Received: 30 August 2023 | Revised: 12 October 2023 | Accepted: 24 October 2023

DOI: 10.1111/cas.16021

ORIGINAL ARTICLE

Cancer Science WILEY

Nationwide prospective registry database of patients with newly diagnosed untreated pleural mesothelioma in Japan

Seiki Hasegawa[1] | Yasushi Shintani[2] | Teruhisa Takuwa[1] | Keisuke Aoe[3] | Katsuya Kato[4] | Nobukazu Fujimoto[5] | Yasuhiro Hida[6] | Masahiro Morise[7] | Yasumitsu Moriya[8] | Takao Morohoshi[9] | Hidemi Suzuki[10] | Masayuki Chida[11] | Shunsuke Endo[12] | Mitsutaka Kadokura[13] | Meinoshin Okumura[2] | Satoshi Hattori[14] | Hiroshi Date[15] | Ichiro Yoshino[10]

[1]Department of Thoracic Surgery, Hyogo Medical University, Hyogo, Japan

[2]Department of General Thoracic Surgery, Osaka University Graduate School of Medicine, Osaka, Japan

[3]Department of Medical Oncology, National Hospital Organization Yamaguchi-Ube Medical Center, Yamaguchi, Japan

[4]Department of Diagnostic Radiology 2, Kawasaki Medical School, Okayama, Japan

[5]Department of Medical Oncology, Okayama Rosai Hospital, Okayama, Japan

[6]Department of Cardiovascular and Thoracic Surgery, Hokkaido University Graduate School of Medicine, Hokkaido, Japan

[7]Department of Respiratory Medicine, Nagoya University Graduate School of Medicine, Aichi, Japan

[8]Division of General Thoracic Surgery, Chiba Rosai Hospital, Chiba, Japan

[9]Division of General Thoracic Surgery, Yokosuka-Kyosai Hospital, Kanagawa, Japan

[10]Department of General Thoracic Surgery, Chiba University Graduate School of Medicine, Chiba, Japan

[11]Department of General Thoracic Surgery, Dokkyo Medical University, Tochigi, Japan

[12]Department of Thoracic Surgery, Jichi Medical University, Shimotsuke, Japan

[13]Division of Chest Surgery, Department of Surgery, Showa University School of Medicine, Tokyo, Japan

[14]Department of Biomedical Statistics, Osaka University Graduate School of Medicine, Osaka, Japan

[15]Department of Thoracic Surgery, Kyoto University Hospital, Kyoto, Japan

Correspondence
Seiki Hasegawa, Department of Thoracic Surgery, Hyogo Medical University, 1-1 Mukogawa-cho, Nishinomiya 663-8501, Japan.
Email: hasegawa@hyo-med.ac.jp

Funding information
The Japanese Joint Committee for Lung Cancer Registry, Grant/Award Number: The 9th project of the Japanese Joint Committee f

Abstract

Due to the scarcity of large-sized prospective databases, the Japanese Joint Committee for Lung Cancer Registry conducted a nationwide prospective registry for newly diagnosed and untreated pleural mesothelioma. All new cases diagnosed pathologically as any subtype of pleural mesothelioma in Japan during the period between April 1, 2017, to March 31, 2019, were included before treatment. Data on survival were collected in April 2021. The eligible 346 patients (285 men [82.3%]; 61 women [17.7%]; median age, 71.0 years [range, 44–88]) were included for analysis. Among these patients, 138 (39.9%) underwent surgery, 164 (47.4%) underwent

Abbreviations: AJCC, American Joint Commission on Cancer; BSC, best supportive care; CI, confidence intervals; EPP, extrapleural pneumonectomy; ET, exploratory thoracotomy; FDG-PET, fluorodeoxyglucose-positron emission tomography; IASLC, International Association for the Study of Lung Cancer; IMIG, International Mesothelioma Interest Group; IQR, interquartile range; JJCLCR, the Japanese Joint Committee for Lung Cancer Registry; MCR, macroscopic complete resection; MTT, maximum tumor thickness; NOS, not otherwise specified; OS, overall survival; P/D, pleurectomy/decortication.; PFS, progression-free survival; PM, pleural mesothelioma; PP, partial pleurectomy; PS, performance status; RT, radiation therapy; STLT, sum of three-level thickness; SUV, standardized uptake value; UICC, Union for International Cancer Control.

non-surgical therapy, and the remaining 44 (12.7%) underwent best supportive care. The median overall survival for all 346 patients was 19.0 months. Survival rates at 1, 2, and 3 years for all patients were, 62.8%, 42.3%, and 26.5%, respectively. Median overall survival was significantly different among patients undergoing surgery, non-surgical treatment, and best supportive care (32.2 months vs. 14.0 months vs. 3.8 months, $p < 0.001$). The median overall survival of patients undergoing pleurectomy/decortication and extrapleural pneumonectomy was 41.8 months and 25.0 months, respectively. Macroscopic complete resection resulted in longer overall survival than R2 resection and partial pleurectomy/exploratory thoracotomy (41.8 months vs. 32.2 months vs. 16.8 months, $p < 0.001$). Tumor shape, maximum tumor thickness, and sum of three level thickness were significant prognostic factors. The data in the prospective database would serve as a valuable reference for clinical practice and further studies for pleural mesothelioma.

KEYWORDS
chemotherapy, database, pleural mesothelioma, staging system, surgery

1 | INTRODUCTION

Pleural mesothelioma (PM) is an aggressive cancer caused by exposure to asbestos. Although many developed countries have banned the use of asbestos, middle- and low-income countries continue to utilize asbestos.[1] The estimated number of global mesothelioma deaths is currently up to 38,000 per year and increasing.[2]

The largest database of PM is the International Association for the Study of Lung Cancer (IASLC) database. The IASLC, in collaboration with the International Mesothelioma Interest Group (IMIG), developed its first international database in 2009[3,4] to update the IMIG staging system introduced in 1994.[5] The staging systems based on the first and second IASLC databases were accepted in the seventh and eighth editions of the Union for International Cancer Control UICC/American Joint Commission on Cancer (AJCC) manuals, respectively.[3,6–8]

The majority of the large number of available retrospective nationwide databases[9–15] are used for epidemiological purposes, while few have complete data on patient treatment, clinical courses, and patient outcomes. Retrospective studies focused on patient prognosis factors,[9,16–22] but only a few were prospective, multicenter studies.[23,24] These limitations lead to difficulties in decision-making regarding treatment strategies for newly diagnosed/untreated PM patients.

Therefore, in our study, we conducted a nationwide prospective registry of newly diagnosed, untreated PM. To the best of our knowledge, this is the first nationwide prospective registry. This study was conducted as the ninth project of the Japanese Joint Committee for Lung Cancer Registry (JJCLCR).[25] JJCLCR has contributed to the establishment of the staging system of lung cancer through several nationwide registries,[26–30] including a prospective one.[29]

The main study aims were to clarify the following issues in newly diagnosed/untreated PM patients in Japan: current status of surgical and non-surgical treatment; surgery completion rate, mortality and morbidity and survival for all patients undergoing surgical intervention; macroscopic complete resection (MCR) as the goal of curative-intent surgery; tumor shape, tumor thickness, and the sum of three-level thickness (STLT) as possible prognostic factors; and feature and prognostic power of the seventh and eighth staging systems.

2 | PATIENTS AND METHODS

2.1 | Study setting

The JJCLCR conducted a prospective observational cohort study enrolling patients first diagnosed with PM between April 1, 2017, and March 31, 2019, in Japan.

The study protocol is described in Supplementary File S1.[25]

2.2 | Inclusion criteria

All patients newly diagnosed according to pathological (including cytology) findings including any subtype of PM in Japan between April 1, 2017, and March 31, 2019, were included. Patients were not given any treatment before registration.

2.3 | Variables

The case report form is shown in Supplementary File S2.[25] The following data were collected and analyzed: (i) demographic characteristics including date of registration, sex, and date of birth; (ii) preoperative status including Eastern Cooperative Oncology Group performance status (PS), preoperative comorbidities (e.g., asbestos exposure and smoking), laboratory values (including tumor markers), radiological findings (tumor shape, tumor thickness, and maximum

standardized uptake value of the pleura on fluorodeoxyglucose-positron emission tomography), and respiratory function tests; (iii) details of diagnosis (e.g., date of diagnosis, diagnostic method, immunohistochemical evaluation results, histologic type, and clinical stage based on both seventh and eighth AJCC/UICC staging systems); (iv) surgical treatments, including induction therapy, surgical interventions, combined resection, status of residual tumor, and postoperative morbidity; (v) postoperative pathological diagnosis and stage based on both seventh and eighth AJCC/UICC staging systems; (vi) chemotherapy regimen; (vii) radiotherapy characteristics, including irradiated sites and type of radiation therapy (RT); and (viii) follow-up data including date of last follow-up, vital signs and symptoms during last follow- up, and date and location of initial relapse.

2.4 | Definitions

2.4.1 | Radiological examination

Localized PM was defined according to Allen's criteria.[31] All the cases were classified into three categories according to the radiological appearance of the tumor: minimal, nodular, or rindlike.[8] Tumor thickness was measured in accordance with the IASLC report.[8] Briefly, measurements of tumor thickness perpendicular to the chest wall or mediastinum on axial imaging were made, representing the upper, middle, and lower third of the hemithorax.[8]

2.4.2 | Diagnosis at registration

In the cases where PM was diagnosed by only cytology, the date of diagnosis was recorded as the date of thoracentesis. In cases where biopsy was performed, the date of diagnosis was the date of biopsy regardless of precedent cytological diagnosis.

2.4.3 | Final diagnosis

In non-surgical cases, diagnosis at registration was the final diagnosis. In surgical cases, the final diagnosis was the diagnosis based on the surgical specimen collected and the date of the final diagnosis was the date of surgery.

2.4.4 | Surgical nomenclature

Surgical nomenclature was defined according to the IASCL/IMIG consensus report.[32]

In this study, MCR was divided into two subgroups: R0-1 was defined as the absence of microscopic tumor cells at the surgical margin, while R1 was defined as microscopic residual tumor cells confirmed at the surgical margin. R2 resection was defined as completion of surgery with macroscopic residual disease. Because both partial pleurectomy (PP) and exploratory thoracotomy (ET) were indicated as incomplete surgery, they were merged into a PP/ET group.

2.5 | Assessments of survival and relapse

Overall survival (OS) was defined as the period from the date of diagnosis at registration to death. Progression-free survival (PFS), defined as the period from surgery to disease progression or death, was calculated in patients who underwent surgery with MCR. Relapse pattern was defined according to Kostron et al.[33]

2.6 | Enrollment and study periods

Patients were enrolled from April 1, 2017, to March 31, 2019.

The study period was between April 1, 2017, and March 31, 2026.

2.7 | Ethics Statement

This study was approved by the institutional review board of Osaka University Hospital, where the registry office is located, on October 11, 2016 (approval number 16038). The registry and the study using the registered data were approved by each institutional review board of all participating institutions. Written informed consent was obtained from all study participants.

This study was registered at the UMIN Clinical Trials Registry as UMIN 000024664 (http://www.umin.ac.jp/ctr/index.htm). This study adhered to the ethical guidelines for epidemiologic studies published jointly by the Japan Ministry of Science, Culture, and Education and the Japan Ministry of Health, Labor, and Welfare on June 17, 2002, and revised on February 28, 2017.

2.8 | Data collection and data analysis

The methods of data management have been previously described.[25] Briefly, patient data were retrieved from the JJCLCR website using a USB drive with a coded institution-individual serial key. Data on survival were collected in April 2021.

2.8.1 | Statistical analysis

Patients' characteristics were summarized with median, interquartile range (IQR) and range (minimum, maximum) for continuous variables and frequencies for categorical variables. For summary statistics, two-tailed 95% confidence intervals (CI) were presented. Survival functions were estimated using the Kaplan–Meier method and their 95% CIs were calculated by using the Greenwood variance with the complementary log–log transformation. Comparisons among

multiple groups were made using the log-rank test, which is referred to as the omnibus test. For ordinal groups, the log-rank test with the linear scores attached was used, referred to as the trend test. Differences between survival functions were evaluated using the log-rank method. Statistical analyses were performed after excluding cases with missing values for relevant variables. No multiplicity adjustment was applied and a *p*-value of less than 0.05 was considered statistically significant. The SAS version 9.4 (SAS Institute, Cary, NC) and R version 4.1.2 (R Core Team; https://www.R-project.org/) were used for statistical analyses. To draw the graphs for the Kaplan–Meier estimates, the *survminer* package for R was used.

3 | RESULTS

3.1 | Clinical characteristics of patients

Between April 1, 2017, and March 31, 2019, a total of 348 cases of PM were registered from 54 institutions. One duplicate case and another case with multiple missing values were removed. The remaining 346 cases were included for analysis (Figure 1).

The clinical characteristics of the 346 patients are shown in Table 1. The median age was 71.0 years (range, 44–88 years). The cohort included 285 men (82.3%) and 61 women (17.7%). Most patients (93.7%) had a good PS score (0 or 1). Asbestos exposure was detected in 67.1% of the patients, and 73.2% of patients were current/former smokers.

3.2 | Diagnosis and pathological findings

Diagnosis at registration was made using biopsy specimens in 97.4% of patietns (337/346) and cell blocks in 2.6% (9/346) (Table 1; Figure 2). Methods of biopsy included open surgery (2.1%, 7/337), video-assisted thoracoscopy under general anesthesia (74.5%, 251/337), thoracoscopy under local anesthesia (11.3%, 38/337), needle biopsy (8.9%, 30/337), and others (3.3%, 11/337). Histological subtype at registration comprised epithelioid (71.5%, 241/337), biphasic (9.5%, 32/337), sarcomatoid (17.8%, 60/337), and not otherwise specified (NOS, 1.2%, 4/337) categories.

Postoperative pathological analysis of surgical specimens was performed in all 138 surgical cases. Diagnosis at registration was made using cell block specimens in six patients, which turned out to be epithelioid ($n = 5$) and biphasic ($n = 1$) subtypes defined during postoperative analysis. In the remaining 132 cases, diagnosis at registration was made using biopsy specimens. We observed and corrected a discrepancy between preoperative and postoperative subtype diagnostics in 8.7% of patients (12/132) as follows: epithelioid to biphasic ($n = 5$), epithelioid to sarcomatoid ($n = 3$), biphasic to epithelioid ($n = 1$), biphasic to sarcomatoid ($n = 1$), biphasic to NOS ($n = 1$), and sarcomatoid to epithelioid ($n = 1$). Consequently, the final diagnosis of 343 patients who underwent biopsy and/or surgery was epithelioid (70.0%, 240/343), biphasic (10.2%, 35/343), sarcomatoid (18.4%, 63/343), and NOS (1.5%, 5/343).

3.3 | Radiological findings

Computed tomography scans and tumor thickness measurements were performed in all cases: 38 (11.0%) localized PM and 299 (89.0%) diffuse PM. Patients were classified as having minimal ($n = 68$, 19.7%), nodular ($n = 96$, 27.7%), and rind-like ($n = 178$, 51.4%) tumors (Table 2). The median maximum tumor thickness (MTT) and the STLT were 11 mm (IQR: 5.0–21.0) and 22 mm (IQR: 11.0–39.0), respectively.

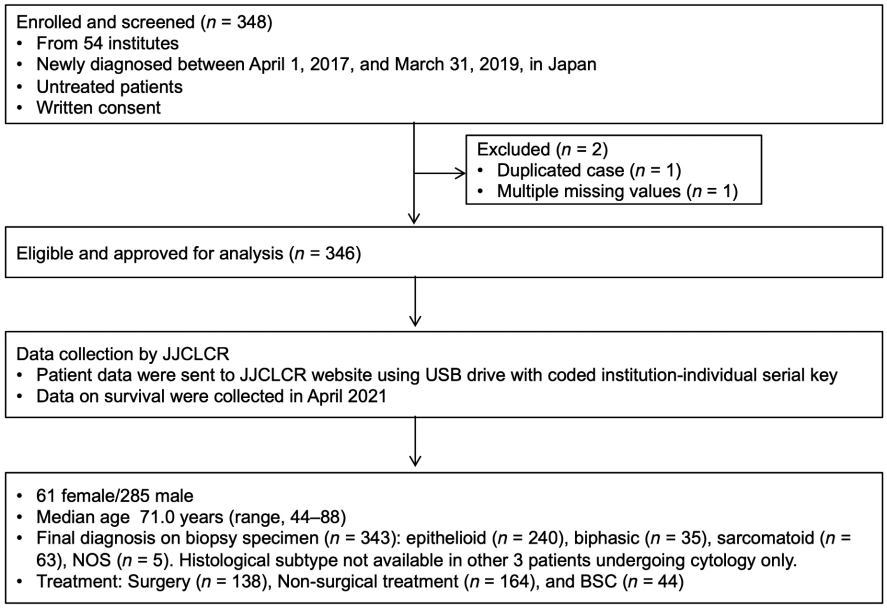

FIGURE 1 CONSORT diagram. Between April 1, 2017, and March 31, 2019, a total of 348 cases of pleural mesothelioma (PM) were registered from 54 institutions. One duplicate case and another case with multiple missing values were removed. The remaining 346 cases were included for analysis. BSC, best supportive care; JJCLCR, Japanese Joint Committee for Lung Cancer Registry; NOS, not otherwise specified.

TABLE 1 Patient's clinical characteristics.

Characteristic	Total ($n = 346$)	Surgery ($n = 138$)	Non-surgical Tx ($n = 164$)	BSC ($n = 44$)
Sex — Number (%)				
Female	61 (17.6)	21 (15.2)	33 (20.1)	7 (15.9)
Male	285 (82.4)	117 (84.8)	131 (79.9)	37 (84.1)
Age — Number (%)				
40–49	5 (1.4)	1 (0.7)	4 (2.4)	0 (0.0)
50–59	27 (7.8)	13 (9.4)	10 (6.1)	4 (9.1)
60–69	114 (32.9)	66 (47.8)	44 (26.8)	4 (9.1)
70–79	154 (44.5)	51 (37.0)	85 (51.8)	18 (40.9)
80–89	46 (13.3)	7 (5.1)	21 (12.8)	18 (40.9)
Age				
Total number	346	138	164	44
Median	71.0	68.5	73.0	78.0
Range	44–88	44–88	45–88	51–88
IQR	66.0–77.0	64.0–73.0	67.0–78.0	71.0–82.0
PS — Number (%)				
0	185 (53.5)	103 (74.6)	69 (42.1)	13 (29.5)
1	139 (40.2)	33 (23.9)	89 (54.3)	17 (38.6)
2	16 (4.6)	1 (0.7)	6 (3.7)	9 (20.5)
3	4 (1.2)	0 (0.0)	0 (0.0)	4 (9.1)
4	2 (0.6)	1 (0.7)	0 (0.0)	1 (2.3)
Asbestos exposure — Number (%)				
Yes	232 (67.1)	94 (68.1)	107 (65.2)	31 (70.5)
No	71 (20.5)	26 (18.8)	36 (22.0)	9 (20.5)
Unknown	43 (12.4)	18 (13.0)	21 (12.8)	4 (9.1)
Smoking — Number (%)				
Never	91 (26.3)	29 (21.0)	46 (28.0)	16 (36.4)
Former	231 (66.8)	95 (68.8)	110 (67.1)	26 (59.1)
Current	22 (6.4)	13 (9.4)	7 (4.3)	2 (4.5)
Unknown	2 (0.6)	1 (0.7)	1 (0.6)	0 (0.7)
Laterality — Number (%)				
Right	209 (60.4)	74 (53.6)	109 (66.5)	26 (59.1)
Left	137 (39.6)	64 (46.4)	55 (33.5)	18 (40.9)
Histology at registration— Number (%)				
Epithelioid	241 (69.7)	112 (81.2)	106 (64.6)	23 (52.3)
Biphasic	32 (9.2)	9 (6.5)	17 (10.4)	6 (13.6)
Sarcomatoid	60 (17.3)	11 (8.0)	36 (22.0)	13 (29.5)
NOS	4 (1.2)	0 (0.0)	2 (1.2)	2 (4.5)
NA (cytology only)	9 (2.6)	6 (4.3)	3 (1.8)	0 (0.0)
Final histology— Number (%)				
Epithelioid	240 (69.4)	111 (80.4)	106 (64.6)	23 (52.3)
Biphasic	35 (10.1)	12 (8.7)	17 (10.4)	6 (13.6)
Sarcomatoid	63 (18.2)	14 (10.1)	36 (22.0)	13 (29.5)
NOS	5 (1.4)	1 (0.7)	2 (1.2)	2 (4.5)
NA (cytology only)	3 (0.9)	0 (0.0)	3 (1.8)	0 (0.0)

Abbreviations: BSC, best supportive care; IQR, interquartile range; NA, not available; NOS, not otherwise specified; Tx, treatment.

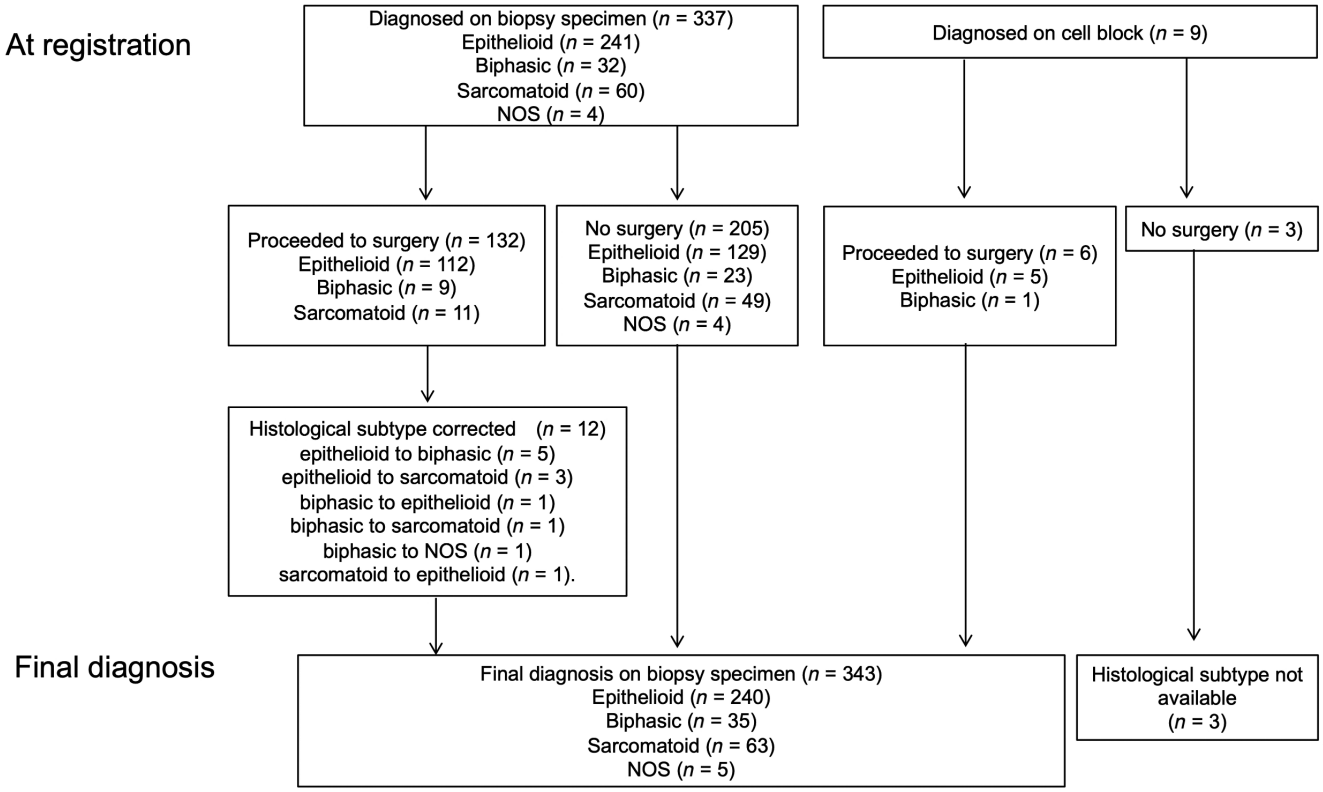

FIGURE 2 Pathological diagnosis at registration and final diagnosis. Pathological diagnosis at registration and final diagnosis are shown. We observed and corrected a discrepancy between preoperative and postoperative subtype diagnostics in 8.7% (12/132). NOS, not otherwise specified.

TABLE 2 Radiological findings.

Characteristic	Total (*n* = 346)	Surgery (*n* = 138)	Non-surgical Tx (*n* = 164)	BSC (*n* = 44)
Diffuse/local — Number (%)				
Diffuse	299 (86.4)	122 (88.4)	136 (82.9)	41 (93.2)
Localized	38 (11.0)	10 (7.2)	25 (15.2)	3 (6.8)
No data	9 (2.6)	6 (4.3)	3 (1.8)	0 (0.0)
Tumor shape — Number (%)				
Minimal	68 (19.7)	32 (23.2)	29 (17.7)	7 (15.9)
Nodular	96 (27.7)	33 (23.9)	49 (29.9)	14 (31.8)
Rind-like	178 (51.4)	71 (51.4)	86 (52.4)	21 (47.7)
Missing data	4 (1.2)	2 (1.4)	0 (0.0)	2 (4.5)
Maximum thickness				
Total number	346	138	164	44
Median (IQR)	11.0 (5.0–21.0)	8.0 (4.0–17.0)	14.0 (7.0–25.0)	12.0 (7.5–18.5)
Range	0–89	0–77	0–89	0–80
Sum of three level thickness				
Total number	346	138	164	44
Median (IQR)	22.0 (11.0–39.0)	18.0 (8.0–31.0)	29.0 (13.0–46.0)	26.5 (15.0–39.5)
Range	0–232	0–154	0–232	0–118
Maximum SUV on FDG-PET				
Total number	234	97	106	31
Median (IQR)	5.8 (3.4–9.6)	4.4 (2.7–7.4)	7.6 (4.0–11.2)	6.5 (3.3–9.5)
Range	0–32	0–23	0–32	0–18

Abbreviations: BSC, best supportive care; FDG-PET, fluorodeoxyglucose-positron emission tomography; IQR, interquartile range; SUV, standardized uptake value; Tx, treatment.

3.4 | Clinical and pathological stages

Clinical stages were defined for all patients. Similarly, for patients undergoing surgery, their pathological stages were determined according to both the seventh and eighth versions of TNM staging systems (Tables 3–5). Stage distribution in the seventh and eighth versions of the staging system is shown in Figure 3. Assessment of the discrepancy between clinical and pathological stages according to the version seventh staging system revealed the following: 54.3% (75/138) unchanged, 39.9% (55/138) upstaged, and 6.5% (9/138) down-staged cancer cases. In contrast, according to the version eighth staging system, the results were as follows: 42.8% (59/138) unchanged, 52.2% (72/138) upstaged, and 5.1% (7/138) down-staged cancer cases.

TABLE 3 Clinical stages according to seventh and eighth TNM staging systems.

Characteristic	Total ($n=346$)	Surgery ($n=138$)	Non-surgical Tx ($n=164$)	BSC ($n=44$)
T (version 7) — Number (%)				
T0, T1a	89 (25.7)	56 (40.6)	25 (15.2)	8 (18.2)
T1b	30 (8.7)	9 (6.5)	18 (11.0)	3 (6.8)
T2	54 (15.6)	29 (21.0)	23 (14.0)	2 (4.5)
T3	104 (30.1)	41 (29.7)	47 (28.7)	16 (36.4)
T4	69 (19.9)	3 (2.2)	51 (31.1)	15 (34.1)
N (version 7) — Number (%)				
N0	267 (77.2)	123 (89.1)	111 (67.7)	33 (75.0)
N1	12 (3.5)	4 (2.9)	7 (4.3)	1 (2.3)
N2	52 (15.0)	11 (8.0)	35 (21.3)	6 (13.6)
N3	15 (4.3)	0 (0.0)	11 (6.7)	4 (9.1)
M (version 7) — Number (%)				
M0	326 (94.2)	137 (99.3)	150 (91.5)	39 (88.6)
M1	20 (5.8)	1 (0.7)	14 (8.5)	5 (11.4)
Stage (version 7) — Number (%)				
Stage I	118 (34.1)	64 (46.4)	43 (26.2)	11 (25.0)
Stage II	41 (11.8)	25 (18.1)	16 (9.8)	0 (0.0)
Stage III	108 (31.2)	45 (32.6)	48 (29.3)	15 (34.1)
Stage IV	79 (22.8)	4 (2.9)	57 (34.8)	18 (40.9)
T (version 8) — Number (%)				
T0, T1	148 (42.8)	80 (58.0)	57 (34.8)	11 (25.0)
T2	25 (7.2)	14 (10.1)	9 (5.5)	2 (4.5)
T3	104 (30.1)	41 (29.7)	47 (28.7)	16 (36.4)
T4	69 (19.9)	3 (2.2)	51 (31.1)	15 (34.1)
N (version 8) — Number (%)				
N0	267 (77.2)	123 (89.1)	111 (67.7)	33 (75.0)
N1	64 (18.5)	15 (10.9)	42 (25.6)	7 (15.9)
N2	15 (4.3)	0 (0.0)	11 (6.7)	4 (9.1)
M (version 8) — Number (%)				
M0	326 (94.2)	137 (99.3)	150 (91.5)	39 (88.6)
M1	20 (5.8)	1 (0.7)	14 (8.5)	5 (11.4)
Stage (version 8) — Number (%)				
Stage IA	142 (41.0)	77 (55.8)	54 (32.9)	11 (25.0)
Stage IB	87 (25.1)	44 (31.9)	31 (18.9)	12 (27.3)
Stage II	12 (3.5)	5 (3.6)	6 (3.7)	1 (2.3)
Stage IIIA	26 (7.5)	8 (5.8)	16 (9.8)	2 (4.5)
Stage IIIB	59 (17.1)	3 (2.2)	43 (26.2)	13 (29.5)
Stage IV	20 (5.8)	1 (0.7)	14 (8.5)	5 (11.4)

Abbreviations: BSC, best supportive care; Tx, treatment; ver., version.

TABLE 4 Clinical stages for surgical cases by seventh and eighth TNM staging systems.

Characteristic	Total ($n=138$)	EPP ($n=26$)	P/D ($n=83$)	PP/ET ($n=26$)	Other surgery ($n=3$)
T (version 7) — Number (%)					
T0, T1a	56 (40.6)	8 (30.8)	44 (53.0)	4 (15.4)	0 (0.0)
T1b	9 (6.5)	1 (3.8)	7 (8.4)	1 (3.8)	0 (0.0)
T2	29 (21.0)	7 (26.9)	14 (16.9)	6 (23.1)	2 (66.7)
T3	41 (29.7)	9 (34.6)	18 (21.7)	13 (50.0)	1 (33.3)
T4	3 (2.2)	1 (3.8)	0 (0.0)	2 (7.7)	0 (0.0)
N (version 7) — Number (%)					
N0	123 (89.1)	25 (96.2)	75 (90.4)	20 (76.9)	3 (100.0)
N1	4 (2.9)	0 (0.0)	4 (4.8)	0 (0.0)	0 (0.0)
N2	11 (8.0)	1 (3.8)	4 (4.8)	6 (23.1)	0 (0.0)
M (version 7) — Number (%)					
M0	137 (99.3)	26 (100.0)	83 (100.0)	25 (96.2)	3 (100.0)
M1	1 (0.7)	0 (0.0)	0 (0.0)	1 (3.8)	0 (0.0)
Stage (version 7) — Number (%)					
Stage I	64 (46.4)	9 (34.6)	50 (60.2)	5 (19.2)	0 (0.0)
Stage II	25 (18.1)	7 (26.9)	10 (12.0)	6 (23.1)	2 (66.7)
Stage III	45 (32.6)	9 (34.6)	23 (27.7)	12 (46.2)	1 (33.3)
Stage IV	4 (2.9)	1 (3.8)	0 (0.0)	3 (11.5)	0 (0.0)
T (version 8) — Number (%)					
T0, T1	80 (58.0)	14 (53.8)	59 (71.1)	7 (26.9)	0 (0.0)
T2	14 (10.1)	2 (7.7)	6 (7.2)	4 (15.4)	2 (66.7)
T3	41 (29.7)	9 (34.6)	18 (21.7)	13 (50.0)	1 (33.3)
T4	3 (2.2)	1 (3.8)	0 (0.0)	2 (7.7)	0 (0.0)
N (version 8) — Number (%)					
N0	123 (89.1)	25 (96.2)	75 (90.4)	20 (76.9)	3 (100.0)
N1	15 (10.9)	1 (3.8)	8 (9.6)	6 (23.1)	0 (0.0)
M (version 8) — Number (%)					
M0	137 (99.3)	26 (100.0)	83 (100.0)	25 (96.2)	3 (100.0)
M1	1 (0.7)	0 (0.0)	0 (0.0)	1 (3.8)	0 (0.0)
Stage (version 8) — Number (%)					
Stage IA	77 (55.8)	14 (53.8)	56 (67.5)	7 (26.9)	0 (0.0)
Stage IB	44 (31.9)	10 (38.5)	19 (22.9)	12 (46.2)	3 (100.0)
Stage II	5 (3.6)	0 (0.0)	5 (6.0)	0 (0.0)	0 (0.0)
Stage IIIA	8 (5.8)	1 (3.8)	3 (3.6)	4 (15.4)	0 (0.0)
Stage IIIB	3 (2.2)	1 (3.8)	0 (0.0)	2 (7.7)	0 (0.0)
Stage IV	1 (0.7)	0 (0.0)	0 (0.0)	1 (3.8)	0 (0.0)

Abbreviations: EPP, extrapleural pneumonectomy; P/D, pleurectomy/decortication; PP/ET, patrial pleurectomy/exploratory thoracotomy; ver., version.

3.5 | Treatment distribution

Among the enrolled 346 patients, 138 (39.9%) underwent surgery, 164 (47.4) underwent non-surgical therapy (i.e., chemotherapy with or without radiation therapy), and the remaining 44 (12.7%) underwent BSC.

3.5.1 | Surgical treatment

One hundred and thirty-eight patients underwent surgery in 35 experienced centers. Of 138 surgeries, 81 (58.7%) were performed in three high-volume centers. Surgical technique consisted of extrapleural pneumonectomy (EPP, $n=26$), pleurectomy/

TABLE 5 Pathological stages for surgical cases by seventh and eighth TNM staging systems.

Characteristic	Total ($n=138$)	EPP ($n=26$)	P/D ($n=83$)	PP/ET ($n=26$)	Other surgery ($n=3$)
T (version 7) — Number (%)					
T0, T1a	17 (12.3)	2 (7.7)	12 (14.5)	3 (11.5)	0 (0.0)
T1b	9 (6.5)	0 (0.0)	7 (8.4)	2 (7.7)	0 (0.0)
T2	30 (21.7)	11 (42.3)	16 (19.3)	2 (7.7)	1 (33.3)
T3	61 (44.2)	11 (42.3)	41 (49.4)	7 (26.9)	2 (66.7)
T4	21 (15.2)	2 (7.7)	7 (8.4)	12 (46.2)	0 (0.0)
N (version 7) — Number (%)					
N0	107 (77.5)	20 (76.9)	62 (74.7)	22 (84.6)	3 (100.0)
N1	4 (2.9)	1 (3.8)	2 (2.4)	1 (3.8)	0 (0.0)
N2	26 (18.8)	5 (19.2)	18 (21.7)	3 (11.5)	0 (0.0)
N3	1 (0.7)	0 (0.0)	1 (1.2)	0 (0.0)	0 (0.0)
M (version 7) — Number (%)					
M0	137 (99.3)	26 (100.0)	83 (100.0)	25 (96.2)	3 (100.0)
M1	1 (0.7)	0 (0.0)	0 (0.0)	1 (3.8)	0 (0.0)
Stage (version 7) — Number (%)					
Stage1	26 (18.8)	2 (7.7)	19 (22.9)	5 (19.2)	0 (0.0)
Stage2	25 (18.1)	8 (30.8)	14 (16.9)	2 (7.7)	1 (33.3)
Stage3	64 (46.4)	14 (53.8)	42 (50.6)	6 (23.1)	2 (66.7)
Stage4	23 (16.7)	2 (7.7)	8 (9.6)	13 (50.0)	0 (0.0)
T (version 8) — Number (%)					
T0, T1	35 (25.4)	5 (19.2)	25 (30.1)	5 (19.2)	0 (0.0)
T2	21 (15.2)	8 (30.8)	10 (12.0)	2 (7.7)	1 (33.3)
T3	61 (44.2)	11 (42.3)	41 (49.4)	7 (26.9)	2 (66.7)
T4	21 (15.2)	2 (7.7)	7 (8.4)	12 (46.2)	0 (0.0)
N (version 8) — Number (%)					
N0	107 (77.5)	20 (76.9)	62 (74.7)	22 (84.6)	3 (100.0)
N1	30 (21.7)	6 (23.1)	20 (24.1)	4 (15.4)	0 (0.0)
N2	1 (0.7)	0 (0.0)	1 (1.2)	0 (0.0)	0 (0.0)
M (version 8) — Number (%)					
M0	137 (99.3)	26 (100.0)	83 (100.0)	25 (96.2)	3 (100.0)
M1	1 (0.7)	0 (0.0)	0 (0.0)	1 (3.8)	0 (0.0)
Stage (version 8) — Number (%)					
Stage IA	32 (23.2)	4 (15.4)	23 (27.7)	5 (19.2)	0 (0.0)
Stage IB	59 (42.8)	14 (53.8)	35 (42.2)	7 (26.9)	3 (100.0)
Stage II	5 (3.6)	3 (11.5)	2 (2.4)	0 (0.0)	0 (0.0)
Stage IIIA	19 (13.8)	3 (11.5)	15 (18.1)	1 (3.8)	0 (0.0)
Stage IIIB	22 (15.9)	2 (7.7)	8 (9.6)	12 (46.2)	0 (0.0)
Stage IV	1 (0.7)	0 (0.0)	0 (0.0)	1 (3.8)	0 (0.0)

Abbreviations: EPP, extrapleural pneumonectomy; P/D, pleurectomy/decortication; PP/ET, patrial pleurectomy/exploratory thoracotomy; ver., version.

decortication (P/D, $n=83$), PP/ET ($n=26$), and other surgeries ($n=3$) (Tables 6 and 7). Surgery alone and surgery as part of a multimodality treatment with chemotherapy and/or radiation therapy were conducted in 29 and 109 patients, respectively. The median age of patients who underwent surgical intervention was 68.5 years (IQR: 64.0–73.0). The median value of operation time and blood loss were 406.5 min (IQR: 282.5–509.5) and 1210 g (IQR: 613.8–1855.8). The resection statuses were R0-1 ($n=41$), R1 ($n=55$), and R2 ($n=42$), respectively, and MCR (R0-1 and R1) was achieved in 69.6% (96/138). Data analysis indicated that 30- and 90-day postoperative deaths were 0.7% (1/138, PP/ET group) and 4.3% (6/138, EPP: 1, P/D: 2, PP/ET: 3). The causes within the

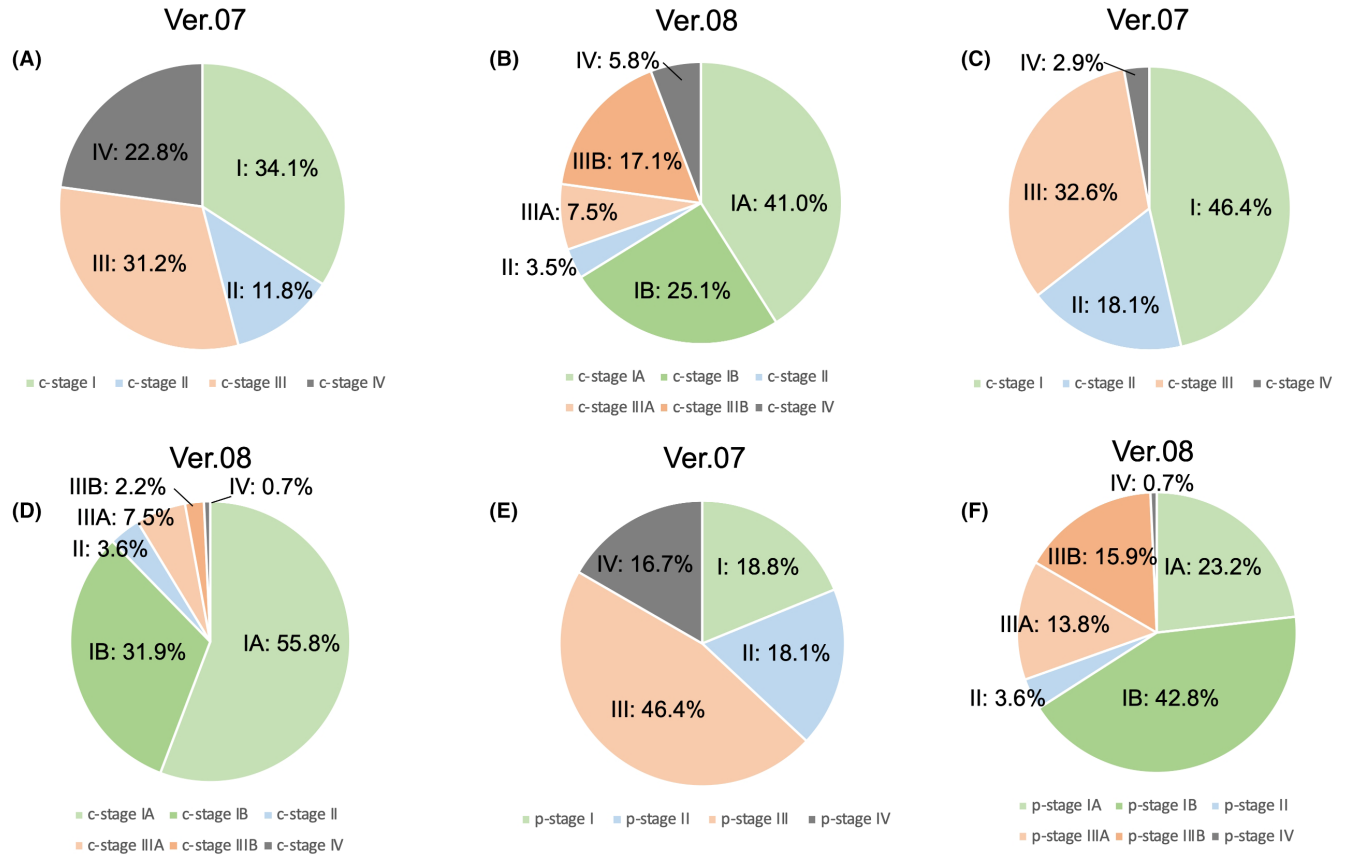

FIGURE 3 Stage distribution in seventh and eighth TNM staging systems. Distributions of clinical stages for all cases are shown in Figure 2A,B, respectively. There were 34.3% of c-stage I and 31.2% of c-stage III patients according to the version 7 staging system (A), and 66.1% cases were classified as c-stage I in the version 8 staging system (B). In surgical cases, 46.4% and 87.7% of cases were classified as c-stage I by version 7 and version 8 staging systems, respectively (C, D). Distributions of pathological stages for surgical cases are shown in Figure 2E,F: There were 46.4% of p-stage III according to the version 7 staging system (E) and 66.0% of p-stage I patients according to the version 8 staging system (F).

90-day mortality range were diagnosed with interstitial pneumonia (two patients) and mesothelioma progression (four patients). Of the 37 patients with localized PM, 10 underwent surgery: P/D ($n=7$), PP ($n=2$), and other surgery ($n=1$). Of these 10 patients, four underwent R0-1 resection, another four underwent R1 resection, and two underwent R2 resection.

3.5.2 | Non-surgical treatment

First-line treatment in 164 patients undergoing non-surgical treatment consisted of concurrent chemoradiotherapy (4.3%, $n=7$), cisplatin plus pemetrexed (51.2%, $n=84$), carboplatin plus pemetrexed (28.7%, $n=47$), pemetrexed alone (6.7, $n=11$), and others (9.1%, $n=15$) (Table 8). Of the 164 patients, 67.7% ($n=111$) and 17.7% ($n=29$) underwent second- and third-line treatment, respectively. A total of 43 patients underwent RT. Post-EPP hemithoracic RT was performed in 21 patients (45–54 Gy, dose unknown in 1). One patient underwent focal adjuvant RT after R2 resection of P/D. Eight patients underwent RT for postoperative recurrence.

3.6 | Survival analysis

Among 346 patients, 242 patients died during the follow-up period. The median follow-up period for the 104 surviving patients was 945.5 days (range, 1–1480 days). At the time of data collection in April 2021, 229 patients died of PM, 13 died of other diseases (seven with PM, six without PM), 85 were alive with PM, and 19 were alive without PM. Median OS was 19.0 months (95% CI: 15.4–22.3). Survival rates at 1, 2, and 3 years for all patients were 62.8% (95% CI: 57.4%–67.6%), 42.3% (95% CI: 37.0%–47.5%), and 26.5% (95% CI: 21.3%–31.9%), respectively (Figure 4A).

In the surgery group, median OS was 32.2 months. In non-surgical treatment group, OS was 14.0 months, while in the BSC group, OS was only 3.8 months. Survival rates at 1, 2, and 3 years in the surgery group were 81.8%, 61.3%, and 41.9%, respectively. Survival rates at 1, 2, and 3 years in non-surgical treatment group were 56.5%, 32.3%, and 17.2%, respectively. Finally, the survival rates in BSC group were 22.9%, 17.8%, and 11.4%, respectively (Figure 4B). These results show significant differences in OS among three groups.

Median OS after multimodality therapy ($n=109$) was significantly longer than that in the surgery alone group ($n=29$): 34.6 months vs.

TABLE 6 Surgical treatments.

	Case No
EPP	26
EPP alone	2
EPP + AC	1
EPP + RT	8
EPP + RT + AC	2
NAC + EPP	2
NAC + EPP + RT	11
P/D	83
P/D alone	13
P/D + AC	18
NAC + P/D	31
NAC + P/D + AC	20
NAC + P/D + RT + AC	1
PP/ET	26
PP/ET alone	12
NAC + PP/ET	14
Other surgery	3
Other surgery alone	2
Other surgery + AC	1
Total	138

Abbreviations: AC, adjuvant chemotherapy; EPP, extrapleural pneumonectomy; ET, exploratory thoracotomy; NAC, neoadjuvant chemotherapy; P/D, pleurectomy/decortication; PP, partial pleurectomy; RT, radiation therapy.

21.0 months (HR = 0.53) (Figure 4C). Median OS by surgical technique is shown in Figure 4D: 25.0 months for EPP, 41.8 months for P/D, and 17.5 months for PP/ET. Survival time of P/D, not EPP, was significantly longer than that for PP/ET.

Median OS for R1 resection, R2 resection, and PP/ET were 39.5 months, 32.2 months, and 16.8 months, respectively (Figure 4E). Median OS for R0-1 group was undefined. There was no significant difference in OS time between R0-1 and R1 groups. Median OS time for the MCR group (R0-1 plus R1) was 41.8 months, which was significantly longer than that for R2 resection and PP/ET (Figure 4F).

The trend of survival in each clinical stage is shown in Table 9A and Figure 5A,B. A significant difference in survival between stage groups was observed using both seventh and eighth staging systems. The survival rates at each pathological stage are shown in Table 9B. No differences in survival rates were observed using the seventh staging system ($p = 0.080$; Figure 5C). A significant difference was observed for pathological stages using the eighth staging system approach ($p = 0.005$; Figure 5D).

The median OS for minimal ($n = 68$), nodular ($n = 96$), and rindlike ($n = 178$) tumor shape groups were 26.7, 21.3, and 15.0 months, respectively (Figure 6A). The survival time in minimal and nodular groups was significantly longer than that in the rindlike group ($p = 0.007$, $p = 0.029$ respectively). The median OS time (27.0 months) was significantly longer in the MTT <5.1 mm group ($n = 91$) than that in the MTT ≥ 5.1 mm group ($n = 255$) (15.5 months) ($p = 0.013$) (Figure 6B). The median OS time (26.3 months) for the STLT <13 mm group ($n = 101$) was significantly longer than that for the 13 ≤ STLT <60 mm group ($n = 203$) (15.5 months) ($p = 0.022$) and the STLT ≥60 mm group ($n = 42$) (12.0 months) ($p = 0.008$) (Figure 6C).

3.7 | Relapse after macroscopic complete resection

Relapse occurred in 74 (77.1%) of the 96 MCR patients and resulted in PM-related death ($n = 36$), death due to other causes with PM ($n = 1$), and survival with PM ($n = 37$). Among 22 patients without recurrence, four died of other causes, while 18 survived. Relapse pattern was described in 71 of 74 relapsed patients. Initial relapse sites were local only in 53 (74.6%), distant only in eight (11.3%), and both in 10 (14.1%) (Table 10). Distant only metastasis was observed in 27.8% (5/18) of EPP patients and 5.9% (3/51) of P/D patients.

The PFS time was calculated in 93 of the 96 MCR cases, excluding three cases without detailed relapse information. Median PFS and survival rates at 1, 2, and 3 years for 93 MCR patients were 16.6 months, 73.1%, 29.3%, and 19.1%, respectively (Figure 7A). Median PFS and PFS rates at 1, 2, and 3 years were 13.6 months and 63.6%, 13.6%, and 13.6% for EPP patients ($n = 22$), and 19.4 months and 76.2%, 34.4%, and 20.7% for P/D patients ($n = 68$), respectively (Figure 7B).

4 | DISCUSSION

The JJLCRC generated several nationwide registries to establish the international staging system of lung cancer.[27,29,30] This study is the first investigation and analysis of a PM registry by JJLCRC. Like previous JJLCRC registries[26–30] this study provides reliable and critical information with few excluded cases and missing values of clinical data. According to the annual report of the Japanese Ministry of Health, Labor, and Welfares,[34] 1555 and 1512 deaths were associated with PM in 2017 and 2018, respectively. According to the National Clinical Database of Japan, 622 curative-intent surgeries for PM were performed between January 2014 and December 2017.[35] Thus, this study represents approximately 10% of all PM cases and 50% of surgical cases in Japan during the study period.

With the nationwide enrollment prospectively, the present study has provided critical information on PM treatment. We found that median OS time for non-surgical treatment groups and BSC groups were 14.0 months and 3.8 months, respectively. These results were in line with a large-scale retrospective study in the United States.[36] This study revealed that prognosis for unresectable PM remains poor. Furthermore, our study provided the surgery completion rate, MCR rate, mortality/morbidity rate, and postoperative survival rate of all patients undergoing surgery, which had been lacking in the literature. Surgery incompletion

TABLE 7 Clinical characteristics of patients with PM surgery.

Characteristic	Total (*n* = 138)	EPP (*n* = 26)	P/D (*n* = 83)	PP/ET (*n* = 26)	Other surgery (*n* = 3)
Gender — Number (%)					
Female	21 (15.2)	4 (15.4)	10 (12.0)	6 (23.1)	1 (33.3)
Male	117 (84.8)	22 (84.6)	73 (88.0)	20 (76.9)	2 (66.7)
Age — Number (%)					
40–49	1 (0.7)	1 (3.8)	0 (0.0)	0 (0.0)	0 (0.0)
50–59	13 (9.4)	4 (15.4)	9 (10.8)	0 (0.0)	0 (0.0)
60–69	66 (47.8)	11 (42.3)	43 (51.8)	11 (42.3)	1 (33.3)
70–79	51 (37.0)	9 (34.6)	27 (32.5)	13 (50.0)	2 (66.7)
80–89	7 (5.1)	1 (3.8)	4 (4.8)	2 (7.7)	0 (0.0)
Total number	138	26	83	26	3
Median (IQR)	68.5 (64.0–73.0)	68.0 (62.0–71.0)	68.0 (64.0–73.0)	71.0 (65.0–75.0)	73.0 (67.0–78.0)
Range	44–88	44–80	55–80	60–88	67–78
Completeness of resection— Number (%)					
R0-1	41 (29.7)	10 (38.5)	30 (36.1)	0 (0.0)	1 (33.3)
R1	55 (39.9)	12 (46.2)	41 (49.4)	1 (3.8)[a]	1 (33.3)
R2	42 (30.4)	4 (15.4)	12 (14.5)	25 (96.2)	1 (33.3)
Surgical time (min.)					
Median (IQR)	406.5 (280.0–510.0)	393.0 (357.0–487.0)	466.0 (372.0–554.0)	175.5 (90.0–233.0)	274.0 (222.0–290.0)
Range	30–885	177–705	68–885	30–544	222–290
Blood loss (gram)					
Median (IQR)	1210.0 (610.0–1861.0)	1186.0 (870.0–1700.0)	1450.0 (860.0–2160.0)	290.0 (34.0–740.0)	270.0 (120.0–670.0)
Range	1–25205	300–8036	5–25205	1–4530	120–670

Abbreviations: EPP, extrapleural pneumonectomy; ET, exploratory thoracotomy; IQR, interquartile range; P/D, pleurectomy/decortication; PM, pleural mesothelioma; PP, partial pleurectomy.

[a]Localized mesothelioma.

TABLE 8 Non-surgical treatment.

First-line Tx (*n* = 164)	Second-line Tx (*n* = 111)	Third-line Tx (*n* = 29)
Chemoradiotherapy (*n* = 7)		
CDDP+PEM (*n* = 84)	CDDP+PEM (*n* = 2)	BSC (*n* = 2)
	CBDCA+PEM (*n* = 8)	Others (*n* = 2), BSC (*n* = 6)
	PEM (*n* = 5)	Others (*n* = 2), RT (*n* = 1), BSC (*n* = 2)
	Others (*n* = 45)	CDDP+PEM (*n* = 1), PEM (*n* = 1), Others (*n* = 4), RT (*n* = 1), BSC (*n* = 38)
	RT (*n* = 1)	Others (*n* = 1)
	BSC (*n* = 23)	
CBDCA+PEM (*n* = 47)	CBDCA+PEM (*n* = 3)	Others (*n* = 1), BSC (*n* = 2)
	PEM (*n* = 1)	BSC (*n* = 1)
	Others (*n* = 19)	CBDCA+PEM (*n* = 1), PEM (*n* = 2), Others (*n* = 2), BSC (*n* = 14)
	RT (*n* = 2)	Others (*n* = 1), BSC (*n* = 1)
	BSC (*n* = 22)	
PEM (*n*=11)	Others (*n* = 5)	Others (*n* = 1), BSC (*n* = 4)
	BSC (*n* = 6)	
Others (*n*=15)	CDDP+PEM (*n* = 3)	Others (*n* = 3)
	CBDCA+PEM (*n* = 2)	Others (*n* = 1), BSC (*n* = 1)
	PEM (*n* = 1)	BSC (*n* = 1)
	Others (*n* = 7)	CBDCA+PEM (*n* = 1), Others (*n* = 2), RT (*n* = 1), BSC (*n* = 3)
	BSC (*n* = 2)	

Abbreviations: BSC, best supportive care; CBDCA, carboplatin; CDDP, cisplatin; PEM, pemetrexed; RT, radiation therapy; Tx, treatment.

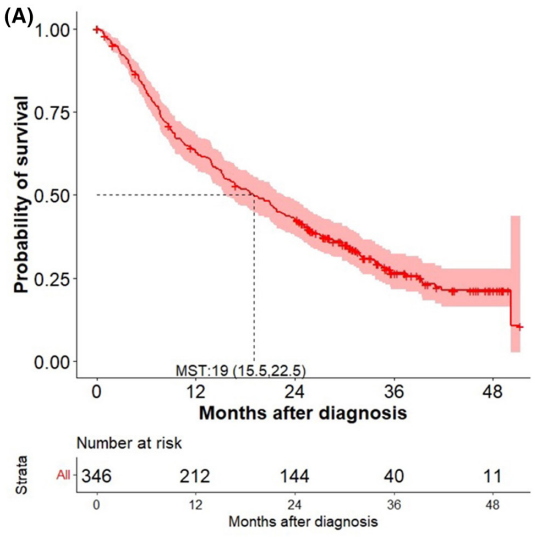

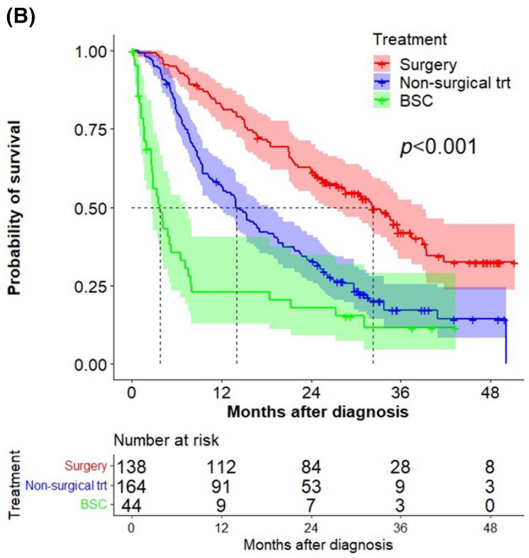

		Number	Survival Probability			MST	HR	
group	n	of event	1 year	2 year	3 year	(95%CI)	(95%CI)	*p*-value
Total	346	242	0.628 (0.574,0.676)	0.423 (0.370,0.475)	0.265 (0.213,0.319)	19.03 (15.37,22.27)		< 0.001 (omnibus)
Surgery	138	77	0.818 (0.743,0.873)	0.613 (0.525,0.688)	0.419 (0.325,0.510)	32.23 (25.60,37.47)	0.22 (0.15, 0.33)	< 0.001
Non-surgical Tx	164	130	0.565 (0.485,0.637)	0.323 (0.252,0.395)	0.172 (0.110,0.245)	14.03 (11.47,17.07)	0.48 (0.33, 0.69)	< 0.001
BSC	44	35	0.229 (0.114,0.367)	0.178 (0.078,0.310)	0.114 (0.036,0.243)	3.80 (2.63,6.53)	1 (reference)	

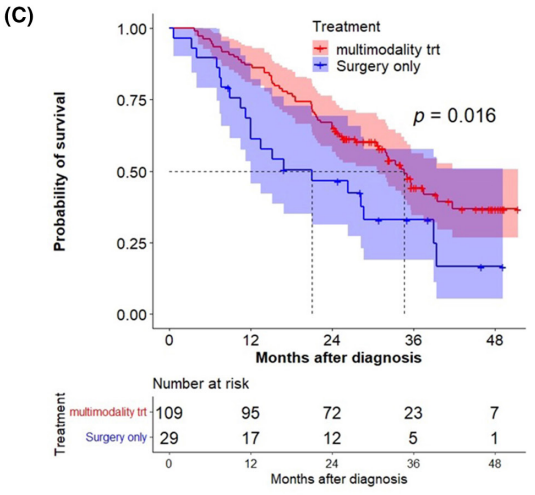

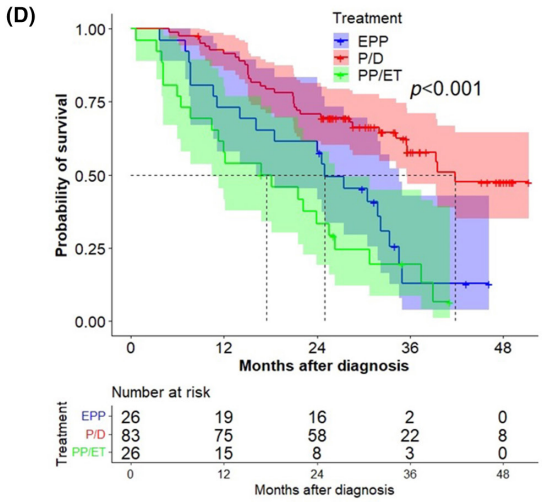

		Number	Survival Probability			MST	HR	
group	n	of event	1 year	2 year	3 year	(95%CI)	(95%CI)	*p*-value
Total	138	77	0.818 (0.743,0.873)	0.613 (0.525,0.688)	0.419 (0.325,0.510)	32.23 (25.60,37.47)		
Multimodality treatment	109	57	0.872 (0.793,0.922)	0.651 (0.554,0.733)	0.441 (0.333,0.544)	34.60 (30.53,41.77)	0.53 (0.32, 0.89)	0.016
Surgery alone	29	20	0.613 (0.410,0.764)	0.466 (0.276,0.636)	0.329 (0.158,0.512)	20.97 (11.27,38.97)	reference	0.016 (omnibus)
EPP	26	20	0.731 (0.517,0.862)	0.577 (0.368,0.739)	0.127 (0.024,0.319)	25.00 (14.03,32.23)	0.67 (0.37, 1.24)	0.203
P/D	83	34	0.915 (0.830,0.959)	0.708 (0.596,0.793)	0.578 (0.448,0.687)	41.77 (35.57,.)	0.27 (0.16, 0.46)	< 0.001
PP/ET	26	22	0.577 (0.368,0.739)	0.333 (0.162,0.515)	0.194 (0.065,0.374)	17.48 (7.67,25.60)	reference	< 0.001 (omnibus)
Other surgery	3	1		0.667 (0.054,0.945)	0.667 (0.054,0.945)	.(20.97,.)	NE	

FIGURE 4 (Continues)

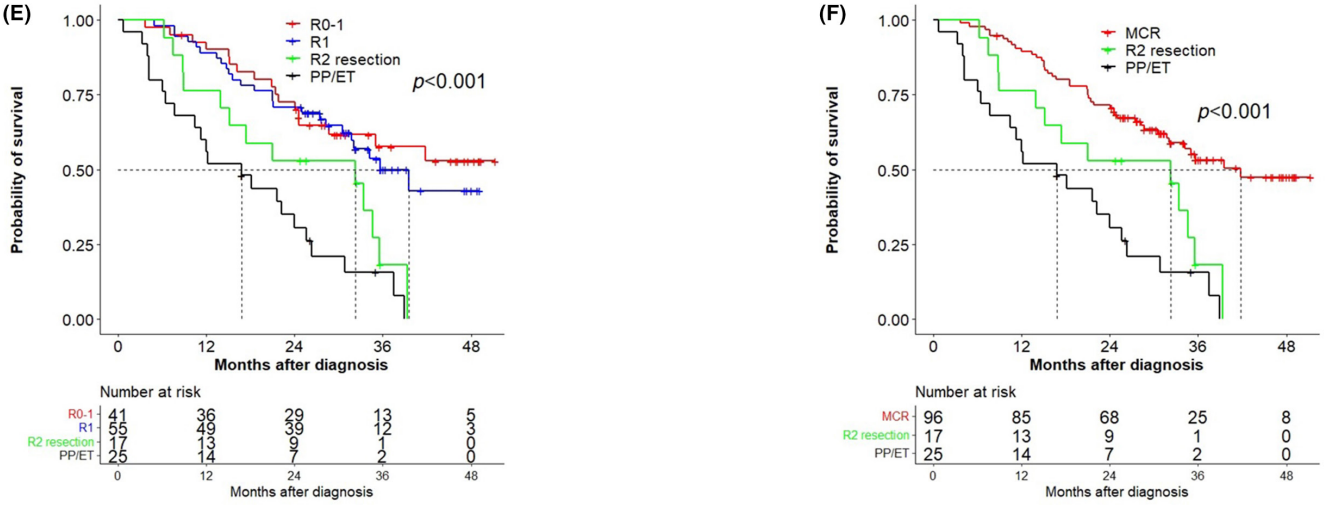

		Number	Survival Probability			MST	HR	
group	n	of event	1 year	2 year	3 year	(95%CI)	(95%CI)	*p*-value
R0-1	41	17	0.901 (0.758,0.962)	0.701(0.534,0.818)	0.576(0.398,0.719)	.(24.60,.)	reference	< 0.001(omnibus)
R1	55	25	0.891 (0.773,0.949)	0.709(0.570,0.811)	0.500(0.341,0.640)	39.50 (30.53,.)	1.20(0.65, 2.24)	0.559
R2 resection	17	13	0.765 (0.488,0.904)	0.529(0.276,0.730)	0.182(0.032,0.430)	32.23 (8.90,35.57)	2.59(1.24, 5.40)	0.011
PP/ET	25	22	0.560 (0.348,0.727)	0.305(0.139,0.491)	0.157(0.043,0.337)	16.83 (7.67,23.93)	4.39(2.29, 8.41)	< 0.001
MCR	96	42	0.895 (0.814,0.942)	0.706 (0.603,0.786)	0.532 (0.415,0.637)	41.77 (31.80,.)	reference	< 0.001 (omnibus)
R2 resection	17	13	0.765 (0.488,0.904)	0.529 (0.276,0.730)	0.182 (0.032,0.430)	32.23 (8.90,35.57)	2.32 (1.24, 4.36)	0.009
PP/ET	25	22	0.560 (0.348,0.727)	0.305 (0.139,0.491)	0.157 (0.043,0.337)	16.83 (7.67,23.93)	3.93 (2.32, 6.67)	< 0.001

FIGURE 4 Overall survival (OS). (A) Median OS and survival rates at 1, 2, and 3 years for all patients were 19.0 months and 62.8%, 42.3%, and 26.5%, respectively. (B) Median OS and survival rates at 1, 2, and 3 years were 32.2 months and 81.8%, 61.3%, and 41.9%, respectively, for the surgery group; at 14.0 months and 56.5%, 32.3%, and 17.2%, respectively, for the non-surgical treatment group; and at 3.8 months, 22.9%, 17.8%, and 11.4% for the BSC group, respectively. (C) Median OS for multimodality therapy ($n = 109$) was significantly longer than surgery alone ($n = 29$): 34.6 months vs. 21.0 months. (D) Median OS by surgical technique were 25.0 months for EPP, 41.8 months for P/D, and 17.5 months for PP/ET. There was a significant difference in OS between P/D and PP/ET. (E) Median OS for R0-1, R1, and R2 resection and PP/ET groups were undefined, 39.5 months, 32.2 months, and 16.8 months. OS for R0-1 and R1 resections were significantly longer for those of R2 resection and PP/ET. There was no significant difference in OS between R0-1 and R1. (F) The median OS for the MCR group was 41.8 months and was significantly longer than those for R2 resection and PP/ET. BSC, best supportive care; EPP, extrapleural pneumonectomy; MCR, macroscopic complete resection; OS, overall survival; P/D, pleurectomy/decortication; PP/ET, patrial pleurectomy/exploratory thoracotomy; Tx, treatment.

rate (i.e., ET/PP) in this study was 18.8%, similar to the result of a previous single-center retrospective study.[37] However, the found rate was relatively high compared to the data from previous prospective studies.[38–42] The relatively high surgery incompletion rate in this study might have reflected that some of participating surgeons were not sufficiently experienced. The ambiguity of surgical nomenclature might also serve as a possible explanation of our findings. Since the distinction of R2 resection, PP, and ET in surgery-intended cases is not clearly described in the consensus paper,[32] surgery incompletion rate might vary according to the surgeon's definition.

The median OS time (32.2 months) for all surgical cases in the present study was longer than that in previous prospective studies (up to 24.4 months).[38,39,43–47] The recent small-scale phase II clinical trial reported an intent-to-treat basis survival of 41.4 months.[42] The present study demonstrated that the postoperative survival for all surgical cases was extending over 30 months.

This study reconfirmed that MCR is a reasonable goal for PM surgery. Since any type of curative-intent surgery for PM provides R1 resection, MCR has become a surgical goal.[48,49] However, some experts were critical of the reliability of MCR, which was subject to the surgeon's discretion.[50] This study revealed that the survival of the MCR group was significantly longer than those of the R2 resection and ET/PP groups. During the planning phase of this study, we hypothesized that a part of MCR surgery might be more radical than the rest. Thus, we divided MCR into two subcategories: R0-1 and

TABLE 9 Overall survival by clinical and pathological stages.

(A) Overall survival by clinical staging								
			1-yr survival, %	2-yr survival, %	3-yr survival, %	MST, mo	HR	*p*-value
	n	Event	(95% CI)	(95% CI)	(95% CI)	(95% CI)	(95% CI)	(95% CI)
T (version 7)								
T0 T1a T1b	119	73	0.771 (0.684, 0.837)	0.581 (0.487, 0.665)	0.334 (0.237, 0.433)	27.00 (21.83, 33.37)	Reference	<0.001 (trend)
T2	54	41	0.778 (0.642, 0.867)	0.407 (0.277, 0.534)	0.258 (0.141, 0.392)	21.03 (15.53, 28.23)	1.29 (0.88, 1.89)	0.196
T3	104	68	0.559 (0.458, 0.649)	0.402 (0.307, 0.496)	0.322 (0.228, 0.420)	18.13 (10.47, 24.03)	1.30 (0.93, 1.81)	0.122
T4	69	60	0.356 (0.244, 0.470)	0.186 (0.103, 0.288)	0.042 (0.005, 0.154)	8.00 (6.57, 11.93)	2.88 (2.03, 4.07)	<0.001
N (version 7)								
No	267	178	0.686 (0.626, 0.738)	0.476 (0.414, 0.534)	0.299 (0.238, 0.362)	21.83 (18.13, 26.23)	Reference	<0.001 (omnibus)
N1-3	79	64	0.427 (0.316, 0.534)	0.240 (0.151, 0.341)	0.147 (0.071, 0.248)	8.87 (6.73, 15.30)	1.83 (1.37, 2.44)	<0.001
M (ver.7)								
Mo	326	227	0.640 (0.585, 0.690)	0.435 (0.380, 0.489)	0.267 (0.214, 0.323)	19.63 (15.77, 22.80)	Reference	0.143 (omnibus)
M1	20	15	0.421 (0.204, 0.625)	0.211 (0.066, 0.410)	0.211 (0.066, 0.410)	11.57 (4.03, 23.93)	1.48 (0.88, 2.49)	0.143
Stage (ver.7)								
Stage I	118	73	0.769 (0.682, 0.835)	0.578 (0.482, 0.662)	0.331 (0.235, 0.430)	27.00 (21.83, 33.37)	Reference	<0.001 (trend)
Stage II	41	31	0.829 (0.675, 0.915)	0.439 (0.286, 0.582)	0.243 (0.114, 0.399)	21.60 (15.53, 32.23)	1.22 (0.80, 1.86)	0.351
Stage III	108	71	0.585 (0.486, 0.672)	0.406 (0.312, 0.497)	0.325 (0.230, 0.422)	18.53 (11.27, 24.03)	1.28 (0.92, 1.77)	0.144
Stage IV	79	67	0.362 (0.257, 0.469)	0.201 (0.120, 0.298)	0.097 (0.038, 0.188)	7.87 (6.60, 11.57)	2.59 (1.86, 3.62)	<0.001
T (ver.8)								
T0-1	148	94	0.782 (0.706, 0.841)	0.562 (0.477, 0.638)	0.319 (0.234, 0.406)	26.73 (21.77, 31.17)	Reference	<0.001 (trend)
T2	25	20	0.720 (0.501, 0.855)	0.320 (0.152, 0.502)	0.240 (0.082, 0.444)	18.43 (12.20, 35.00)	1.44 (0.89, 2.34)	0.137
T3	104	68	0.559 (0.458, 0.649)	0.402 (0.307, 0.496)	0.322 (0.228, 0.420)	18.13 (10.47, 24.03)	1.26 (0.92, 1.72)	0.145
T4	69	60	0.356 (0.244, 0.470)	0.186 (0.103, 0.288)	0.042 (0.005, 0.154)	8.00 (6.57, 11.93)	2.80 (2.01, 3.89)	<0.001
N (ver.8)								
N0	267	178	0.686 (0.626, 0.738)	0.476 (0.414, 0.534)	0.299 (0.238, 0.362)	21.83 (18.13, 26.23)	Reference	<0.001 (omnibus)
N1-3	79	64	0.427 (0.316, 0.534)	0.240 (0.151, 0.341)	0.147 (0.071, 0.248)	8.87 (6.73, 15.30)	1.83 (1.37, 2.44)	<0.001
M (ver.8)								
M0	326	227	0.640 (0.585, 0.690)	0.435 (0.380, 0.489)	0.267 (0.214, 0.323)	19.63 (15.77, 22.80)	Reference	0.143 (omnibus)
M1	20	15	0.421 (0.204, 0.625)	0.211 (0.066, 0.410)	0.211 (0.066, 0.410)	11.57 (4.03, 23.93)	1.48 (0.88, 2.49)	0.143
Stage (version 8)								
Stage IA	142	90	0.787 (0.710, 0.846)	0.571 (0.485, 0.649)	0.320 (0.233, 0.409)	27.00 (21.83, 31.80)	Reference	<0.001 (omnibus)
Stage IB, II	99	65	0.629 (0.525, 0.717)	0.402 (0.305, 0.498)	0.337 (0.238, 0.439)	18.13 (12.23, 22.50)	1.22 (0.88, 1.67)	0.23
Stage IIIA-IV	105	87	0.407 (0.312, 0.500)	0.238 (0.161, 0.324)	0.115 (0.055, 0.200)	8.87 (7.13, 11.97)	2.26 (1.68, 3.04)	<0.001

(Continues)

TABLE 9 (Continued)

(B) Overall survival by pathological stage								
	n	Event	1-year survival, % (95% CI)	2-year survival, % (95% CI)	3-year survival, % (95% CI)	MST, mo (95% CI)	HR (95% CI)	*p*-value
T (version 7)								
T0T1aT1b	26	9	0.921 (0.721, 0.980)	0.757 (0.537, 0.883)	0.580 (0.336, 0.762)	(26.30, NE)	Reference	0.013 (trend)
T2	30	15	0.867 (0.683, 0.948)	0.733 (0.537, 0.857)	0.442 (0.241, 0.626)	32.23 (27.50, NE)	1.39 (0.61, 3.19)	0.431
T3	61	38	0.820 (0.698, 0.896)	0.525 (0.393, 0.641)	0.349 (0.215, 0.487)	24.60 (20.97, 35.63)	2.04 (0.99, 4.22)	0.055
T4	21	15	0.619 (0.381, 0.788)	0.524 (0.297, 0.709)	0.393 (0.179, 0.602)	32.03 (10.47, 38.97)	2.45 (1.07, 5.60)	0.034
N (version 7)								
No	107	55	0.840 (0.756, 0.898)	0.631 (0.532, 0.715)	0.470 (0.360, 0.572)	35.57 (26.30, 39.50)	Reference	0.125 (omnibus)
N1-3	31	22	0.742 (0.550, 0.862)	0.548 (0.360, 0.703)	0.269 (0.118, 0.446)	25.60 (17.43, 34.60)	1.47 (0.90, 2.42)	0.125
M (ver.7)								
Mo	137	76	0.817 (0.741, 0.872)	0.617 (0.530, 0.693)	0.422 (0.327, 0.513)	32.23 (25.60, 37.47)	Reference	0.454 (omnibus)
M1	1	1		0.000 (0.000, 0.000)	0.000 (0.000, 0.000)	23.93 (NE, NE)	2.13 (0.29, 15.38)	0.454
Stage (ver.7)								
Stage I	26	9	0.921 (0.721, 0.980)	0.757 (0.537, 0.883)	0.580 (0.336, 0.762)	NE (26.30, NE)	Reference	0.080 (trend)
Stage II	25	11	0.880 (0.673, 0.960)	0.760 (0.542, 0.884)	0.539 (0.320, 0.715)	NE (27.50, NE)	1.22 (0.51, 2.95)	0.657
Stage III	64	40	0.828 (0.711, 0.901)	0.547 (0.418, 0.659)	0.340 (0.211, 0.474)	25.60 (20.97, 35.57)	2.00 (0.97, 4.12)	0.061
Stage IV	23	17	0.609 (0.383, 0.774)	0.478 (0.268, 0.661)	0.359 (0.163, 0.560)	23.93 (10.47, 38.97)	2.62 (1.17, 5.89)	0.02
T (ver.8)								
T0-1	35	12	0.942 (0.787, 0.985)	0.762 (0.580, 0.873)	0.597 (0.392, 0.752)	NE (30.80, NE)	Reference	0.007 (trend)
T2	21	12	0.810 (0.569, 0.924)	0.714 (0.472, 0.860)	0.337 (0.113, 0.580)	30.53 (21.83, NE)	2.02 (0.91, 4.51)	0.086
T3	61	38	0.820 (0.698, 0.896)	0.525 (0.393, 0.641)	0.349 (0.215, 0.487)	24.60 (20.97, 35.63)	2.24 (1.17, 4.30)	0.015
T4	21	15	0.619 (0.381, 0.788)	0.524 (0.297, 0.709)	0.393 (0.179, 0.602)	32.03 (10.47, 38.97)	2.69 (1.26, 5.75)	0.011
N (ver.8)								
N0	107	55	0.840 (0.756, 0.898)	0.631 (0.532, 0.715)	0.470 (0.360, 0.572)	35.57 (26.30, 39.50)	Reference	0.125 (omnibus)
N1-3	31	22	0.742 (0.550, 0.862)	0.548 (0.360, 0.703)	0.269 (0.118, 0.446)	25.60 (17.43, 34.60)	1.47 (0.90, 2.42)	0.125
M (ver.8)								
M0	137	76	0.817 (0.741, 0.872)	0.617 (0.530, 0.693)	0.422 (0.327, 0.513)	32.23 (25.60, 37.47)	Reference	0.454 (omnibus)
M1	1	1		0.000 (0.000, 0.000)	0.000 (0.000, 0.000)	23.93 (NA, NE)	2.13 (0.29, 15.38)	0.454
Stage (version 8)								
Stage IA	32	10	0.936 (0.769, 0.984)	0.772 (0.581, 0.885)	0.637 (0.422, 0.790)	NE (30.80, NE)	Reference	0.005 (trend)
Stage IB, II	64	37	0.828 (0.711, 0.901)	0.594 (0.463, 0.702)	0.363 (0.226, 0.501)	30.53 (20.97, 39.50)	2.22 (1.10, 4.46)	0.026
Stage IIIA-IV	42	30	0.714 (0.552, 0.826)	0.524 (0.364, 0.661)	0.343 (0.195, 0.496)	25.07 (18.53, 35.00)	2.82 (1.38, 5.77)	0.005

Abbreviations: HR, hazard ration; MST, median survival time; NE, not evaluable.

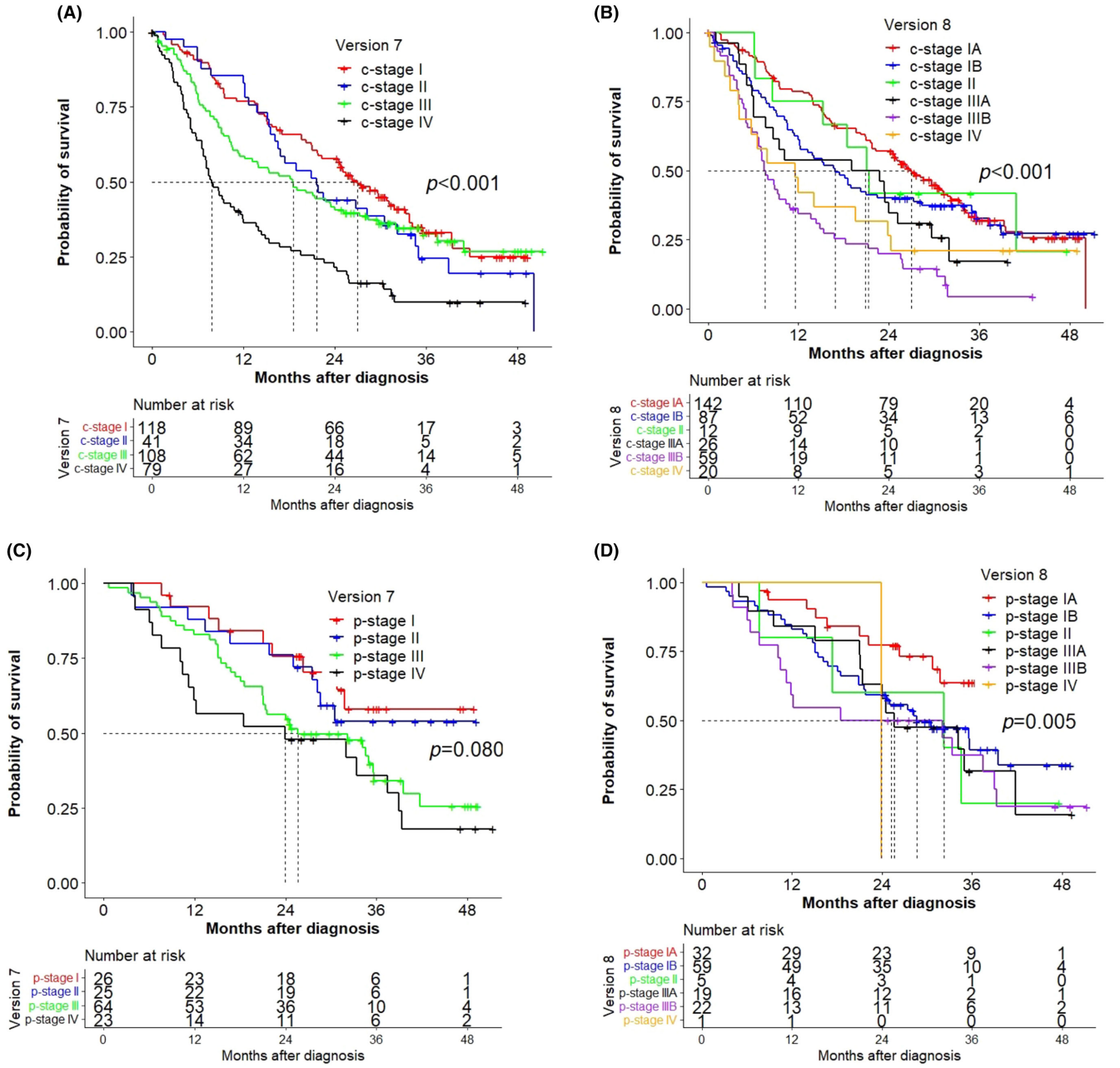

FIGURE 5 Overall survival by clinical and pathological stages. (A, B) A significant survival difference between clinical stage groups was observed in both seventh (A) and eighth (B) staging systems. (C) There was not a significant survival difference at the seventh version pathological stages. (D) A significant survival difference was observed at the eighth version pathological stages.

R1. However, R0-1 and R1 groups had similar survival rates. Thus, the results confirmed that MCR is a reliable and practical goal of PM surgery.

In the present study, P/D, not EPP, showed a significantly longer survival than PP/ET. Because this study may contain patient selection bias, including conversion from P/D to EPP,[40] it is not appropriate to draw any conclusion on the comparison of different surgical techniques. However, the results of this study might suggest that we should be cautious in indicating surgical intervention for EPP.

Our study confirmed the prognostic power of both tumor shape and tumor thickness that had been found in the previous IASLC registry.[8] The reliability of MTT and STLT was previously confirmed by single-center studies.[51,52] To the best of our knowledge, this study was the first to validate that tumor shape is a reliable prognostic variable. Since tumor shape and thickness are readily accessible to practicians, they are promising candidates for the next T descriptors.

We verified and compared the prognostic power using the seventh and eighth versions of the TNM staging system. Approximately two-thirds of patients were categorized as c- and p-stage I in the eighth TNM staging system. The results of the present study concur with previously reported data of a retrospective study that validated

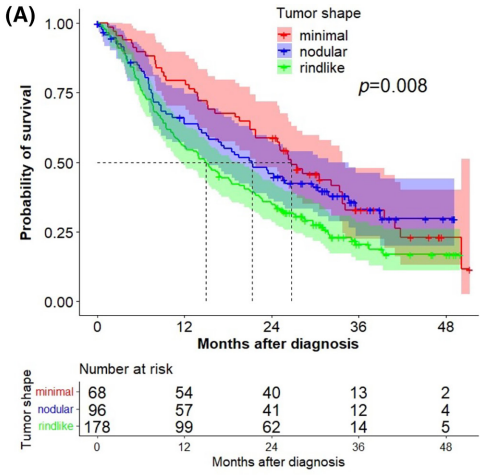

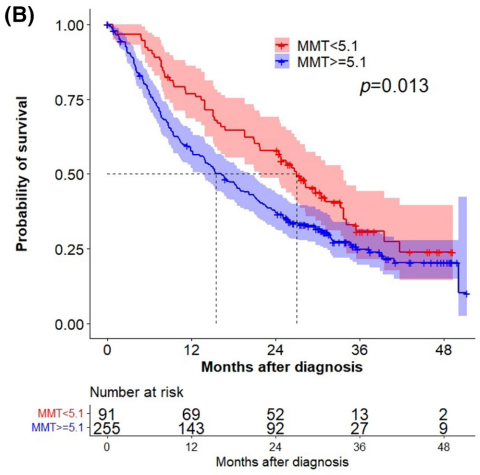

		Number	Survival Probability			MST	HR	
Tumor shape	n	of event	1 year	2 year	3 year	(95%CI)	(95%CI)	*p*-value
minimal	68	46	0.794 (0.677,0.873)	0.588 (0.462,0.694)	0.328 (0.209,0.451)	26.73 (21.03,33.77)	0.63 (0.45, 0.88)	0.007
nodular	96	58	0.639 (0.531,0.728)	0.448 (0.344,0.547)	0.329 (0.222,0.440)	21.33 (14.40,30.40)	0.71 (0.52, 0.97)	0.029
rindlike	178	136	0.556 (0.480,0.626)	0.347 (0.278,0.417)	0.204 (0.141,0.276)	14.97 (11.27,18.43)	reference	0.008 (omnibus)
data lacking	4	2	0.750 (0.128,0.961)	0.375 (0.011,0.808)	0.375 (0.011,0.808)	15.13 (0.80,..)	NE	

		Number	Survival Probability			MST	HR	
MTT	n	of event	1 year	2 year	3 year	(95%CI)	(95%CI)	*p*-value
< 5.1 mm	91	58	0.768 (0.667,0.842)	0.579 (0.471,0.673)	0.308 (0.202,0.420)	27.00 (21.03,33.37)	reference	0.013 (omnibus)
≥ 5.1 mm	255	184	0.577 (0.513,0.635)	0.366 (0.306,0.426)	0.249 (0.191,0.310)	15.53 (13.23,19.53)	1.46 (1.08, 1.96)	0.013

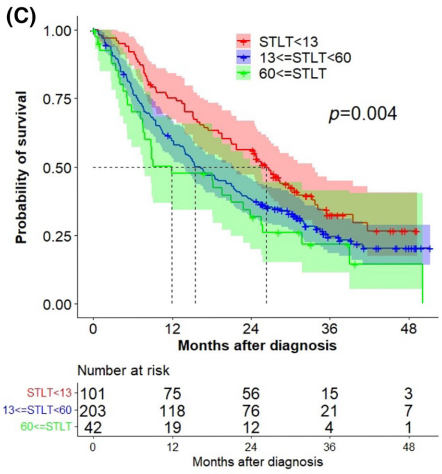

		Number	Survival Probability			MST	HR	
STLT	n	of event	1 year	2 year	3 year	(95%CI)	(95%CI)	*p*-value
< 13 mm	101	64	0.752 (0.655,0.825)	0.561 (0.459,0.652)	0.324 (0.224,0.429)	26.30 (19.63,31.17)	reference	0.004 (trend)
≥ 13, < 60 mm	203	146	0.596 (0.524,0.660)	0.373 (0.307,0.440)	0.244 (0.179,0.313)	15.53 (13.70,21.10)	1.41 (1.05, 1.89)	0.022
≥ 60 mm	42	32	0.476 (0.316,0.619)	0.317 (0.180,0.464)	0.216 (0.097,0.366)	11.97 (7.47,22.80)	1.77 (1.16, 2.72)	0.008

FIGURE 6 Overall survival (OS) by tumor shape and tumor thickness. (A) Median overall survival for minimal ($n = 68$), nodular ($n = 96$), and rind-like ($n = 178$) groups were 26.7, 21.3, and 15.0 months, respectively. Survivals for minimal and nodular groups were significantly longer than for the rind-like group. (B) Median OS was significantly longer in the MTT <5.1 mm group ($n = 91$) than that in the MTT ≥5.1 mm group ($n = 255$): 27.0 months vs. 15.5 months. (C) The median OS for the STLT <13 mm group ($n = 101$) was significantly longer than those for the 13 ≤ STLT <60 mm group ($n = 203$) and the STLT ≥60 mm group ($n = 42$): 26.3 months vs. 15.5 months and 12.0 months, respectively. MTT, maximum tumor thickness; OS, overall survival; STLT, sum of three-level thickness.

the sixth and eighth TNM staging system using the surveillance, epidemiology, and end results (SEER) database.[53] This study revealed the "bulky stage I" issue of the eighth version as a task for the ninth version of the TNM staging system.

This study has some limitations. First, there may be sampling bias because this study did not collect all the Japanese PM cases during the study period. This study might have not reflected the real-world situation in Japan because the majority of the participating institutions were academic centers or large hospitals. Second, the results of this study might not directly translate to other countries because of differences in racial composition, cultural habits, and medical systems.[54] Complimentary periodic medical checkups

TABLE 10 Relapse pattern and sites.

Relapse pattern	Relapse site (local)		Relapse site (distant)	
	Site	No (EPP/PD/Other)	Site	No (EPP/PD/Other)
Local only ($n=53$)	Total	53 (11/40/2)		
	Ipsilateral chest wall	45 (9/34/2)		
	Ipsilateral diaphragm	1 (1/0/0)		
	Ipsilateral mediastinal LN	11 (0/11/0)		
	Ipsilateral axillar/supraclavicular LN	2 (1/1/0)		
	Pericardium	4 (3/1/0)		
Distant only ($n=8$)			Total	8 (5/3/0)
			Contralateral chest wall	3 (2/1/0)
	Abdomen			2 (2/0/0)
	Contralateral LN			1 (1/0/0)
	Intrapulmonary			3 (1/2/0)
Local + distant ($n=10$)	Total	10 (2/8/0)		
	Ipsilateral chest wall	6 (2/4/0)	Contralateral chest wall	1 (0/1/0)
	Ipsilateral diaphragm	1 (0/1/0)	Abdomen	1 (0/1/0)
	Ipsilateral mediastinal LN	4 (0/4/0)	Contralateral LN	1 (1/0/0)
	Ipsilateral axillar/supraclavicular LN	1 (1/0/0)	Intrapulmonary	8 (2/6/0)
	Pericardium	1 (0/1/0)		

Abbreviation: EPP, extrapleural pneumonectomy; LN, lymph node; P/D, pleurectomy/decortication.

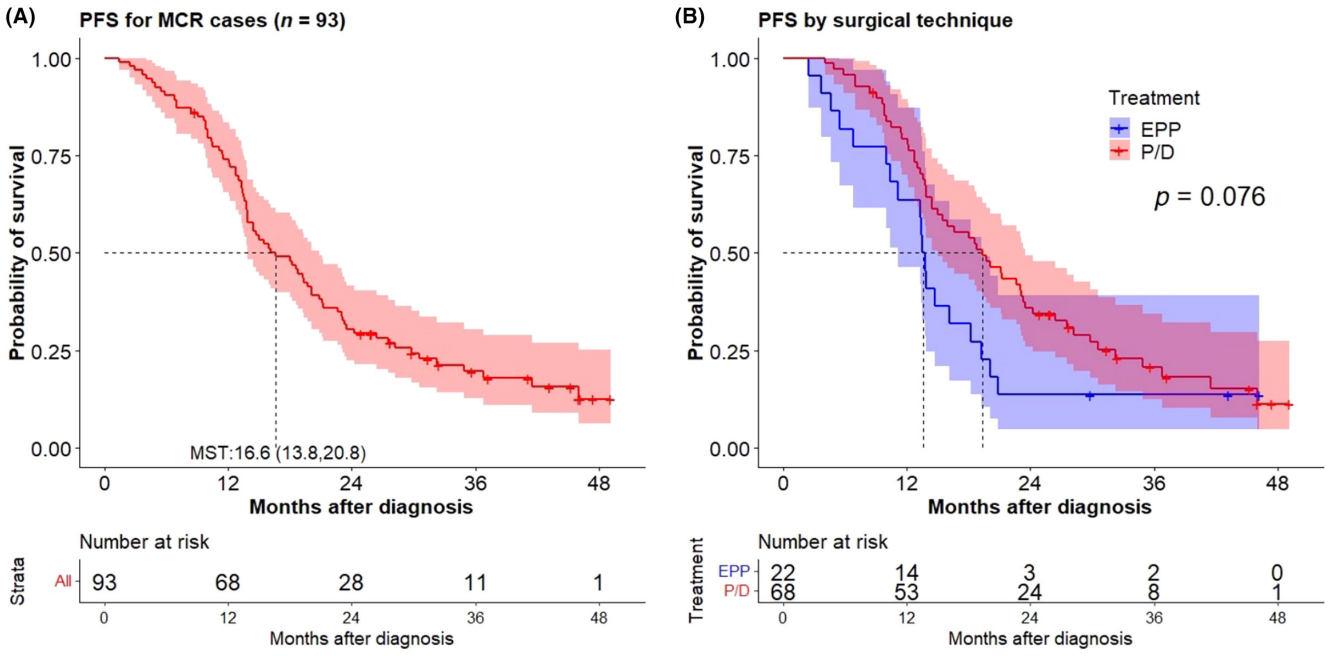

		Number	Progression-free Survival Probability			MST	HR	
	n	of event	1 year	2 year	3 year	(95%CI)	(95%CI)	p-value
Total	93	75	0.719 (0.615,0.799)	0.294 (0.205,0.389)	0.197 (0.119,0.289)	16.63 (13.83,20.10)		
EPP	22	19	0.636 (0.403,0.799)	0.136 (0.034,0.309)	0.136 (0.034,0.309)	13.62 (10.03,18.20)	1.61 (0.95, 2.73)	0.076
P/D	68	54	0.762 (0.642,0.847)	0.344 (0.233,0.457)	0.207 (0.114,0.320)	19.37 (14.47,23.33)	reference	0.076 (omnibus)
PP/ET	1	0				.(.,.)	NE	
Other surgery	2	2	0.000 (0.000,0.000)	0.000 (0.000,0.000)	0.000 (0.000,0.000)	2.15 (1.43,2.87)	NE	

FIGURE 7 (Legend on next page)

FIGURE 7 Progression-free survival. (A) Median PFS and survival rates at 1, 2, and 3 years for MCR patients ($n=93$) were 16.6 months and 73.1%, 29.3%, and 19.1%, respectively. (B) Median PFS and PFS rates at 1, 2, and 3 years were 13.6 months and 63.6%, 13.6%, and 13.6% for EPP patients ($n=22$), and 19.4 months and 76.2%, 34.4%, and 20.7% for P/D patients ($n=68$), respectively. EPP, extrapleural pneumonectomy; MCR, macroscopic complete resection; P/D: pleurectomy/decortication; PFS, progression-free survival.

for high-risk populations and complimentary medical interventions for patients with PM are available in Japan. Third, nivolumab treatment was not considered in the questionnaire of the case report form because registration of this study was started in April 2017, a year before the approval of nivolumab in Japan. Although most of the chemotherapeutic agents listed as "others" were presumed to be nivolumab, this cannot be verified. It is also presumed that nivolumab had an additional effect on the prognosis of both surgical and non-surgical cases.

AUTHOR CONTRIBUTIONS

Seiki Hasegawa: Conceptualization; investigation; methodology; project administration; validation; writing – original draft; writing – review and editing. **Yasushi Shintani:** Data curation; validation; writing – original draft; writing – review and editing. **Teruhisa Takuwa:** Investigation; writing – original draft. **Keisuke Aoe:** Investigation. **Katsuya Kato:** Investigation. **Nobukazu Fujimoto:** Investigation. **Yasuhiro Hida:** Investigation. **Masahiro Morise:** Investigation. **Yasumitsu Moriya:** Investigation. **Takao Morohoshi:** Investigation. **Hidemi Suzuki:** Investigation; project administration. **Masayuki Chida:** Investigation. **Shunsuke Endo:** Data curation. **Mitsutaka Kadokura:** Investigation. **Meinoshin Okumura:** Funding acquisition; supervision. **Satoshi Hattori:** Data curation; formal analysis; visualization; writing – original draft. **Hiroshi Date:** Funding acquisition; supervision. **Ichiro Yoshino:** Funding acquisition; supervision; writing – original draft; writing – review and editing.

ACKNOWLEDGMENTS

The authors thank all patients and investigators from participating institutions.

FUNDING INFORMATION

The Japanese Joint Committee for Lung Cancer Registry (JJCLCR) runs thanks to donations from participating medical associations, including the Japanese Respiratory Society, the Japanese Lung Cancer Society, the Japanese Association for Chest Surgery, the Japanese Association for Thoracic Surgery, the Japanese Society for Respiratory Endoscopy, the Japanese Association for Research on the Thymus, and the Japan Asbestos and Mesothelioma Interest Group.

CONFLICT OF INTEREST STATEMENT

Seiki Hasegawa received an endowed course from Kubota Corporation. Yasushi Shintani received grants from Immunomedicine, and Ishihara Sangyo Kaisya. Keisuke Aoe received grants from Astra Zeneka, Novartis, Phizer, Bristol-Meyer Squib, and MSD. Masahiro Morise received grants from Behringer Ingelheim and Eli Lilly. The other authors declare that they have no conflicts of interest.

ETHICS STATEMENT

This study was approved by the institutional review board of Osaka University Hospital, where the registry office is located, on October 11, 2016 (approval number 16038). The registry and the study using the registered data were approved by each institutional review board of all participating institutions.

Informed consent statement: This study complied with the Declaration of Helsinki. Written informed consent was obtained from all study participants.

This study adhered to the ethical guidelines for epidemiologic studies published jointly by the Japan Ministry of Science, Culture, and Education and the Japan Ministry of Health, Labor, and Welfare on June 17, 2002, and revised on February 28, 2017.

Clinical Trial Registration: UMIN 000024664.

Animal Studies: N/A.

DATA AVAILABILITY STATEMENT

Under Japan's Personal Information Protection Law (Amended version in 2022), it is obligatory to obtain re-consent from research participants when providing data to a third-party. Since it is impossible to obtain consent again from the research participants, we cannot provide the data.

DISCLAIMER

The findings and conclusions of this study are those of the authors and do not necessarily represent the views of the Japanese Joint Committee for Lung Cancer Registry or its participating medical associations.

ORCID

Seiki Hasegawa https://orcid.org/0000-0002-0386-1952
Yasushi Shintani https://orcid.org/0000-0002-2540-5288
Nobukazu Fujimoto https://orcid.org/0000-0002-4516-0433

REFERENCES

1. Brims F. Epidemiology and clinical aspects of malignant pleural mesothelioma. *Cancers (Basel)*. 2021;13:13. doi:10.3390/cancers13164194
2. Odgerel CO, Takahashi K, Sorahan T, et al. Estimation of the global burden of mesothelioma deaths from incomplete national mortality data. *Occup Environ Med*. 2017;74:851-858. doi:10.1136/oemed-2017-104298
3. Pass H, Giroux D, Kennedy C, et al. The IASLC mesothelioma staging project: improving staging of a rare disease through international participation. *J Thorac Oncol*. 2016;11:2082-2088. doi:10.1016/j.jtho.2016.09.123
4. Rusch VW, Giroux D. Do we need a revised staging system for malignant pleural mesothelioma? Analysis of the IASLC database. *Ann Cardiothorac Surg*. 2012;1:438-448. doi:10.3978/j.issn.2225-319X.2012.11.10

5. Rusch VW. A proposed new international TNM staging system for malignant pleural mesothelioma. From the international mesothelioma interest group. *Chest*. 1995;108:1122-1128. doi:10.1378/chest.108.4.1122
6. Rusch VW, Giroux D, Kennedy C, et al. Initial analysis of the international association for the study of lung cancer mesothelioma database. *J Thorac Oncol*. 2012;7:1631-1639. doi:10.1097/JTO.0b013e31826915f1
7. Rusch VW, Chansky K, Kindler HL, et al. The IASLC mesothelioma staging project: proposals for the M descriptors and for revision of the TNM stage groupings in the forthcoming (eighth) edition of the TNM classification for mesothelioma. *J Thorac Oncol*. 2016;11:2112-2119. doi:10.1016/j.jtho.2016.09.124
8. Nowak AK, Chansky K, Rice DC, et al. The IASLC mesothelioma staging project: proposals for revisions of the T descriptors in the forthcoming eighth edition of the TNM classification for pleural mesothelioma. *J Thorac Oncol*. 2016;11:2089-2099. doi:10.1016/j.jtho.2016.08.147
9. Baas P, Daumont MJ, Lacoin L, et al. Treatment patterns and outcomes for patients with malignant pleural mesothelioma in England in 2013-2017: a nationwide CAS registry analysis from the I-O optimise initiative. *Lung Cancer*. 2021;162:185-193. doi:10.1016/j.lungcan.2021.11.001
10. Beckett P, Edwards J, Fennell D, Hubbard R, Woolhouse I, Peake MD. Demographics, management and survival of patients with malignant pleural mesothelioma in the National Lung Cancer Audit in England and Wales. *Lung Cancer*. 2015;88:344-348. doi:10.1016/j.lungcan.2015.03.005
11. Beebe-Dimmer JL, Fryzek JP, Yee CL, et al. Mesothelioma in the United States: a surveillance, epidemiology, and end results (SEER)-Medicare investigation of treatment patterns and overall survival. *Clin Epidemiol*. 2016;8:743-750. doi:10.2147/CLEP.S105396
12. Gemba K, Fujimoto N, Aoe K, et al. Treatment and survival analyses of malignant mesothelioma in Japan. *Acta Oncol*. 2013;52:803-808. doi:10.3109/0284186X.2012.709948
13. Neumann V, Günthe S, Mülle KM, et al. Malignant mesothelioma—German mesothelioma register 1987–1999. *Int Arch Occup Environ Health*. 2001;74:383-395. doi:10.1007/s004200100240
14. Tomasson K, Gudmundsson G, Briem H, Rafnsson V. Malignant mesothelioma incidence by nation-wide cancer registry: a population-based study. *J Occup Med Toxicol*. 2016;11:37. doi:10.1186/s12995-016-0127-4
15. van Kooten JP, Belderbos RA, von der Thusen JH, et al. Incidence, treatment and survival of malignant pleural and peritoneal mesothelioma: a population-based study. *Thorax*. 2022;77:1260-1267. doi:10.1136/thoraxjnl-2021-217709
16. Brims FJ, Meniawy TM, Duffus I, et al. A novel clinical prediction model for prognosis in malignant pleural mesothelioma using decision tree analysis. *J Thorac Oncol*. 2016;11:573-582. doi:10.1016/j.jtho.2015.12.108
17. Curran D, Sahmoud T, Therasse P, van Meerbeeck J, Postmus PE, Giaccone G. Prognostic factors in patients with pleural mesothelioma: the European Organization for Research and Treatment of cancer experience. *J Clin Oncol*. 1998;16:145-152. doi:10.1200/JCO.1998.16.1.145
18. Edwards JG, Abrams KR, Leverment JN, Spyt TJ, Waller DA, O'Byrne KJ. Prognostic factors for malignant mesothelioma in 142 patients: validation of CALGB and EORTC prognostic scoring systems. *Thorax*. 2000;55:731-735. doi:10.1136/thorax.55.9.731
19. Linton A, Pavlakis N, O'Connell R, et al. Factors associated with survival in a large series of patients with malignant pleural mesothelioma in New South Wales. *Br J Cancer*. 2014;111:1860-1869. doi:10.1038/bjc.2014.478
20. Yeap BY, De Rienzo A, Gill RR, et al. Mesothelioma risk score: a new prognostic pretreatment, clinical-molecular algorithm for malignant pleural mesothelioma. *J Thorac Oncol*. 2021;16:1925-1935. doi:10.1016/j.jtho.2021.06.014
21. Opitz I, Friess M, Kestenholz P, et al. A new prognostic score supporting treatment allocation for multimodality therapy for malignant pleural mesothelioma: a review of 12 Years' experience. *J Thorac Oncol*. 2015;10:1634-1641. doi:10.1097/JTO.0000000000000661
22. Fournel L, Charrier T, Huriet M, et al. Prognostic impact of inflammation in malignant pleural mesothelioma: a large-scale analysis of consecutive patients. *Lung Cancer*. 2022;166:221-227. doi:10.1016/j.lungcan.2022.03.014
23. Hooper CE, Lyburn ID, Searle J, et al. The south west area mesothelioma and pemetrexed trial: a multicentre prospective observational study evaluating novel markers of chemotherapy response and prognostication. *Br J Cancer*. 2015;112:1175-1182. doi:10.1038/bjc.2015.62
24. Rusch VW, Venkatraman E. The importance of surgical staging in the treatment of malignant pleural mesothelioma. *J Thorac Cardiovasc Surg*. 1996;111:815–825; discussion 825-816.-826. doi:10.1016/s0022-5223(96)70342-2
25. Shintani Y, Hasegawa S, Takuwa T, et al. Prospective registry database of patients with malignant mesothelioma: directions for a future Japanese registry-based lung cancer study. *J Thorac Dis*. 2018;10:1968-1971. doi:10.21037/jtd.2018.03.53
26. Asamura H, Goya T, Koshiishi Y, et al. A Japanese lung cancer registry study: prognosis of 13,010 resected lung cancers. *J Thorac Oncol*. 2008;3:46-52. doi:10.1097/JTO.0b013e31815e8577
27. Nagai K, Sohara Y, Tsuchiya R, Goya T, Miyaoka E. Prognosis of resected non-small cell lung cancer patients with intrapulmonary metastases. *J Thorac Oncol*. 2007;2:282-286. doi:10.1097/01.JTO.0000263709.15955.8a
28. Sakurai H, Asamura H, Goya T, et al. Survival differences by gender for resected non-small cell lung cancer: a retrospective analysis of 12,509 cases in a Japanese lung cancer registry study. *J Thorac Oncol*. 2010;5:1594-1601. doi:10.1097/JTO.0b013e3181f1923b
29. Sawabata N, Asamura H, Goya T, et al. Japanese lung cancer registry study: first prospective enrollment of a large number of surgical and nonsurgical cases in 2002. *J Thorac Oncol*. 2010;5:1369-1375. doi:10.1097/JTO.0b013e3181e452b9
30. Sawabata N, Miyaoka E, Asamura H, et al. Japanese lung cancer registry study of 11,663 surgical cases in 2004: demographic and prognosis changes over decade. *J Thorac Oncol*. 2011;6:1229-1235. doi:10.1097/JTO.0b013e318219aae2
31. Allen TC, Cagle PT, Churg AM, et al. Localized malignant mesothelioma. *Am J Surg Pathol*. 2005;29:866-873. doi:10.1097/01.pas.0000165529.78945.dc
32. Rice D, Rusch V, Pass H, et al. Recommendations for uniform definitions of surgical techniques for malignant pleural mesothelioma: a consensus report of the international association for the study of lung cancer international staging committee and the international mesothelioma interest group. *J Thorac Oncol*. 2011;6:1304-1312. doi:10.1097/JTO.0b013e3182208e3f
33. Kostron A, Friess M, Crameri O, et al. Relapse pattern and second-line treatment following multimodality treatment for malignant pleural mesothelioma. *Eur J Cardiothorac Surg*. 2016;49:1516-1523. doi:10.1093/ejcts/ezv398
34. https://www.mhlw.go.jp/toukei/saikin/hw/jinkou/tokusyu/chuuhisyu20/dl/chuuhisyu.pdf (last access 7 April 2023)
35. Hashimoto M, Yamamoto H, Endo S, et al. Japanese current status of curative-intent surgery for malignant pleural mesothelioma. *Ann Thorac Surg*. 2022;113:1348-1353. doi:10.1016/j.athoracsur.2021.04.042
36. Verma V, Ahern CA, Berlind CG, et al. Facility volume and postoperative outcomes for malignant pleural mesothelioma: a National Cancer Data Base analysis. *Lung Cancer*. 2018;120:7-13. doi:10.1016/j.lungcan.2018.03.019

37. Burt BM, Lee HS, Raghuram AC, et al. Preoperative prediction of unresectability in malignant pleural mesothelioma. *J Thorac Cardiovasc Surg*. 2020;159:2512-2520.e2511. doi:10.1016/j.jtcvs.2019.11.035
38. Van Schil PE, Baas P, Gaafar R, et al. Trimodality therapy for malignant pleural mesothelioma: results from an EORTC phase II multicentre trial. *Eur Respir J*. 2010;36:1362-1369. doi:10.1183/09031936.00039510
39. Krug LM, Pass HI, Rusch VW, et al. Multicenter phase II trial of neoadjuvant pemetrexed plus cisplatin followed by extrapleural pneumonectomy and radiation for malignant pleural mesothelioma. *J Clin Oncol*. 2009;27:3007-3013. doi:10.1200/JCO.2008.20.3943
40. Nakamura A, Hashimoto M, Matsumoto S, Kondo N, Kijima T, Hasegawa S. Outcomes of conversion to Extrapleural pneumonectomy from pleurectomy/decortication for malignant pleural mesothelioma. *Semin Thorac Cardiovasc Surg*. 2021;33:873-881. doi:10.1053/j.semtcvs.2021.02.003
41. Cho BCJ, Donahoe L, Bradbury PA, et al. Surgery for malignant pleural mesothelioma after radiotherapy (SMART): final results from a single-Centre, phase 2 trial. *Lancet Oncol*. 2021;22:190-197. doi:10.1016/S1470-2045(20)30606-9
42. Hasegawa S, Yokoi K, Okada M, et al. Neoadjuvant pemetrexed plus cisplatin followed by pleurectomy for malignant pleural mesothelioma. *J Thorac Cardiovasc Surg*. 2022;163:1940-1947. doi:10.1016/j.jtcvs.2021.07.017
43. Weder W, Stahel RA, Bernhard J, et al. Multicenter trial of neo-adjuvant chemotherapy followed by extrapleural pneumonectomy in malignant pleural mesothelioma. *Ann Oncol*. 2007;18:1196-1202. doi:10.1093/annonc/mdm093
44. Treasure T, Lang-Lazdunski L, Waller D, et al. Extra-pleural pneumonectomy versus no extra-pleural pneumonectomy for patients with malignant pleural mesothelioma: clinical outcomes of the mesothelioma and radical surgery (MARS) randomised feasibility study. *Lancet Oncol*. 2011;12:763-772. doi:10.1016/S1470-2045(11)70149-8
45. Stahel RA, Riesterer O, Xyrafas A, et al. Neoadjuvant chemotherapy and extrapleural pneumonectomy of malignant pleural mesothelioma with or without hemithoracic radiotherapy (SAKK 17/04): a randomised, international, multicentre phase 2 trial. *Lancet Oncol*. 2015;16:1651-1658. doi:10.1016/S1470-2045(15)00208-9
46. Hasegawa S, Okada M, Tanaka F, et al. Trimodality strategy for treating malignant pleural mesothelioma: results of a feasibility study of induction pemetrexed plus cisplatin followed by extrapleural pneumonectomy and postoperative hemithoracic radiation (Japan mesothelioma interest group 0601 trial). *Int J Clin Oncol*. 2016;21:523-530. doi:10.1007/s10147-015-0925-1
47. Rimner A, Zauderer MG, Gomez DR, et al. Phase II study of Hemithoracic intensity-modulated pleural radiation therapy (IMPRINT) As part of lung-sparing multimodality therapy in patients with malignant pleural mesothelioma. *J Clin Oncol*. 2016;34:2761-2768. doi:10.1200/JCO.2016.67.2675
48. Friedberg JS, Culligan MJ, Tsao AS, et al. A proposed system toward standardizing surgical-based treatments for malignant pleural mesothelioma, from the joint National Cancer Institute-International Association for the Study of Lung Cancer-Mesothelioma Applied Research Foundation taskforce. *J Thorac Oncol*. 2019;14:1343-1353. doi:10.1016/j.jtho.2019.04.029
49. Sugarbaker DJ. Macroscopic complete resection: the goal of primary surgery in multimodality therapy for pleural mesothelioma. *J Thorac Oncol*. 2006;1:175-176.
50. Batirel HF, Metintas M, Caglar HB, et al. Macroscopic complete resection is not associated with improved survival in patients with malignant pleural mesothelioma. *J Thorac Cardiovasc Surg*. 2018;155:2724-2733. doi:10.1016/j.jtcvs.2017.12.131
51. Hashimoto M, Takeuchi J, Takuwa T, et al. Pleural thickness after neoadjuvant chemotherapy is a prognostic factor in malignant pleural mesothelioma. *J Thorac Cardiovasc Surg*. 2019;157:404-413. doi:10.1016/j.jtcvs.2018.09.106
52. Ito T, Nakamura S, Kadomatsu Y, et al. Impact of pleural thickness on occurrence of postoperative complications in patients with malignant pleural mesothelioma. *Ann Surg Oncol*. 2023;30:1574-1583. doi:10.1245/s10434-022-12790-9
53. Abdel-Rahman O. Challenging a dogma; AJCC 8th staging system is not sufficient to predict outcomes of patients with malignant pleural mesothelioma. *Lung Cancer*. 2017;113:128-133. doi:10.1016/j.lungcan.2017.09.015
54. Ikeda N, Saito E, Kondo N, et al. What has made the population of Japan healthy? *Lancet*. 2011;378:1094-1105. doi:10.1016/S0140-6736(11)61055-6

SUPPORTING INFORMATION

Additional supporting information can be found online in the Supporting Information section at the end of this article.

How to cite this article: Hasegawa S, Shintani Y, Takuwa T, et al. Nationwide prospective registry database of patients with newly diagnosed untreated pleural mesothelioma in Japan. *Cancer Sci*. 2024;115:507-528. doi:10.1111/cas.16021

International Journal of
Molecular Sciences

MDPI

Article

Functional Roles of CD26/DPP4 in Bleomycin-Induced Pulmonary Hypertension Associated with Interstitial Lung Disease

Tadasu Okaya [1], Takeshi Kawasaki [1,*], Shun Sato [1,2], Yu Koyanagi [1], Koichiro Tatsumi [1], Ryo Hatano [3], Kei Ohnuma [3], Chikao Morimoto [3], Yoshitoshi Kasuya [4], Yoshinori Hasegawa [5], Osamu Ohara [5] and Takuji Suzuki [1,2]

[1] Department of Respirology, Graduate School of Medicine, Chiba University, Chiba 260-8670, Japan
[2] Synergy Institute for Futuristic Mucosal Vaccine Research and Development, Chiba University, Chiba 260-8670, Japan
[3] Department of Therapy Development and Innovation for Immune Disorders and Cancers, Graduate School of Medicine, Juntendo University, Tokyo 113-8421, Japan
[4] Department of Biomedical Science, Graduate School of Medicine, Chiba University, Chiba 260-8670, Japan
[5] Department of Applied Genomics, Kazusa DNA Research Institute, Chiba 292-0818, Japan
* Correspondence: kawatake@chiba-u.jp

Abstract: Pulmonary hypertension (PH) with interstitial lung diseases (ILDs) often causes intractable conditions. CD26/Dipeptidyl peptidase-4 (DPP4) is expressed in lung constituent cells and may be related to the pathogenesis of various respiratory diseases. We aimed to clarify the functional roles of CD26/DPP4 in PH-ILD, paying particular attention to vascular smooth muscle cells (SMCs). *Dpp4* knockout (*Dpp4*KO) and wild type (WT) mice were administered bleomycin (BLM) intraperitoneally to establish a PH-ILD model. The BLM-induced increase in the right ventricular systolic pressure and the right ventricular hypertrophy observed in WT mice were attenuated in *Dpp4*KO mice. The BLM-induced vascular muscularization in small pulmonary vessels in *Dpp4*KO mice was milder than that in WT mice. The viability of TGFβ-stimulated human pulmonary artery SMCs (hPASMCs) was lowered due to the *DPP4* knockdown with small interfering RNA. According to the results of the transcriptome analysis, upregulated genes in hPASMCs with TGFβ treatment were related to pulmonary vascular SMC proliferation via the Notch, PI3K-Akt, and NFκB signaling pathways. Additionally, *DPP4* knockdown in hPASMCs inhibited the pathways upregulated by TGFβ treatment. These results suggest that genetic deficiency of *Dpp4* protects against BLM-induced PH-ILD by alleviating vascular remodeling, potentially through the exertion of an antiproliferative effect via inhibition of the TGFβ-related pathways in PASMCs.

Keywords: CD26; dipeptidyl peptidase-4; pulmonary hypertension; interstitial lung disease

Citation: Okaya, T.; Kawasaki, T.; Sato, S.; Koyanagi, Y.; Tatsumi, K.; Hatano, R.; Ohnuma, K.; Morimoto, C.; Kasuya, Y.; Hasegawa, Y.; et al. Functional Roles of CD26/DPP4 in Bleomycin-Induced Pulmonary Hypertension Associated with Interstitial Lung Disease. *Int. J. Mol. Sci.* **2024**, *25*, 748. https://doi.org/10.3390/ijms25020748

Academic Editor: Longshuang Huang

Received: 24 November 2023
Revised: 30 December 2023
Accepted: 4 January 2024
Published: 6 January 2024

1. Introduction

Pulmonary hypertension (PH) is defined by elevated mean pulmonary arterial pressure (>20 mmHg [1]). Patients with PH often develop right heart failure if no appropriate treatment is administered. PH is classified into five clinical phenotypes according to its pathophysiology. Each phenotypic group requires a different treatment strategy and shows a different prognosis [2]. Among the five phenotypes, the prognosis of patients with pulmonary arterial hypertension (PAH) has remarkably improved in recent years with continuous intravenous prostaglandin I_2 therapy [3] and upfront combination therapy with pulmonary vasodilators [4].

Group III PH develops secondary to chronic lung diseases such as interstitial lung diseases (ILDs) and chronic obstructive pulmonary disease. A proportion of patients with ILDs comprises those with chronic progressive lung diseases characterized by varying

degrees of inflammation and fibrosis in the lung interstitium. Idiopathic pulmonary fibrosis (IPF) is a clinical phenotype of ILDs that often develops into an intractable condition, and approximately 8–15% of IPF cases are associated with PH [5]. In general, the effects of pulmonary vasodilators are limited in PH with ILD (PH-ILD), and patients with PH-ILD often exhibit clinical worsening with pulmonary vasodilators [6–8], although inhaled prostaglandin I_2 therapy does improve exercise tolerance [9]. Therefore, the prognosis of patients with PH-ILDs has remained worse than that of patients with PAH [10], and a better understanding of PH-ILD pathogenesis is necessary to develop new treatment strategies other than using pulmonary vasodilators.

In patients with PH, the main pathological findings include vascular remodeling of the small pulmonary arteries [11], partly due to the persistent pressure overload of the pulmonary circulatory system. They are characterized by thickening of the tunica media accompanied by an increase in pulmonary artery smooth muscle cells (PASMCs) and luminal narrowing with cell proliferation of the intima and fibrosis. Plexiform lesions are sometimes observed as the disease progresses in the final stage of pulmonary circulatory failure. In Group III PH, which encompasses both pulmonary vascular and parenchymal lung lesions, the pathology of pulmonary vascular remodeling differs from that of PAH, and thickening of the tunica media is the primary pathological feature [12].

Bleomycin (BLM) is an anticancer drug used against malignant lymphoma and testicular cancer, which inhibits DNA synthesis and introduces single or double-strand scissions in DNA. However, BLM is known to cause lung fibrosis as a severe adverse effect [13]. Therefore, it is used to establish not only ILD models in mice and rats [14] but also PH-ILD models in mice [15]. Intratracheal administration is common for BLM exposure; however, intravenous, intraperitoneal, and intranasal administration have also been used [14]. Intraperitoneal BLM administration is especially used in establishing a PH-ILD model, assuming uniform vascular remodeling in the lungs of mice.

CD26/Dipeptidyl peptidase-4 (DPP4) is a protein with a molecular weight of 110 kDa. It is expressed as a type II membrane-bound protein on the surface of multiple types of human and rodent cells [16]. The soluble form of DPP4 enters blood circulation after shedding from the cell surface. The enzymatic activity of CD26/DPP4, such as degradation and inactivation of incretins, has been the focus of many studies, and DPP4 inhibitors have been used clinically for the treatment of diabetes mellitus [17]. CD26/DPP4 was originally established as a T-cell activation antigen that participates in immune stimulation [18]. It plays multiple roles, including those in the progression of inflammation and fibrosis in various diseases [19]. DPP4 inhibitors can not only improve respiratory diseases [20], such as acute respiratory distress syndrome [21] and ILDs [22], but also cardiovascular diseases [23], such as left heart dysfunction [24] and atherosclerosis [25].

DPP4 inhibitors could be a new treatment option for patients with PH [26]. These inhibitors may prevent the pathological progression of PH by influencing pulmonary vascular cells and lung fibroblasts. In vivo, sitagliptin, a DPP4 inhibitor, mitigated the elevation of right ventricular systolic pressure (RVSP) in a hypoxia-induced PH rat model and attenuated pulmonary artery remodeling by decreasing the number of PASMCs in the media [27]. Moreover, sitagliptin treatment suppressed PDGF-BB-induced migration of cultured human PASMCs in vitro [28]. Based on the above-mentioned observations, we speculated that CD26/DPP4 plays mechanistic roles in the pathogenesis of PH-ILD. Through this study, we aimed to clarify the functional roles of CD26/DPP4 in PH-ILD using *Dpp4*-deficient mice in a BLM administration model and using DPP4-siRNA in cultured human PASMCs.

2. Results

2.1. BLM-Induced Pulmonary Hypertension Was Attenuated in Dpp4KO Mice

First, we evaluated the expression levels of CD26/DPP4 in the cellular components of the lungs of wild-type (WT) and *Dpp4* knockout (*Dpp4*KO) mice. Real-time quantitative PCR analysis showed that *Dpp4* expression was significantly lower in *Dpp4*KO mice than

that in WT mice (Figure 1a). Flow cytometric analysis also showed that CD26/DPP4 expression was substantially low or nearly absent in *Dpp4*KO mice (Figure 1b,c).

In BLM-administered WT mice, RVSP, cardiac output (CO), and the maximum rate of pressure rise (Max dP/dt) were higher compared with those in PBS-administered WT mice (Figure 1d,f,g), although the difference in heart rate (HR) (Figure 1e) was minor. These hemodynamic changes after the BLM challenge were attenuated in *Dpp4*KO mice (WT/BLM versus *Dpp4*KO/BLM, RVSP: 33.0 versus 26.6 mmHg [$p < 0.01$], CO: 0.98 versus 0.79 [$p = 0.068$], and Max dP/dt: 2.55 versus 1.49 [$p < 0.05$]) (Figure 1d,f,g). Regarding right ventricular hypertrophy, the weight ratio of the right ventricle to the left ventricle plus the ventricular septum (RV/LV + S) and RV/body were greater in WT mice after the BLM challenge. The increase in RV/LV + S was significantly alleviated in *Dpp4*KO mice (WT/BLM versus *Dpp4*KO, 0.39 versus 0.30 [$p < 0.05$]) (Figure 1h,i). No apparent difference in mortality was observed either for WT/PBS and *DPP4*KO/PBS mice or for WT/BLM and *DPP4*KO/BLM mice (Supplemental Figure S1a,b).

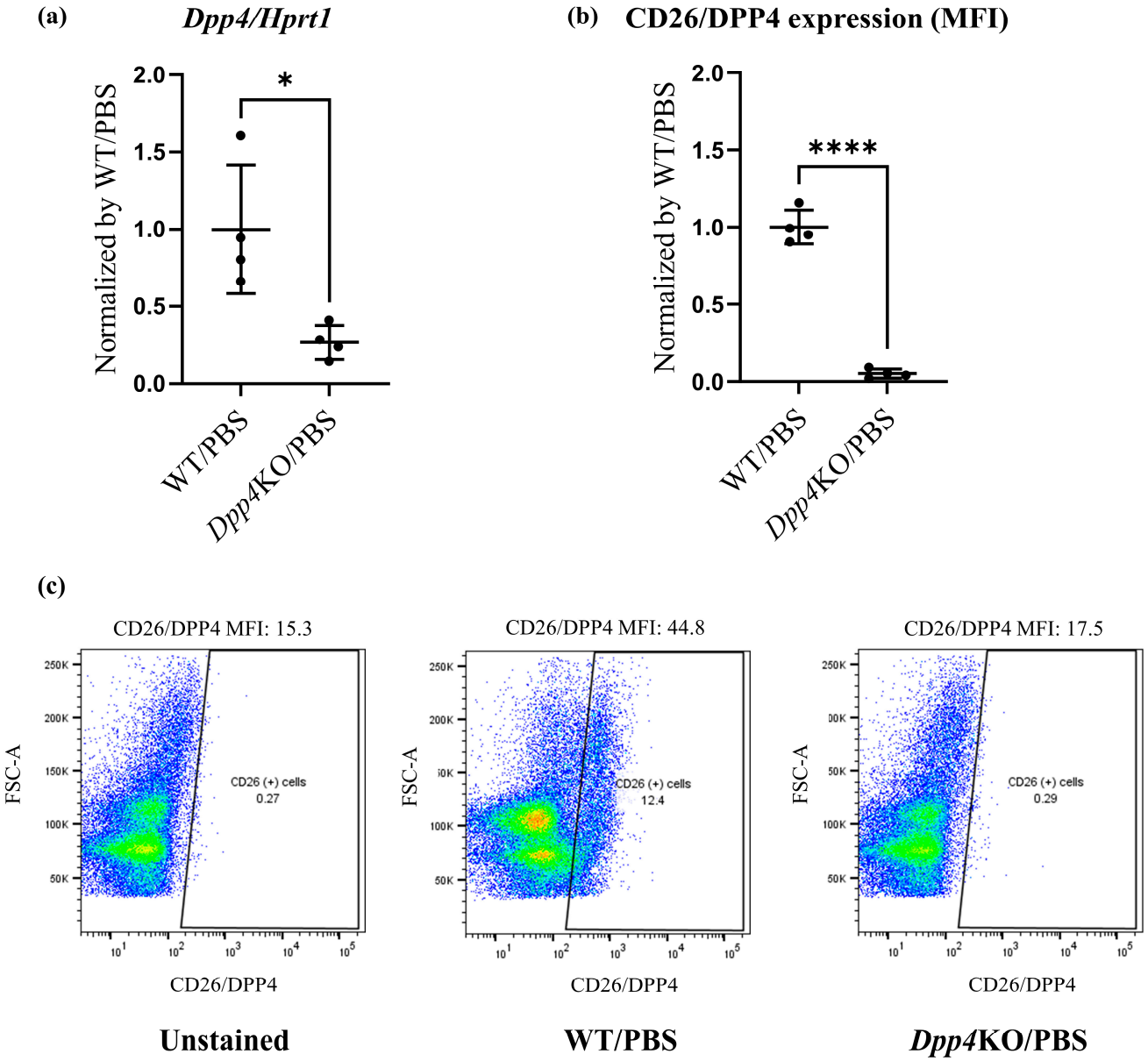

Figure 1. *Cont.*

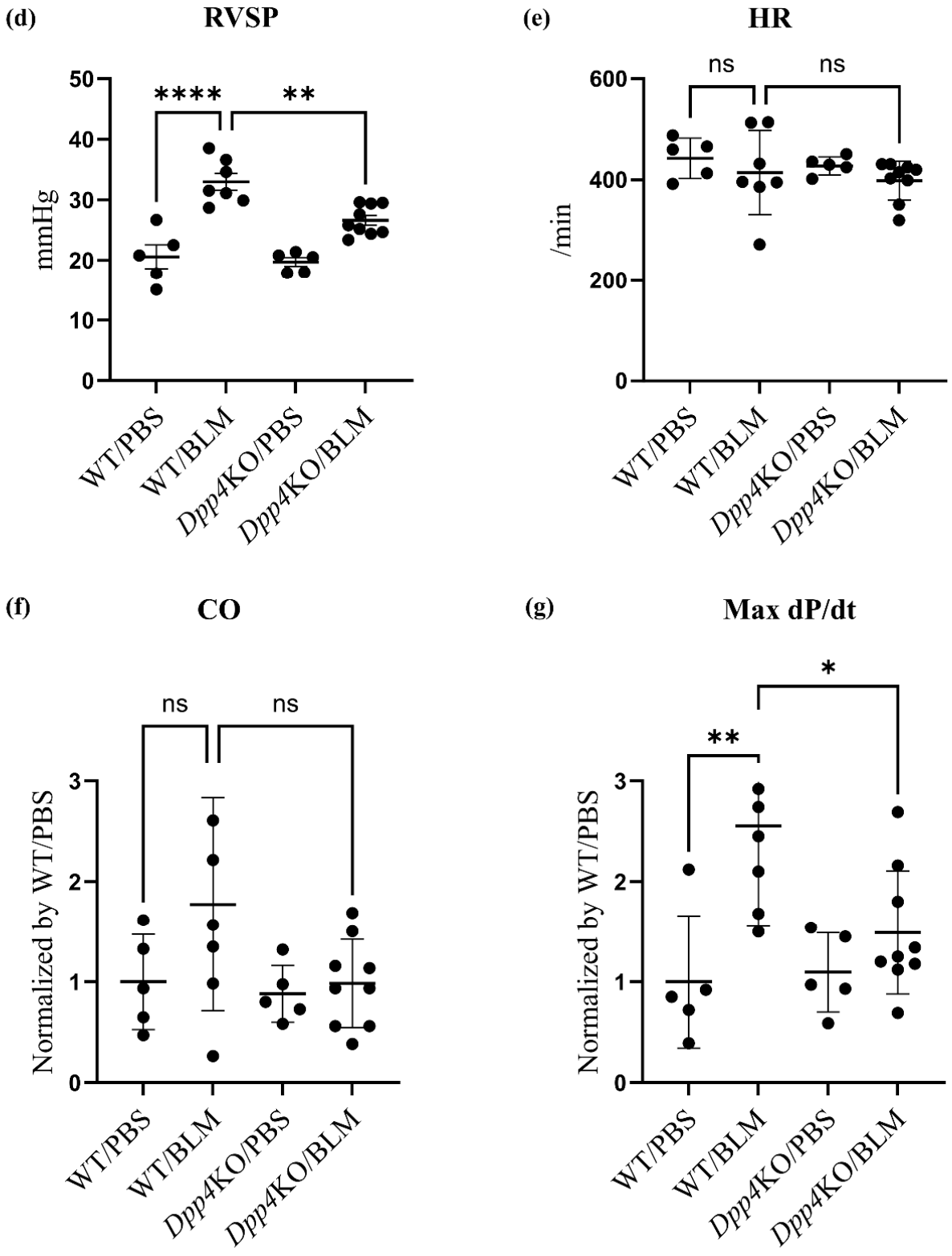

Figure 1. *Cont.*

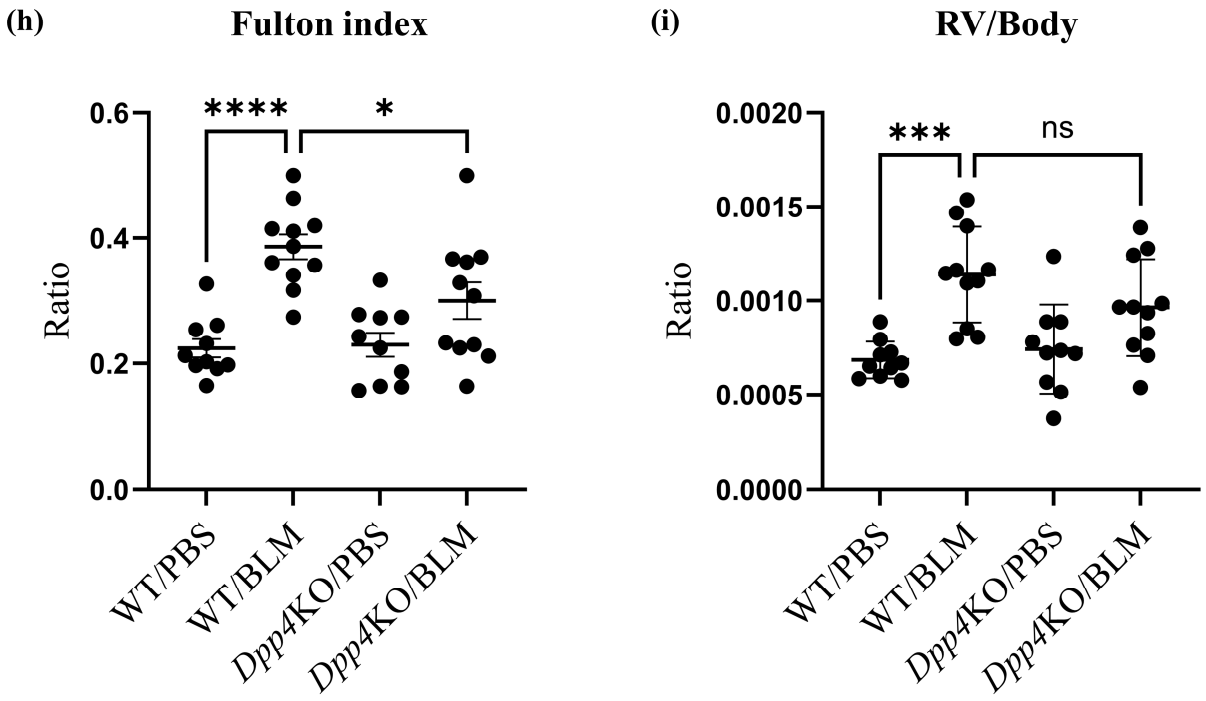

Figure 1. Pulmonary hemodynamic evaluation of bleomycin (BLM)-induced pulmonary hypertension (PH) in wild type (WT) and *Dpp4*KO mice. CD26/DPP4 expression in whole lung cells of WT and *Dpp4*KO mice was measured using (**a**) real-time quantitative PCR and (**b**) flow cytometry. Panel (**c**) shows representative images of dotted plots. The pulmonary hemodynamic parameters evaluated by right heart catheterization were as follows: (**d**) right ventricular (RV) systolic pressure (RVSP), (**e**) heart rate (HR), (**f**) cardiac output (CO), and (**g**) maximal rate of pressure rise (max dP/dt) in RV. RV hypertrophy was evaluated by calculating (**h**) the Fulton index (weight ratio of the right ventricle to the left ventricle plus the ventricular septum) or (**i**) RV/body. ns, not significant; * $p < 0.05$, ** $p < 0.01$, *** $p < 0.001$, **** $p < 0.0001$.

2.2. Media Thickening in Small Pulmonary Vessels Was Attenuated in Dpp4KO Mice

The BLM challenge thickened the media of the small pulmonary vessels in WT mice (WT/BLM) compared with that in PBS-treated mice (WT/PBS); however, the media thickness was attenuated in BLM-treated *Dpp4*KO mice (*Dpp4*KO/BLM) (Figure 2a). As evident from the quantitative evaluation of vascular muscularization in small pulmonary arteries, the number of partially or fully muscularized vessels was significantly greater in WT/BLM mice than that in WT/PBS mice (partially muscularized: $p < 0.001$ and fully muscularized: $p < 0.05$). The total number of muscularized vessels (partially and fully) in *Dpp4*KO/BLM mice was significantly lower than that in WT/BLM mice ($p < 0.05$) (Figure 2b), whereas no individual differences were observed between WT/BLM and *Dpp4*KO/BLM (partially muscularized: $p = 0.29$ and fully muscularized: $p = 0.32$) (Figure 2c).

The expression levels of α-SMA in $CD31^{+}CD45^{-}$ pulmonary cells (partial endothelial-to-mesenchymal transition cells), evaluated as mean fluorescence intensity (MFI), were higher after the BLM challenge (WT/PBS versus WT/BLM: $p < 0.05$). Notably, the expression levels were significantly lower in *Dpp4*KO/BLM than those in WT/BLM ($p < 0.05$). The expression levels of α-SMA in whole lung cells of WT/BLM were not significantly different from those in *Dpp4*KO/BLM ($p = 0.36$) (Figure 2d,e,f).

The BLM challenge caused fibrosis in the lungs and the right ventricle in both WT and *Dpp4*KO mice (Figure 2g,h). The Ashcroft scale, a quantitative lung fibrosis histological evaluation, in WT/BLM was more severe than that in WT/PBS ($p < 0.001$); however, it was not significantly different between WT/BLM and *Dpp4*KO/BLM ($p = 0.95$) (Figure 2i).

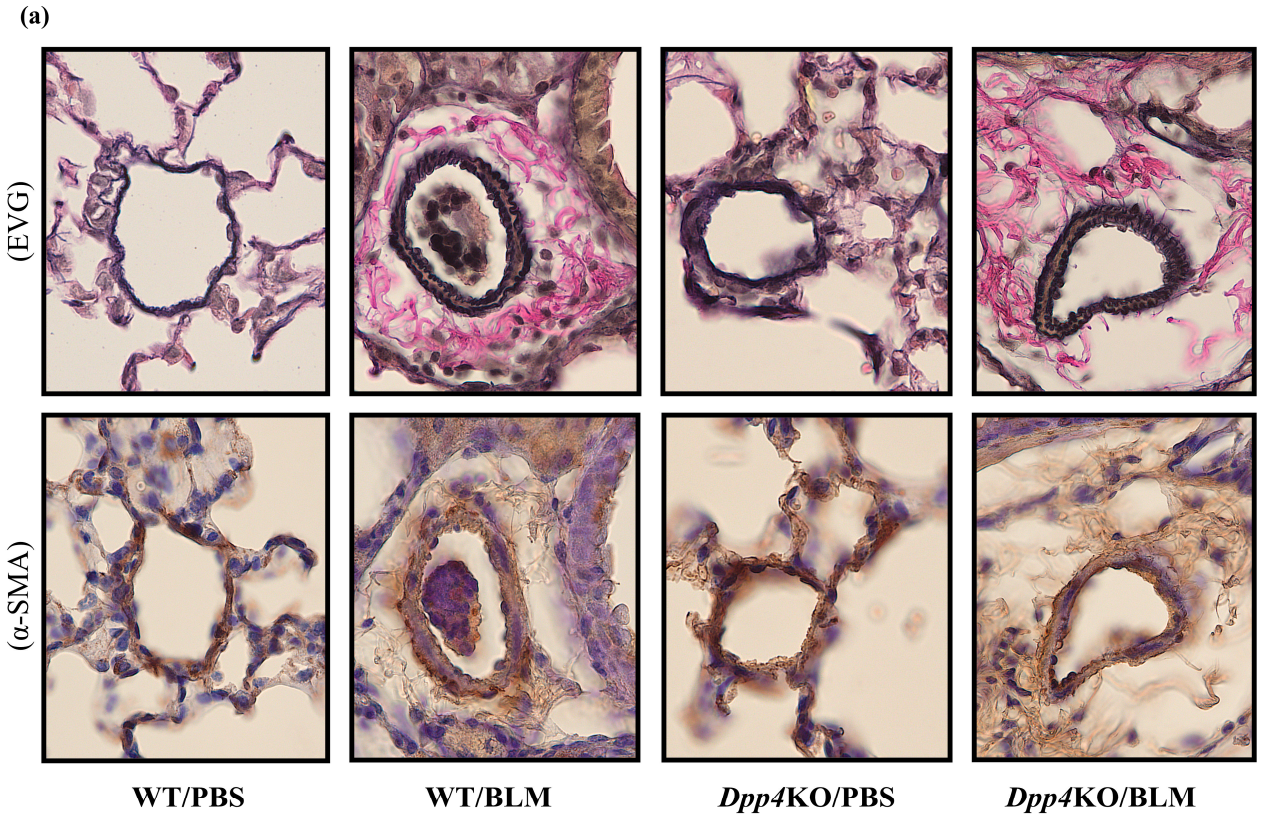

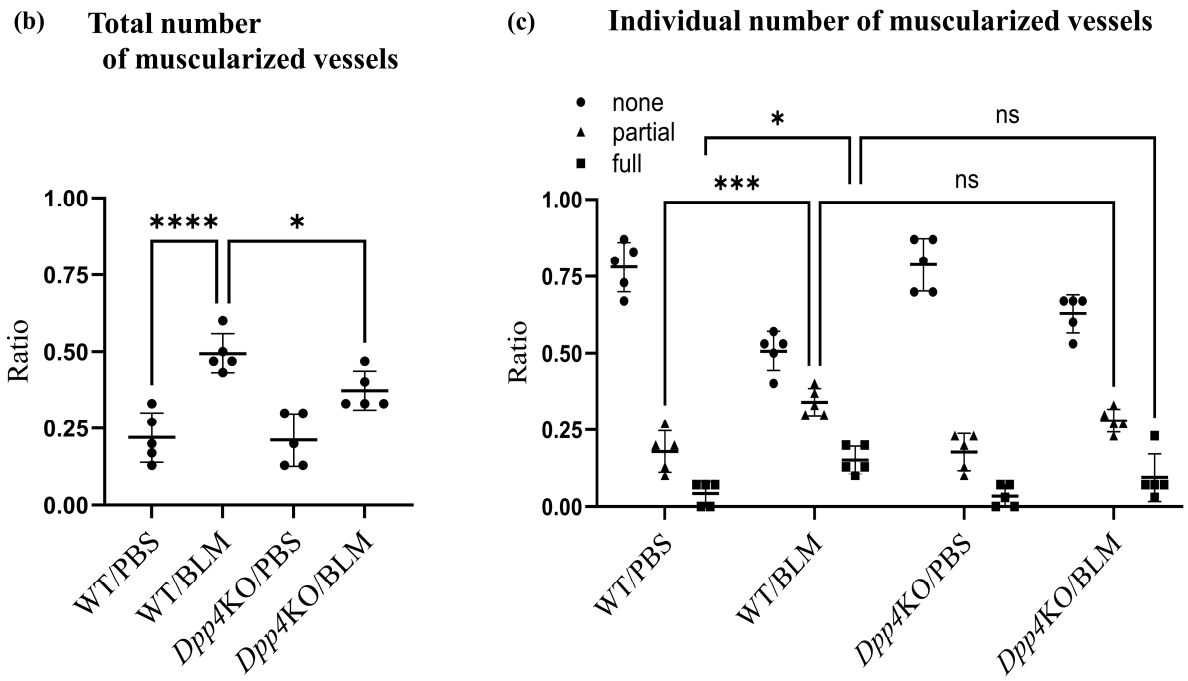

Figure 2. *Cont.*

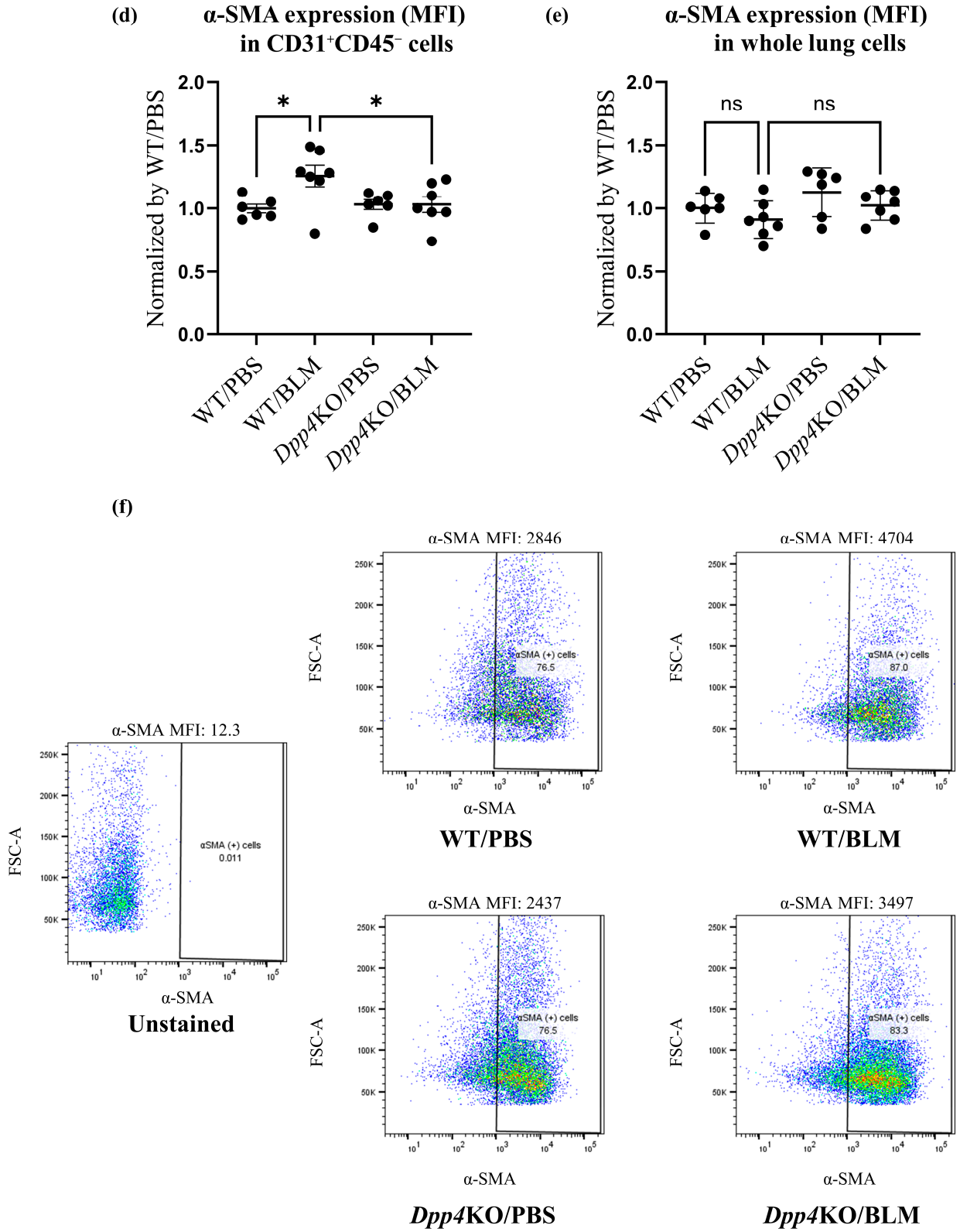

Figure 2. *Cont.*

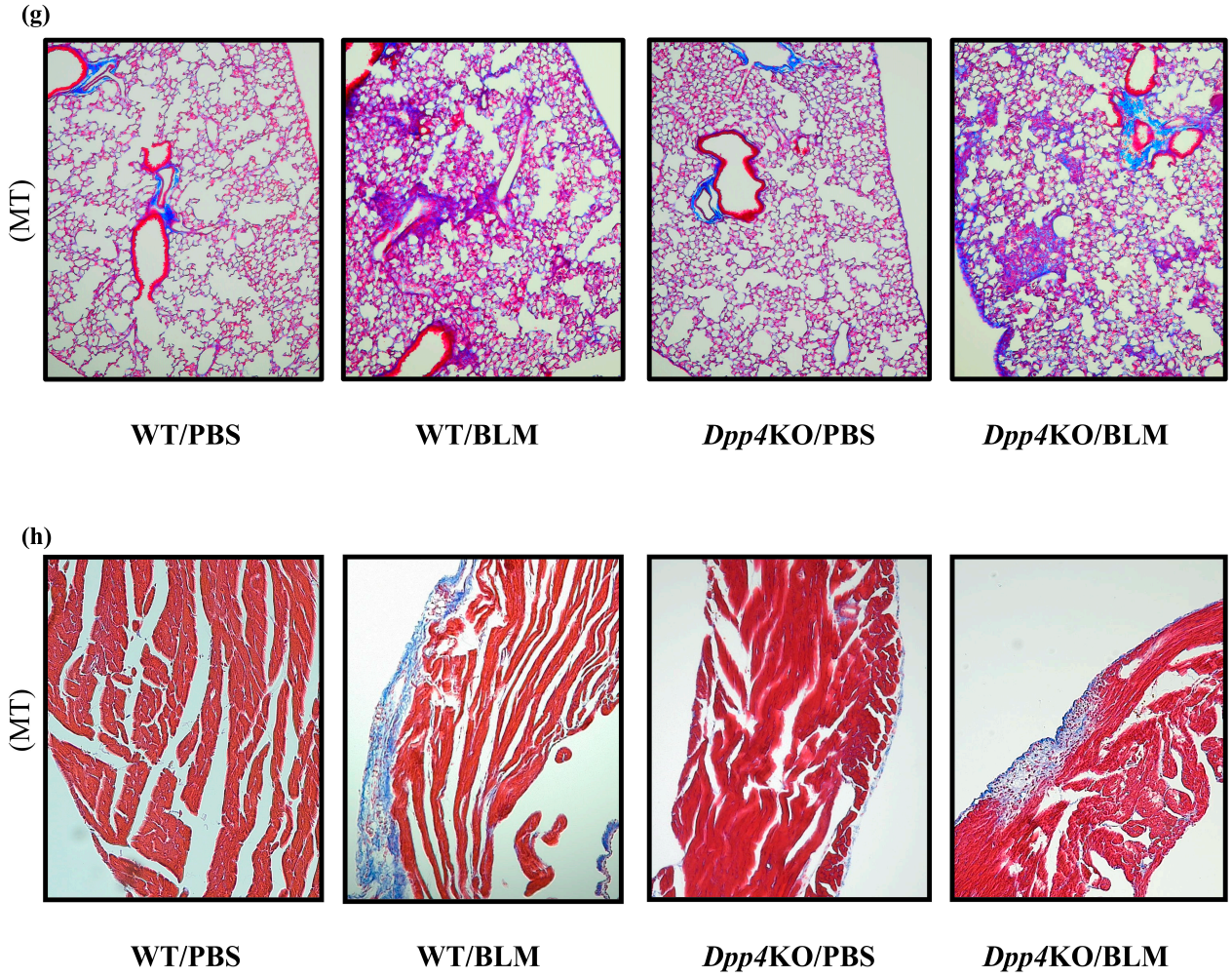

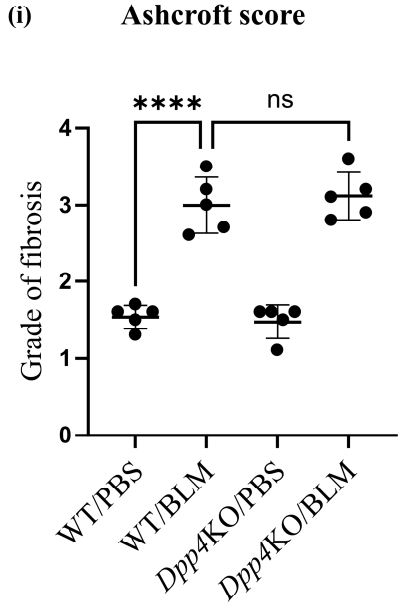

Figure 2. Evaluation of pulmonary small vessel remodeling of BLM-induced pulmonary hypertension in WT and *Dpp4*KO mice. The representative images of small pulmonary vessels of four groups are

shown in (**a**): staining with Elastica van Gieson (EVG) and α-SMA; observed under ×400 magnification. The extent of vascular muscularization (n = 5 in each group) is summarized in (**b**): the total number of partially and fully muscularized vessels, and in (**c**): individual number of muscularized vessels. The mean fluorescence intensity of α-SMA in $CD31^+CD45^-$ pulmonary vascular endothelial cells and whole lung cells is shown in (**d**,**e**). Representative dot plot images of $CD31^+CD45^-$ pulmonary vascular endothelial cells are shown in panel (**f**). The representative images of four groups are shown in (**g**): lung tissues (Masson's trichrome (MT); ×40 magnification), and in (**h**): right ventricle free wall (Masson's trichrome; ×40 magnification). To evaluate lung fibrosis, the Ashcroft score (n = 5 for each group) was calculated (**i**). ns, not significant; * $p < 0.05$, *** $p < 0.001$, **** $p < 0.0001$.

2.3. Cell Proliferation and Cytotoxicity Were Reduced by DPP4-siRNA Treatment in Cultured hPASMCs

Expression levels of CD26/DPP4 in cultured human PASMCs (hPASMCs) treated with either control-siRNA (Control) or *DPP4*-siRNA (*DPP4* knockdown, *DPP4*KD) were examined in vitro. Real-time quantitative PCR revealed that the mRNA expression level of *DPP4* was reduced by *DPP4*-siRNA (Figure 3a). Flow cytometric analysis also revealed that the expression levels of CD26/DPP4 were reduced by *DPP4*-siRNA treatment (Figure 3b,c).

Proliferation and cytotoxicity assays were performed to explore the potential role of CD26/DPP4 in the proliferation and cytotoxicity of PASMCs. A proliferation assay of cultured hPASMCs revealed that the enhanced cell viability induced by TGFβ treatment was suppressed by *DPP4*-siRNA treatment (Figure 3d). A cytotoxicity assay revealed that cell damage was unchanged after TGFβ treatment, whereas it was significantly lower in *DPP4*-siRNA-treated cells than that in the control cells (Figure 3e).

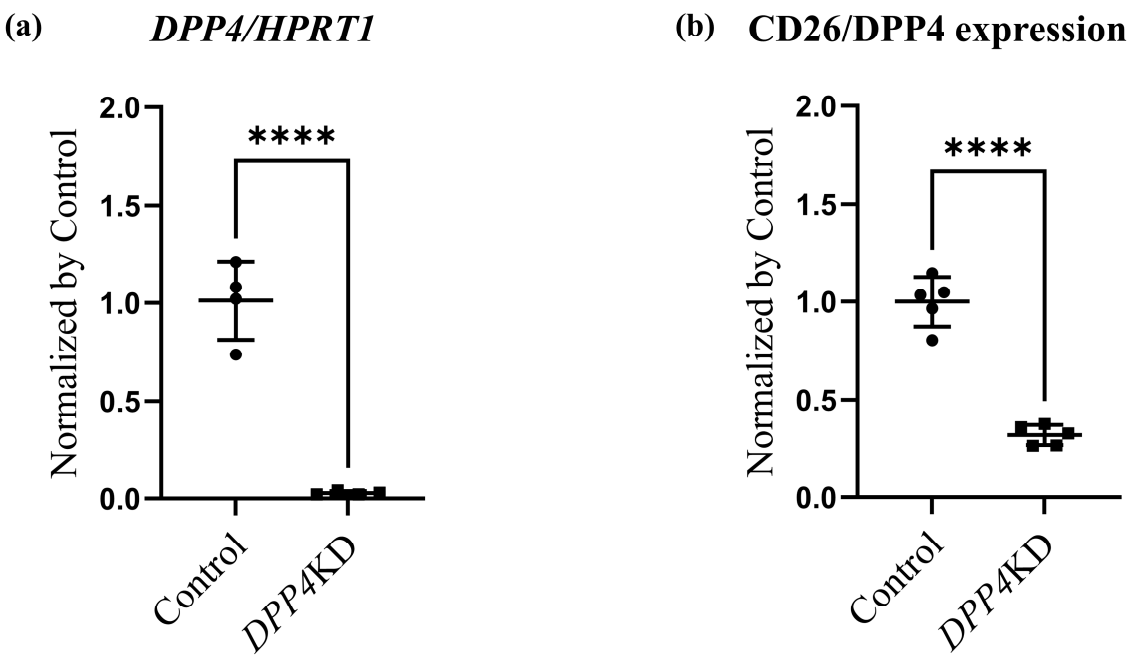

Figure 3. *Cont.*

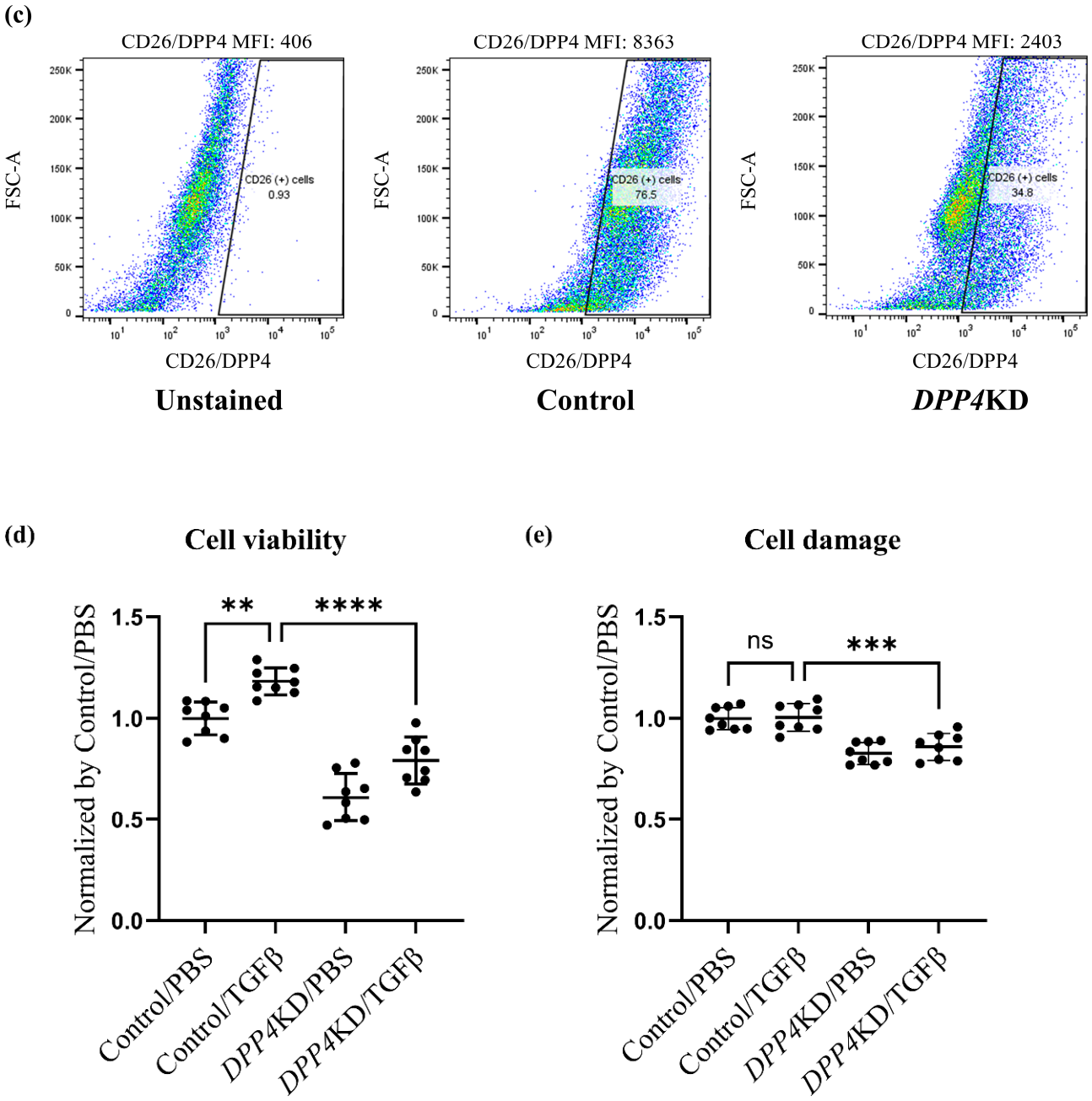

Figure 3. Cell viability and damage in cultured hPASMCs were reduced by *DPP4* knockdown. Expression levels of CD26/DPP4 in cultured hPASMCs were evaluated using real-time quantitative PCR (**a**) and flow cytometry (**b**). Representative dot plots of flow cytometry are shown in panel (**c**). Cell viability and cytotoxicity were evaluated using (**d**): Cell Counting Kit-8 assay and (**e**): LDH assay, respectively. Control: hPASMCs treated with nonspecific control siRNA; *DPP4* knockdown (*DPP4*KD): hPASMCs treated with *DPP4*-siRNA; ns: not significant; ** $p < 0.01$, *** $p < 0.001$, **** $p < 0.0001$.

2.4. Transcriptome Analysis of Cultured hPASMCs after Treatment with TGFβ and DPP4-siRNA

To explore the potential effects of TGFβ treatment on the transcriptome signature of cultured hPASMCs, a comparison between Control/PBS and Control/TGFβ groups was performed. Principal component analysis and heat maps with hierarchical clustering revealed that gene expression patterns differed between the groups (Figure 4a,b). Similarly, to reveal the effects of *DPP4*-siRNA, a comparison between the Control/PBS and *DPP4*KD/PBS groups was carried out (Figure 4c,d). Furthermore, to reveal the ef-

fects of *DPP4*-siRNA under TGFβ treatment, a comparison between Control/TGFβ and *DPP4*KD/TGFβ groups was conducted (Figure 4e,f).

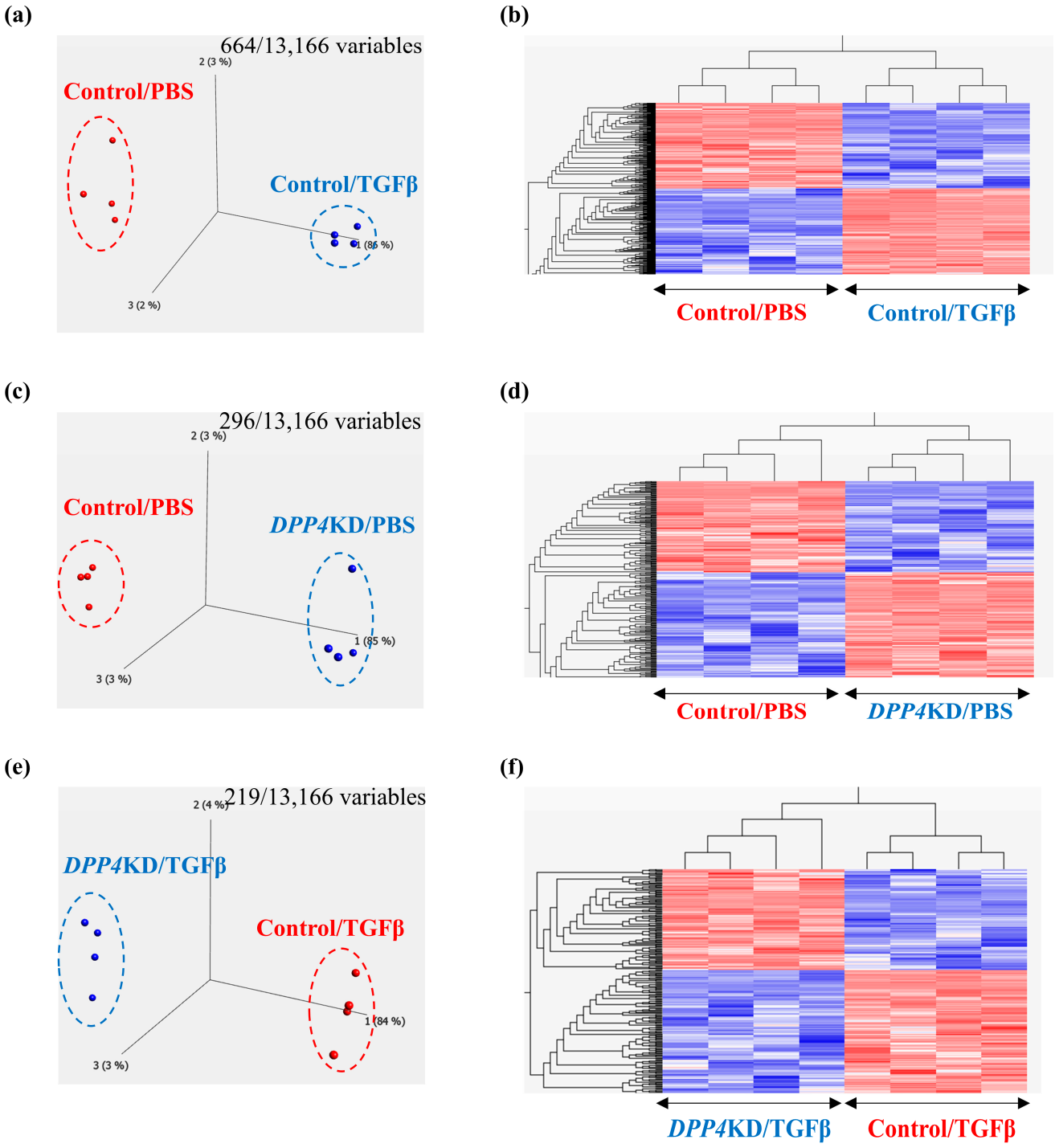

Figure 4. *Cont.*

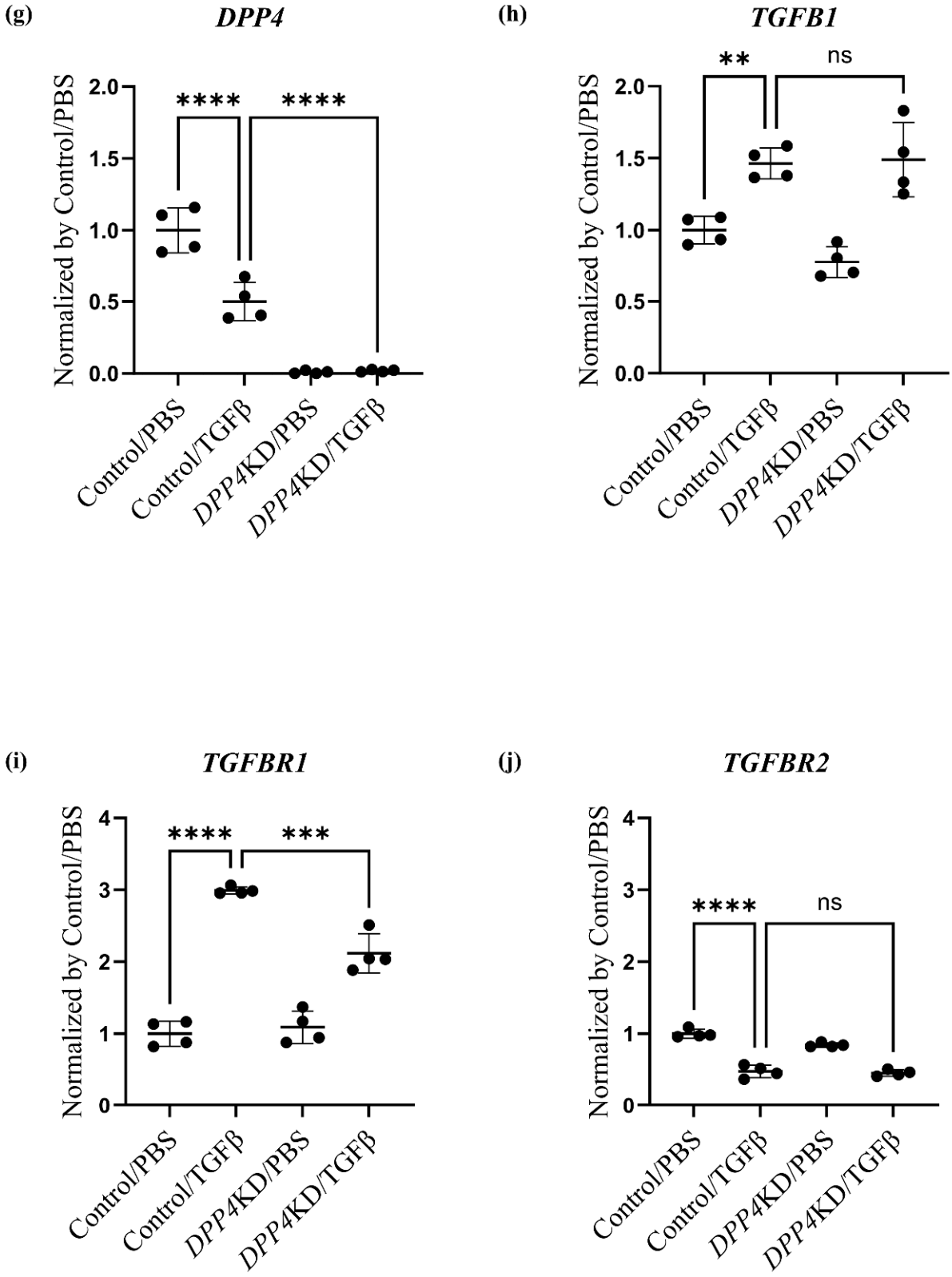

Figure 4. *Cont.*

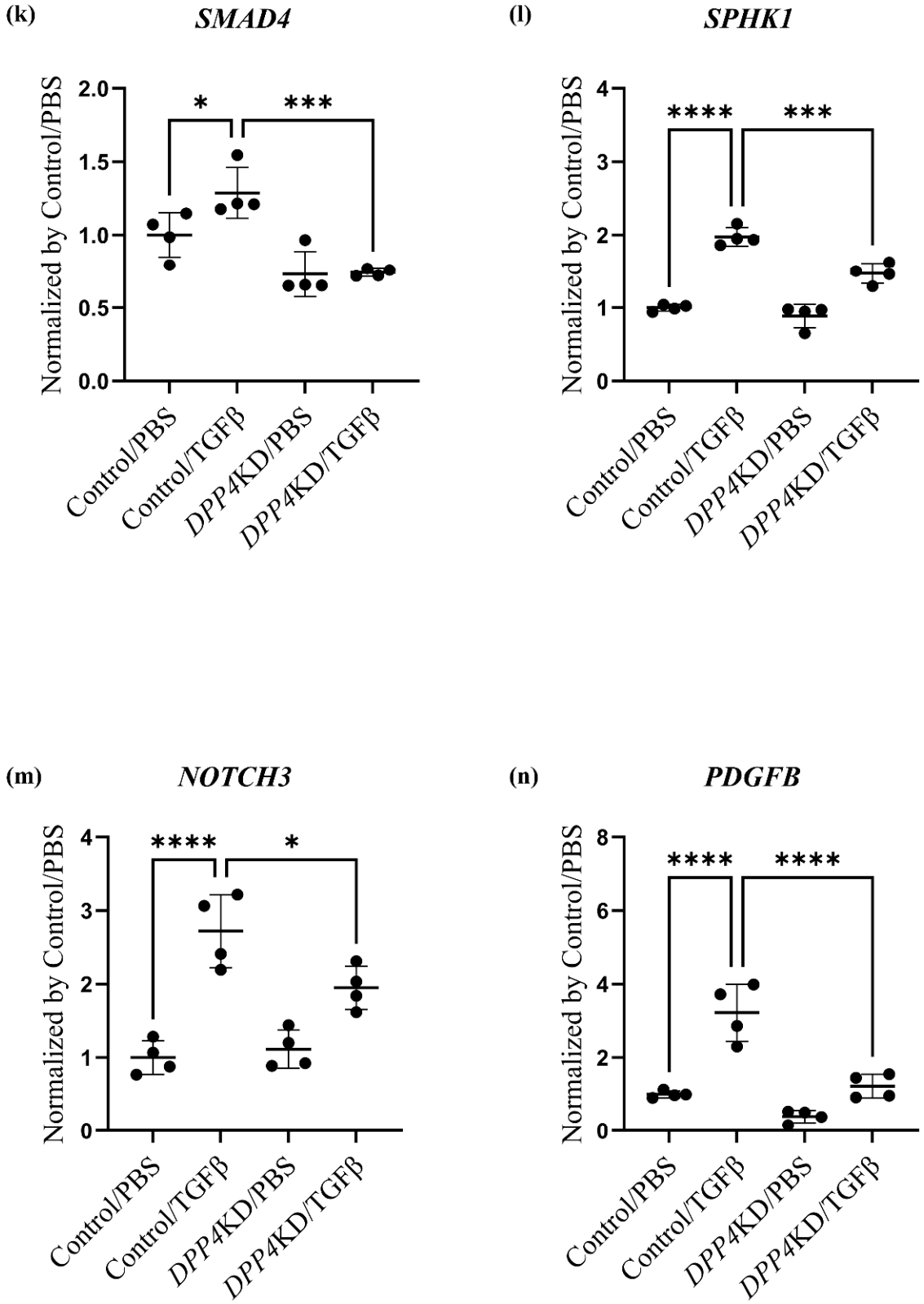

Figure 4. *Cont.*

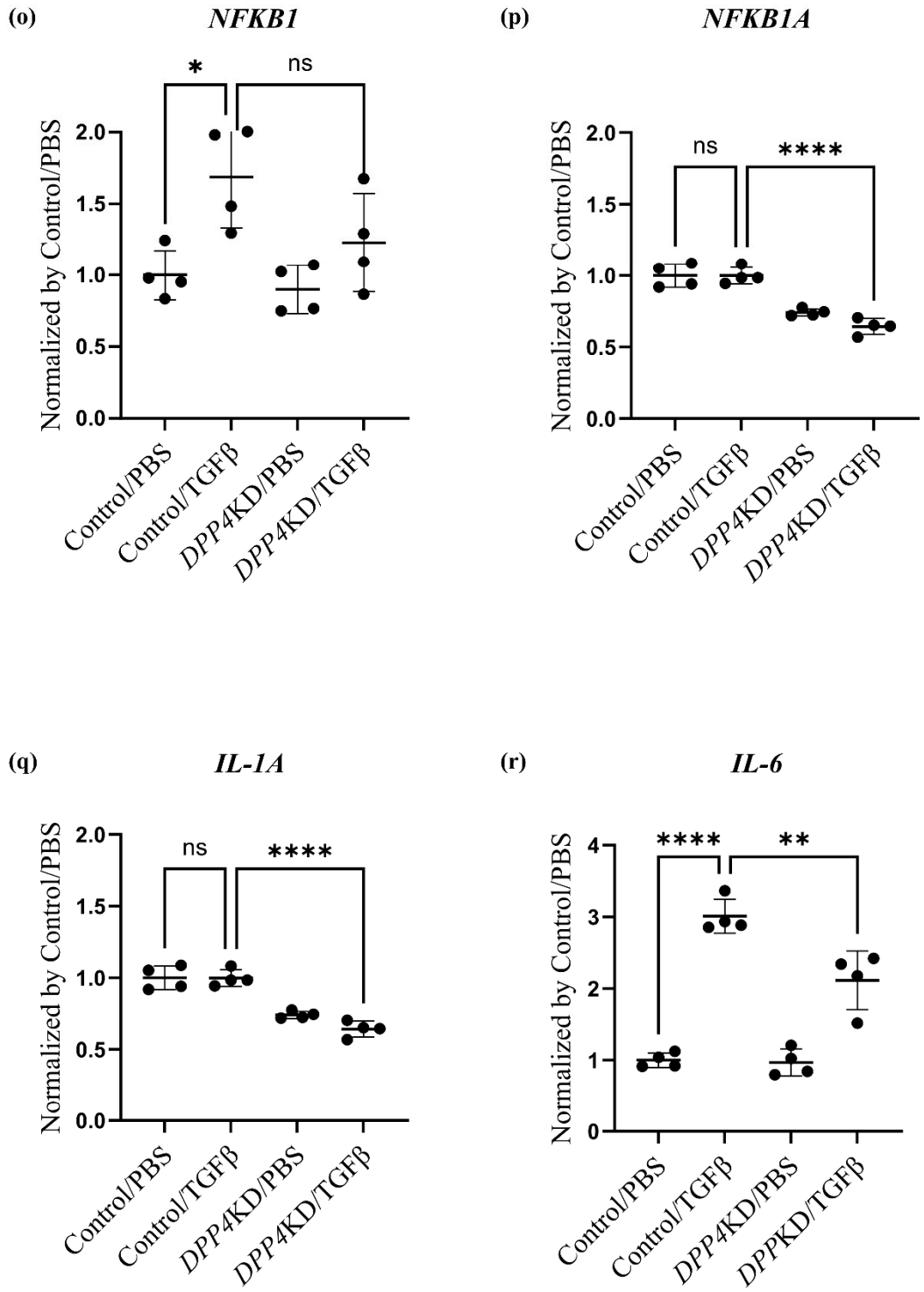

Figure 4. Transcriptome analysis of cultured hPASMCs treated with TGFβ and *DPP4*-siRNA. Cultured hPASMCs were treated as follows (each group: $n = 4$): Control/PBS (treated with non-specific control siRNA followed by PBS), Control/TGFβ (treated with non-specific control siRNA followed by TGFβ treatment), *DPP4*KD/PBS (hPASMCs treated with *DPP4*-siRNA followed by PBS), *DPP4*KD/TGFβ (hPASMCs treated with *DPP4*-siRNA followed by TGFβ treatment). Principal component analysis and heat map with hierarchical clustering of differentially expressed genes between the Control/PBS and Control/TGFβ (**a**,**b**), Control/PBS and *DPP4*KD/PBS (**c**,**d**), and Control/TGFβ and *DPP4*KD/TGFβ groups (**e**,**f**) are shown. mRNA expression levels of TGFβ pathway-related genes in hPASMCs are shown (**g**–**r**). ns; not significant, * $p < 0.05$, ** $p < 0.01$, *** $p < 0.001$, **** $p < 0.0001$.

Enrichment analysis (gene ontology [GO] and Kyoto Encyclopedia of Genes and Genomes [KEGG] pathways) comparing the Control/PBS and Control/TGFβ groups suggested that TGFβ treatment upregulated genes related to smooth muscle cell (SMC) proliferation and differentiation, growth factor stimulation, further TGFβ production, augmentation of TGFβ and TGFβ receptor responses, and pulmonary vascular SMC proliferation in hPASMCs (Table 1A). As an intervening pathway of TGFβ treatment, the genes related to pathways such as Notch, PI3K-Akt, and NFκB signaling pathways were upregulated according to the KEGG pathway analysis (Table 1B).

Table 1. Enrichment analysis of transcriptomic data (Control/PBS vs. Control/TGFβ).

(A): GO: relevant terms were excerpted	
Terms with upregulated genes following TGFβ treatment	*p*-value
Regulation of SMC differentiation (GO: 0051150)	0.0041
Cellular response to growth factor stimulus (GO: 0071363)	0.0051
Regulation of vascular associated SMC migration (GO: 1904754)	0.0057
Regulation of SMC proliferation (GO: 0048660)	0.013
Pathway-restricted SMAD protein phosphorylation (GO: 0060393)	0.020
Response to TGF-beta (GO: 0071559)	0.026
Regulation of TGF-beta production (GO: 0071634)	0.030
Notch signaling pathway (GO: 0007219)	0.030
Regulation of TGF-beta receptor signaling pathway (GO: 0017015)	0.041
Regulation of vascular associated SMC proliferation (GO: 1904707)	0.045
(B): KEGG: relevant pathways were excerpted	
Pathways with upregulated genes following TGFβ treatment	*p*-value
PI3K-Akt signaling pathway	<0.0001
Cytokine–cytokine receptor interaction	0.013
Notch signaling pathway	0.018
TGF-beta signaling pathway	0.076
NF-kappa B signaling pathway	0.10

DPP4-siRNA treatment seemed to downregulate the genes and pathways that were upregulated by TGFβ treatment (Table 2). Gene expression levels associated with the *DPP4*, the *TGF* family, and the Notch and NFκB pathways were measured; the results are summarized in Table 3 and Figure 4g–r. The expression levels of *TGFBR1* after TGFβ treatment were downregulated by *DPP4*-siRNA (Table 3A and Figure 4i). Additionally, the expression levels of genes related to the Notch3 and NFκB signaling pathways were downregulated by *DPP4*-siRNA (Table 3B,C and Figure 4k–r).

Table 2. Enrichment analysis of transcriptomic data (Control/TGFβ vs. *DPP4*KD/TGFβ).

(A): GO: relevant terms were excerpted	
Terms with downregulated genes following *DPP4*-siRNA treatment	*p*-value
Cellular response to growth factor stimulus (GO: 0071363)	<0.0001
Cellular response to cytokine stimulus (GO: 0071345)	<0.0001
Notch signaling pathway (GO: 0007219)	0.0018
Pathway-restricted SMAD protein phosphorylation (GO: 0060389)	0.0031
SMAD protein signal transduction (GO: 0060395)	0.0036
Regulation of TGF-beta receptor signaling pathway (GO: 0017015)	0.029
Regulation of vascular associated SMC differentiation (GO: 1905063)	0.035
Positive regulation of NIK/NF-kappa B signaling (GO: 1901224)	0.040
Regulation of vascular associated SMC migration (GO: 1904754)	0.041
Regulation of SMC proliferation (GO: 0048660)	0.042

Table 2. *Cont.*

(B): KEGG: relevant pathways were excerpted	
Pathways with downregulated genes following *DPP4*-siRNA treatment	*p*-value
Cytokine–cytokine receptor interaction	0.0020
PI3K-Akt signaling pathway	0.020
NF-kappa B signaling pathway	0.0036
TGF-beta signaling pathway	0.019
Notch signaling pathway	0.049

Table 3. Differences in gene expression levels in hPASMCs.

(A): Genes related to *DPP4* and the *TGF*β family					
Gene ID	Control /PBS	Control /TGFβ	*DPP4*KD /PBS	*DPP4*KD /TGFβ	*p*-value
DPP4	43.50	21.74	0.37	0.81	<0.0001
TGFB1	55.25	80.83	42.85	82.31	<0.0001
TGFBR1	25.78	77.10	28.13	54.63	<0.0001
TGFBR2	116.50	55.40	98.17	52.79	<0.0001
(B): Genes related to the canonical pathway (Notch pathway)					
Gene ID	Control /PBS	Control /TGFβ	*DPP4*KD /PBS	*DPP4*KD /TGFβ	*p*-value
SMAD2	52.51	39.64	46.69	44.30	0.064
SMAD4	16.08	20.70	11.76	11.93	0.0003
SPHK1	49.69	98.18	44.09	73.12	<0.0001
S1PR3	38.57	113.9	33.89	74.95	<0.0001
NOTCH3	21.81	59.39	24.31	42.56	<0.0001
PDGFB	6.55	21.10	2.59	8.01	<0.0001
(C): Genes related to the non-canonical pathway (NFκB pathway)					
Gene ID	Control /PBS	Control /TGFβ	*DPP4*KD /PBS	*DPP4*KD /TGFβ	*p*-value
NFKB1	22.19	38.16	19.97	27.27	0.0077
RELA	44.16	49.64	46.41	50.99	0.56
NFKB1A	170.20	170.00	126.10	109.50	<0.0001
IL-1A	38.41	46.95	20.57	18.31	0.0003
IL-6	44.71	134.60	44.34	94.56	<0.0001
CXCL8	939.60	821.60	518.10	360.10	<0.0001

3. Discussion

In the present study, we demonstrated that BLM-induced pulmonary vascular remodeling associated with media thickening was attenuated in *Dpp4*KO mice. In vitro experiments showed that the TGFβ-enhanced proliferative capacity of cultured hPASMCs was suppressed by *DPP4*-siRNA treatment. Transcriptome analysis revealed that TGFβ treatment of cultured hPASMCs upregulated genes related to pulmonary vascular SMC proliferation, involving the Notch, PI3K-Akt, and NFκB signaling pathways in cultured hPASMCs. Conversely, application of *DPP4*-siRNA to cultured hPASMCs canceled these TGFβ-induced events. Specifically, *TGFBR1* and genes associated with the Notch3 and NFκB signaling pathways were downregulated by *DPP4*-siRNA. These results suggest that genetic deficiency of *Dpp4* provides protection against BLM-induced PH-ILD by alleviating vascular remodeling. This is attributed to the antiproliferative effect achieved via inhibition of TGFβ-related pathways on PASMCs.

BLM-induced pulmonary vascular remodeling with thickening of media was attenuated in *Dpp4*KO mice in this study. Because pulmonary vascular remodeling is a hallmark of structural changes in PH, which comprise the abnormal proliferation of PASMCs and/or endothelial cells, pulmonary adventitial fibrosis, and inflammatory cell infiltration in

the vascular walls, CD26/DPP4 could intervene somewhere in these mechanisms. This study focused on vascular SMC proliferation in PH-ILD models and clearly demonstrated in vitro that upregulated genes related to SMC proliferation and differentiation can be suppressed by *DPP4* knockdown. These findings suggest that media thickening in small pulmonary vessels was the main target in *Dpp4*KO mice. Treatment with sitagliptin, a DPP4 inhibitor, alleviates pulmonary artery remodeling in BLM-treated rats [28]. DPP4 inhibitors can decrease its enzymatic activity by binding to CD26/DPP4 on the surface of the lung constituent cells or the soluble form of DPP4 present in the circulating blood [29]. The downregulated CD26/DPP4 enzymatic activity in the targeting cells or in the circulating blood may contribute to the inhibition of pulmonary vascular remodeling in PH model animals.

The degree of BLM-induced lung fibrosis in this study was similar between the two genotypes, whereas previous studies have shown that intratracheally administered BLM-induced lung fibrosis in mice was attenuated by *Dpp4* deficiency or treatment with the DPP4 inhibitor vildagliptin [22,30]. This discrepancy could be explained by the differences in BLM exposure methods: schedule, doses, and route of administration—especially intraperitoneal or intratracheal administration, which was reported to cause greater direct reactions in lungs [31]. The degree of involvement of *Dpp4*KO may be different between the development of PH and lung fibrosis induced by BLM administration.

TGFβ production can be augmented in fibroblasts and macrophages by BLM challenge, which may play a central role in lung fibrosis and vascular remodeling [32]. To explore potential functional roles of CD26/DPP4 in PASMC in the BLM-induced PH model, *DPP4*-siRNA was used in cultured hPASMCs. The proliferation of hPASMCs was enhanced by TGFβ treatment, and this enhancement was suppressed by *DPP4*-siRNA (Figure 4d). Moreover, sitagliptin, a DPP4 inhibitor, inhibits the proliferation of hPASMCs induced by PDGF-BB [28]. PDGF-BB is a well-known potent mitogen implicated in proliferation and migration of PASMCs similar to TGFβ, playing a key role in the progression of PH. A reduction in DPP4 activity could suppress the proliferation of hPASMCs upon stimulation with cell growth factor. Moreover, the cytotoxicity assay revealed that LDH release from hPASMCs was not significantly changed by TGFβ treatment and was reduced by *DPP4*-siRNA treatment (Figure 4e). These results suggest that *DPP4*-siRNA can reduce cell damage in hPASMCs whereas the decrease in cell numbers, which was seen in proliferation assay, may also affect LDH concentration.

The molecular mechanisms, by which *DPP4*-siRNA suppresses SMC proliferation, were explored via transcriptome analysis of the cultured hPASMCs (Figure 5). The existence of CD26/DPP4 is essential for TGFβ receptor assembly [33]. This functional aid of CD26/DPP4 for the TGFβ receptors was observed in human microvascular endothelial cells and fibroblasts [34,35]. In this study, *TGFBR1* expression in hPASMCs was increased upon TGFβ stimulation, and this increase was suppressed by *DPP4*-siRNA treatment, indicating the existence of functional association of *DPP4* with *TGFBR1* in PASMCs. Moreover, transcriptome analysis showed that cell surface CD26/DPP4 could modulate intracellular TGF-β signaling via canonical and non-canonical pathways, leading to proliferation of PASMCs in PH pathobiology.

Enrichment analysis suggested that TGFβ signaling pathways including canonical and non-canonical pathways were downregulated by *DPP4*-siRNA treatment. The canonical pathway of TGFβ/Smad signaling could be related to the onset and development of PH [36], whereas Smad/Notch3 signaling activated by TGFβ stimulation promotes the proliferation of PASMCs via upregulation of SphK1/S1P [37]. Moreover, NOTCH3 overexpression in small pulmonary artery SMCs is a crucial signaling factor associated with the severity of PH in humans and rodents [38]. In the present study, *DPP4*-siRNA treatment downregulated TGFβ signaling possibly by interfering with canonical pathways, especially Notch3 pathways, and suppressed the proliferation of hPASMCs. On the contrary, TGFβ stimulation enhanced intracellular non-canonical pathways, which was suppressed by *DPP4*-siRNA treatment. TGFβ stimulation enhances non-canonical pathways including NFκB, RAF-

MEK-ERK, p38 MAPK, JNK, and PI3K-Akt-mTOR [39]. Among these pathways, NFκB pathway is known to be associated with monocrotaline-induced PH by promoting vascular remodeling and increasing inflammation [40]. Furthermore, it has been suggested that the crosstalk between NFκB and Akt–mTOR signaling pathways may promote hypoxia-induced PH by increasing *DPP4* expression in PASMCs [27]. In this study, enrichment analysis on gene sets from hPASMCs demonstrated that the upregulation of PI3K-Akt and NFκB signaling by TGFβ stimulation was downregulated by *DPP4*-siRNA treatment.

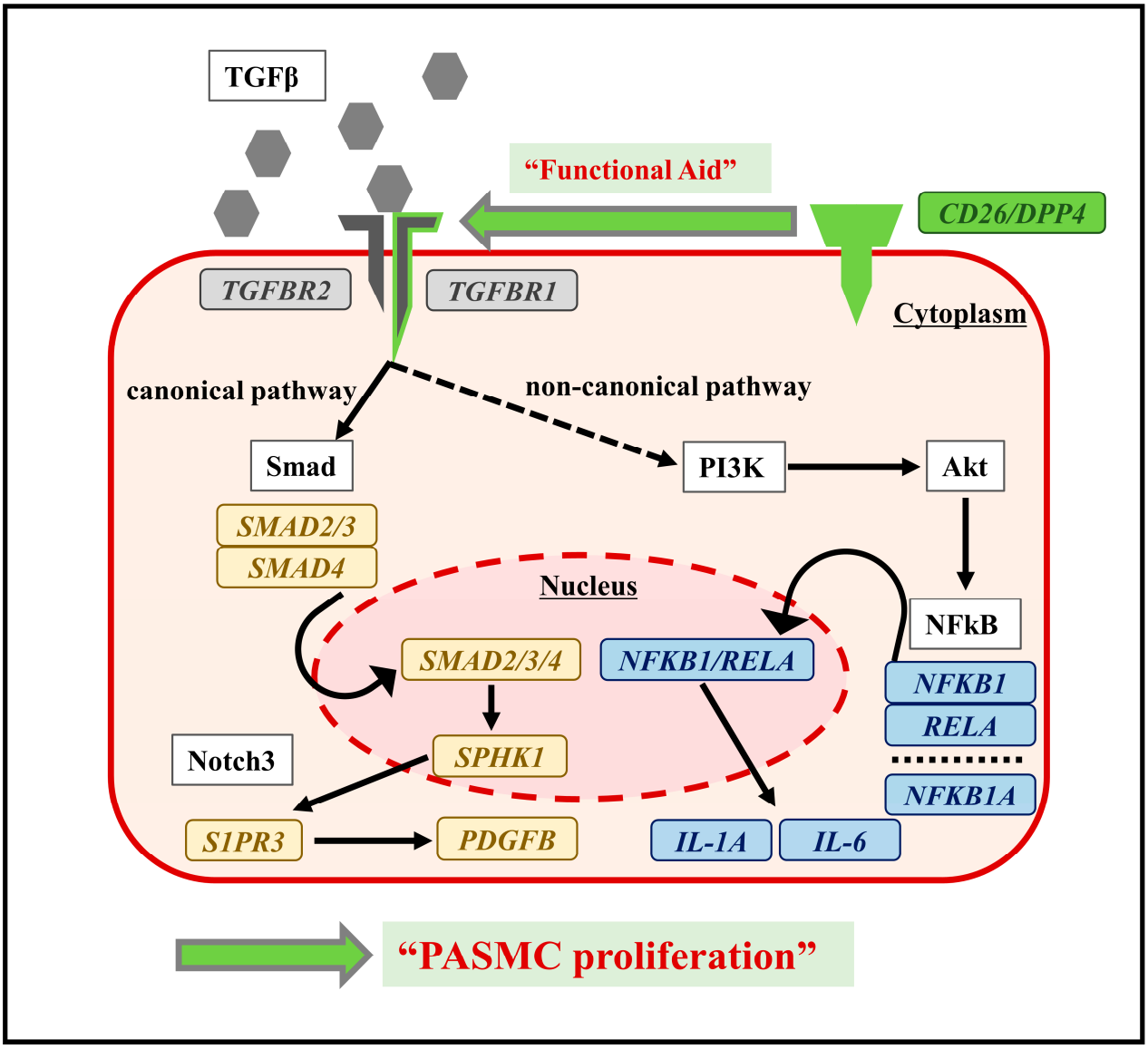

Figure 5. Conceptual diagram of functional association of CD26/DPP4 with TGFβ via signaling pathways in hPASMCs. Potential mechanisms of PASMC proliferation are also shown. Transcriptome analysis of hPASMCs suggested that the functional aid of CD26/DPP4 for TGFβ receptors might activate canonical and non-canonical pathways, causing PASMC proliferation.

This study has several limitations. First, we focused on the proliferation of PASMCs as a mechanism of vascular remodeling in this PH-ILD model based on the pathological findings of media thickening. However, various mechanisms, such as endothelial dysfunction, endothelial-to-mesenchymal transition, extracellular matrix production of fibroblasts, and release of inflammatory cytokines from macrophages, are related to vascular remodeling in patients with PH-ILD. Therefore, further evaluation is required to clarify the mechanisms underlying the in vivo roles of CD26/DPP4, including those in cell–cell interactions and cell

transformation in endothelial cells, fibroblasts, and macrophages. Second, the molecular pathways related to hPASMC proliferation were explored using transcriptome analysis by RNA sequencing. However, verification of mRNA and protein expression should be performed using real-time quantitative PCR and/or Western blotting, and further independent confirmatory experiments to investigate molecular mechanisms are required. Third, it would be meaningful to explore if PASMC functions are different between patients with PH-ILD and healthy controls and are associated with CD26/DPP4 expression levels. Finally, it would be helpful to identify the substrates of CD26/DPP4 involved in pulmonary vascular remodeling and examine the effects of CD26/DPP4 activation on media component cells, including PASMCs or other cell types. Further studies are warranted to better understand the functional role of CD26/DPP4 in PH-ILD.

4. Materials and Methods

4.1. Animal Model of Pulmonary Hypertension with Interstitial Pneumonia

Five-to six-week-old male C57BL/6J mice (body weight: 18–20 g) were purchased from CLEA Japan, Inc. (Tokyo, Japan) and used as WT mice. *Dpp4*KO mice with a C57BL/6 background were provided by the Department of Therapy Development and Innovation for Immune Disorders and Cancers, Graduate School of Medicine, Juntendo University (Japan). All mice were housed in ventilated cages with microisolator lids and were kept at an ambient temperature of 22 °C and in a 12 h light-dark cycle. All experiments were conducted according to protocols approved by the Review Board for Animal Experiments of Chiba University (Japan). To establish the PH-ILD model, WT and *Dpp4*KO mice were intraperitoneally administered 0.035 mg/g of BLM (Nippon Kayaku Co., Ltd. Tokyo, Japan) or phosphate-buffered saline (PBS; 0.035 mg/g) twice weekly for 4 weeks as previously described [41]. In this experimental design, mice were assigned to one of the following four groups: WT/PBS, WT/BLM, *Dpp4*KO/PBS, and *Dpp4*KO/BLM. All mice were tested under anesthesia and euthanized on day 33.

4.2. Hemodynamic Analysis

Pulmonary hemodynamics were assessed while the mice were under mild anesthesia induced using isoflurane (3% for induction, 1% for maintenance), and their body temperatures were maintained at 37 °C. Right heart catheterization was performed according to the manufacturer's protocol [42], whilst the mice were maintained under spontaneous breathing. The mice were then placed in the supine position, and a small incision was made on the right side of the neck, where the right jugular vein was identified. A 1.4F microtip pressure catheter (SPR-671. Millar OEM Solutions. Houston, TX, USA) was advanced through the incision into the RV. Using a Power-Lab data acquisition system (AD Instruments. Dunedin, New Zealand), RVSP, CO, HR and Max dP/dt in RV were continuously monitored and recorded. After completion of the measurements, the mice were euthanized with 5% isoflurane and their hearts were removed. The RV free wall was carefully dissected from the left ventricle and septum (LV + S) and weighed to calculate RV/LV + S (Fulton index) as an indicator of RV hypertrophy.

4.3. Histological Analysis

After the mice were euthanized, the lungs were perfused via the right ventricle with PBS and fixed in 10% formalin after expansion of the lung tissues. The left lungs were cut sagitally into two sections, embedded in paraffin, sectioned (2 μm), and mounted on slides. The specimens were stained with Masson's trichrome (MT). The severity of pulmonary fibrosis was semiquantitatively assessed according to the method proposed by Ashcroft using the mean of 10 fields (magnification, ×100) per mouse, as previously described [43]. The extent of muscularization in small pulmonary vessels (<100 μm diameter) was examined using Elastica van Gieson (EVG) and α-smooth muscle actin (α-SMA) staining. Vessels were identified as non-muscularized (no α-SMA staining), partially muscularized (α-SMA staining in the part of vessels), or fully muscularized (α-SMA staining in the whole

circumference of the vessels), and then the distribution (%) of the three categories was calculated using a previously reported method [44]. The values obtained represent the mean for 30 vessels (magnification, ×100) per mouse. The RV free wall was also processed into 2 μm sections and stained with MT to evaluate fibrosis in the RV.

4.4. Cell Culture and Treatments of Small Interfering RNA and TGF-β1

hPASMCs were purchased from PromoCell (Heidelberg, Germany) and cultured in Smooth Muscle Cell Growth Medium 2 (PromoCell) supplemented with 10% fetal bovine serum. hPASMCs were incubated at 37 °C in a 5% CO_2 incubator and used at passages 4–6 for all experiments. For small interfering RNA (siRNA) transfection, *DPP4* siRNA (Cat# 4392421, siRNA ID: s4255) and non-specific control siRNA (Cat# 4390843, Silencer™ Select Negative Control No. 1 siRNA) were purchased from Thermo Fisher Scientific (Waltham, MA, USA). Using the Lipofectamine™ RNAiMAX Transfection Reagent (Thermo Fisher Scientific), hPASMCs were transfected with siRNA for 48 h according to the manufacturer's protocol. After the siRNA treatment, the cells were stimulated with recombinant human transforming growth factor-b1 (TGFβ) (PEPROTECH. Cranbury, NJ, USA) at a concentration of 10 ng/mL as previously reported [45] or with PBS at the same concentration for 24 h.

4.5. Proliferation and Cytotoxicity Assay

Cultured hPASMCs were treated with *DPP4* siRNA or control siRNA, detached using ACCUTASE (Thermo Fisher Scientific), and cultured in serum-free medium for 24 h and subsequently challenged with TGFβ or PBS. For the proliferation assay, the Cell Counting Kit-8 (WST-8. Dojindo Molecular Technologies. Kumamoto, Japan) was used according to the manufacturer's protocol. In brief, the treated cells were added to a 96-well plate, 10 μL of WST-8 was added to each well, and the plate was incubated at 37 °C for 2 h. Cell viability was determined by measuring the absorbance at 450 nm using a microplate reader. For the cytotoxicity assay, a Cytotoxicity LDH Assay Kit-WST (Dojindo Molecular Technologies) was used to measure LDH expression levels according to the manufacturer's protocol. The treated cells were added to a 6-well plate and 100 μL of LDH substrate solution was added to the wells, followed by incubation of the plates for 30 min at room temperature. The absorbance at 450 nm was measured using a microplate reader.

4.6. Real-Time Quantitative PCR Analysis

The total RNA was extracted from whole mouse lungs or cultured hPASMCs using the TRIzol reagent and the Direct-Zol RNA MiniPrep Plus Kit (ZYMO RESEARCH Corporation. Irvine, CA, USA). The extracted RNA was reverse transcribed via PCR using the SuperScript IV VILO Master Mix (Thermo Fisher Scientific) to synthesize single-stranded cDNA. cDNA samples both from mouse lungs and cultured hPASMCs were amplified using qPCR with the Fast SYBR Green PCR Master Mix (Thermo Fisher Scientific) and the GeneAmp PCR System (Thermo Fisher Scientific). Specific primers (the details of primer sequences are provided in Supplemental Table S1) were designed using an online software from the Universal Probe Library Assay Design Center (URL: https://lifescience.roche.com/en_us/brands/universal-probe-library.html#assay-design-center/) accessed on 13 June 2016 (Roche Applied Science. Upper Bavaria, Germany). The expression levels of target genes were normalized to hypoxanthine phosphoribosyl transferase 1 threshold cycle (CT) values and calculated using the $2^{-\Delta\Delta Ct}$ method (ΔΔCT = [target gene CT of experimental group − reference gene CT of experimental group] − [target gene CT of control group − reference gene CT of control group]).

4.7. Flow Cytometry Analysis

In vivo, mouse lungs were perfused from the right ventricle until they were blood-free, using 20 mL of PBS containing 10 U/mL heparin (Mochida. Tokyo, Japan). The whole lungs were then minced and digested in an enzyme cocktail of Dulbecco's mod-

ified Eagle's medium (Sigma-Aldrich. Saint Louis, MO, USA) containing 1% bovine serum albumin (BSA) (Sigma), 2 mg/mL collagenase (Worthington. Lakewood, NJ, USA), 100 μg/mL DNase (Sigma), and 2.5 mg Dispase II (Sigma) at 37 °C for 60 min, followed by meshing through a 70 μm nylon cell strainer. The single cell suspensions were pretreated with an anti-CD16/32 antibody (BioLegend. San Diego, CA, USA) for 10 min to block Fc receptors, then incubated with specific antibodies in the dark at 4 °C for 15 min. The following antibodies were used for cell-surface staining: anti-CD26-PE, anti-CD31-PE/Cy7, and anti-CD45-Alexa Fluor 700 (BioLegend). After surface staining, the lung cells were fixed, permeabilized, and further incubated with anti-α-SMA (Thermo Fisher Scientific), followed by donkey anti-rabbit IgG-PE (Invitrogen. Boston, MA, USA) as the secondary antibody for 15 min in the dark at 4 °C. Cell fluorescence was measured with the BD FACS Canto™ II (BD Biosciences), and the data were analyzed using the FlowJo software ver. 10.8.1 (Becton, Dickinson and Company. Franklin Lakes, NJ, USA). To evaluate protein expression levels, the MFI of each sample was calculated (MFI = MFI of a sample stained with an antibody − MFI of an unstained sample [autofluorescence of the sample]). In vitro, cultured hPASMCs were pretreated with the anti CD16/32 antibody (BioLegend) for 10 min to block Fc receptors and then stained with anti-CD26-PE/Cy7 (BioLegend).

4.8. Transcriptome Analysis

Total RNA was isolated from the PASMCs and stored in Isogen (Nippon Gene. Tokyo, Japan). One milliliter of this solution was vigorously vortexed and then centrifuged after adding 200 μL of chloroform. The supernatants were removed, and 10 μg of glycogen (Roche. Basel, Switzerland) was added. RNA was precipitated by adding 500 μL of isopropyl alcohol. The solution was then vortexed vigorously and centrifuged. The RNA pellets were washed with 75% ethanol and then dissolved in 10 μL RNase-free water. The concentration and quality of RNA were verified using an Agilent 2100 Bioanalyzer (Agilent Technologies. Santa Clara, CA, USA). Purified total RNA (200 ng) with an RIN value > 9 was used for RNA library preparation according to the instructions of the QuantSeq 3′mRNA-Seq Library Prep Kit FWD for Illumina (Lexogen. Vienna, Austria). Libraries were amplified via 13 PCR cycles. RNA libraries were sequenced using an Illumina (San Diego, California, USA) NextSeq 500 system (75 cycles). The FASTQ files were prepared with reads using bcl2fastq ver2.20 (Illumina). The quality of FASTQ sequence data was assessed using FastQC v0.11.9 (Illumina). After removing adapter sequences from the raw reads, the trimmed reads were aligned using STAR v2.7.6a to the GRCh38 human reference genome. Reads per million values were calculated using Samtools v1.15, and htseq count v1.99.2. The expression levels of the genes identified in the transcriptome were normalized and compared. Principal component analysis and heat maps with hierarchical clustering were created using the Qlucore Omics Exploration software ver. 3.9.9 (Qlucore AB. Lund, Sweden). The fold change between each group was >4.0 ($p < 0.001$). Significantly over-represented functional categories were identified using Enrichr online tool (http://amp.pharm.mssm.edu/Enrichr/) accessed on 1 October 2023. Genes with significantly upregulated expression between Control/PBS and Control/TGFβ or downregulated expression between Control/TGFβ and *DPP4*KD/TGFβb were annotated. GO terms and KEGG pathways were also identified and considered significant at $p < 0.05$.

4.9. Statistical Analysis

Data are presented as the mean ± standard deviation. Unpaired two-tailed *t*-tests were used for comparisons of two groups. One-way ANOVA was used for multiple group comparisons, followed by Bonferroni's post hoc test. Statistical significance was set at $p < 0.05$. Statistical analyses were performed using GraphPad Prism version 9.3 (GraphPad Software, Inc. San Diego, CA, USA).

5. Conclusions

This study demonstrated that genetic deficiency of *Dpp4* has protective effects on BLM-induced PH in mice by alleviating vascular remodeling, potentially by exerting an antiproliferative effect on PASMCs via the Notch, PI3K-Akt, and NFκB signaling pathways. Therefore, CD26/DPP4 may be a potential therapeutic target in patients with PH associated with ILDs.

Supplementary Materials: The following supporting information can be downloaded at: https://www.mdpi.com/article/10.3390/ijms25020748/s1.

Author Contributions: Conceptualization, T.O., T.K. and K.T.; data curation, T.O.; formal analysis, T.O., T.K. and Y.H.; funding acquisition, T.K., K.T. and T.S.; investigation, T.O.; methodology, T.O., T.K., S.S., Y.K. (Yu Koyanagi), Y.K. (Yoshitoshi Kasuya), Y.H. and O.O.; project administration, T.K.; resources, R.H., K.O. and C.M.; supervision, K.T., C.M., Y.K. (Yoshitoshi Kasuya), O.O. and T.S.; writing—original draft, T.O. and T.K.; writing—review and editing, S.S., Y.K. (Yu Koyanagi), K.T., R.H., K.O., C.M., Y.K. (Yoshitoshi Kasuya), Y.H., O.O. and T.S. All authors have read and agreed to the published version of the manuscript.

Funding: This research was funded by JSPS KAKENHI (Grant Numbers 19K17663, 22K16163, and 22H03076), GSK Japan Research Grant 2019, Therapeutics Research Initiative Grant from Chiba University School of Medicine 2019-G6, AMED-CREST (JP21gm1210003), AMED (223fa627003h0001), and a research grant from the Intractable Respiratory Diseases and Pulmonary Hypertension Research Group, Ministry of Health, Labor and Welfare, Japan (Grant Numbers 20FC1027 and 23FC1031).

Institutional Review Board Statement: Animal experiments were conducted according to protocols approved by the Review Board for Animal Experiments of Chiba University (Japan).

Informed Consent Statement: Not applicable.

Data Availability Statement: The datasets presented in this study can be found online in the NCBI database (accession number: GSE248794).

Acknowledgments: We are grateful to Tomoko Misawa, Akiko Moriya, and Sumina Atarashi, for their technical advice, and to Chieko Handa and Tamie Hirano for their administrative support.

Conflicts of Interest: The authors declare no conflicts of interest.

References

1. Humbert, M.; Kovacs, G.; Hoeper, M.M.; Badagliacca, R.; Berger, R.M.F.; Brida, M.; Carlsen, J.; Coats, A.J.S.; Escribano-Subias, P.; Ferrari, P.; et al. 2022 ESC/ERS Guidelines for the diagnosis and treatment of pulmonary hypertension. *G. Ital. Cardiol.* **2023**, *24*, 1e–116e. [CrossRef] [PubMed]
2. Gall, H.; Felix, J.F.; Schneck, F.K.; Milger, K.; Sommer, N.; Voswinckel, R.; Franco, O.H.; Hofman, A.; Schermuly, R.T.; Weissmann, N.; et al. The Giessen Pulmonary Hypertension Registry: Survival in pulmonary hypertension subgroups. *J. Heart Lung Transplant.* **2017**, *36*, 957–967. [CrossRef] [PubMed]
3. Gomberg-Maitland, M.; Olschewski, H. Prostacyclin therapies for the treatment of pulmonary arterial hypertension. *Eur. Respir. J.* **2008**, *31*, 891–901. [CrossRef]
4. Boucly, A.; Savale, L.; Jais, X.; Bauer, F.; Bergot, E.; Bertoletti, L.; Beurnier, A.; Bourdin, A.; Bouvaist, H.; Bulifon, S.; et al. Association between Initial Treatment Strategy and Long-Term Survival in Pulmonary Arterial Hypertension. *Am. J. Respir. Crit. Care Med.* **2021**, *204*, 842–854. [CrossRef] [PubMed]
5. Nathan, S.D.; Barbera, J.A.; Gaine, S.P.; Harari, S.; Martinez, F.J.; Olschewski, H.; Olsson, K.M.; Peacock, A.J.; Pepke-Zaba, J.; Provencher, S.; et al. Pulmonary hypertension in chronic lung disease and hypoxia. *Eur. Respir. J.* **2019**, *53*, 1801914. [CrossRef] [PubMed]
6. Prins, K.W.; Duval, S.; Markowitz, J.; Pritzker, M.; Thenappan, T. Chronic use of PAH-specific therapy in World Health Organization Group III Pulmonary Hypertension: A systematic review and meta-analysis. *Pulm. Circ.* **2017**, *7*, 145–155. [CrossRef] [PubMed]
7. Raghu, G.; Nathan, S.D.; Behr, J.; Brown, K.K.; Egan, J.J.; Kawut, S.M.; Flaherty, K.R.; Martinez, F.J.; Wells, A.U.; Shao, L.; et al. Pulmonary hypertension in idiopathic pulmonary fibrosis with mild-to-moderate restriction. *Eur. Respir. J.* **2015**, *46*, 1370–1377. [CrossRef]
8. Nathan, S.D.; Behr, J.; Collard, H.R.; Cottin, V.; Hoeper, M.M.; Martinez, F.J.; Corte, T.J.; Keogh, A.M.; Leuchte, H.; Mogulkoc, N.; et al. Riociguat for idiopathic interstitial pneumonia-associated pulmonary hypertension (RISE-IIP): A randomised, placebo-controlled phase 2b study. *Lancet Respir. Med.* **2019**, *7*, 780–790. [CrossRef]

9. Waxman, A.; Restrepo-Jaramillo, R.; Thenappan, T.; Ravichandran, A.; Engel, P.; Bajwa, A.; Allen, R.; Feldman, J.; Argula, R.; Smith, P.; et al. Inhaled Treprostinil in Pulmonary Hypertension Due to Interstitial Lung Disease. *N. Engl. J. Med.* **2021**, *384*, 325–334. [CrossRef]
10. Tanabe, N.; Kumamaru, H.; Tamura, Y.; Taniguchi, H.; Emoto, N.; Yamada, Y.; Nishiyama, O.; Tsujino, I.; Kuraishi, H.; Nishimura, Y.; et al. Multi-Institutional Prospective Cohort Study of Patients With Pulmonary Hypertension Associated With Respiratory Diseases. *Circ. J.* **2021**, *85*, 333–342. [CrossRef]
11. Heath, D.; Edwards, J.E. The pathology of hypertensive pulmonary vascular disease; a description of six grades of structural changes in the pulmonary arteries with special reference to congenital cardiac septal defects. *Circulation* **1958**, *18*, 533–547. [CrossRef] [PubMed]
12. Eddahibi, S.; Chaouat, A.; Morrell, N.; Fadel, E.; Fuhrman, C.; Bugnet, A.S.; Dartevelle, P.; Housset, B.; Hamon, M.; Weitzenblum, E.; et al. Polymorphism of the serotonin transporter gene and pulmonary hypertension in chronic obstructive pulmonary disease. *Circulation* **2003**, *108*, 1839–1844. [CrossRef] [PubMed]
13. Della Latta, V.; Cecchettini, A.; Del Ry, S.; Morales, M.A. Bleomycin in the setting of lung fibrosis induction: From biological mechanisms to counteractions. *Pharmacol. Res.* **2015**, *97*, 122–130. [CrossRef] [PubMed]
14. Moore, B.B.; Hogaboam, C.M. Murine models of pulmonary fibrosis. *Am. J. Physiol. Lung Cell. Mol. Physiol.* **2008**, *294*, L152–L160. [CrossRef] [PubMed]
15. Santos-Ribeiro, D.; Lecocq, M.; de Beukelaer, M.; Bouzin, C.; Palmai-Pallag, M.; Yakoub, Y.; Huaux, F.; Horman, S.; Perros, F.; Pilette, C.; et al. Bleomycin-induced lung injury: Revisiting an old tool to model group III PH associated with pulmonary fibrosis. *Pulm. Circ.* **2023**, *13*, e12177. [CrossRef] [PubMed]
16. Mulvihill, E.E.; Drucker, D.J. Pharmacology, physiology, and mechanisms of action of dipeptidyl peptidase-4 inhibitors. *Endocr. Rev.* **2014**, *35*, 992–1019. [CrossRef] [PubMed]
17. Green, B.D.; Flatt, P.R.; Bailey, C.J. Dipeptidyl peptidase IV (DPP IV) inhibitors: A newly emerging drug class for the treatment of type 2 diabetes. *Diab. Vasc. Dis. Res.* **2006**, *3*, 159–165. [CrossRef] [PubMed]
18. Morimoto, C.; Schlossman, S.F. The structure and function of CD26 in the T-cell immune response. *Immunol. Rev.* **1998**, *161*, 55–70. [CrossRef]
19. Klemann, C.; Wagner, L.; Stephan, M.; von Horsten, S. Cut to the chase: A review of CD26/dipeptidyl peptidase-4's (DPP4) entanglement in the immune system. *Clin. Exp. Immunol.* **2016**, *185*, 1–21. [CrossRef]
20. Zhang, T.; Tong, X.; Zhang, S.; Wang, D.; Wang, L.; Wang, Q.; Fan, H. The Roles of Dipeptidyl Peptidase 4 (DPP4) and DPP4 Inhibitors in Different Lung Diseases: New Evidence. *Front. Pharmacol.* **2021**, *12*, 731453. [CrossRef]
21. Kawasaki, T.; Chen, W.; Htwe, Y.M.; Tatsumi, K.; Dudek, S.M. DPP4 inhibition by sitagliptin attenuates LPS-induced lung injury in mice. *Am. J. Physiol. Lung Cell. Mol. Physiol.* **2018**, *315*, L834–L845. [CrossRef] [PubMed]
22. Liu, Y.; Qi, Y. Vildagliptin, a CD26/DPP4 inhibitor, ameliorates bleomycin-induced pulmonary fibrosis via regulating the extracellular matrix. *Int. Immunopharmacol.* **2020**, *87*, 106774. [CrossRef] [PubMed]
23. Chen, S.Y.; Kong, X.Q.; Zhang, K.F.; Luo, S.; Wang, F.; Zhang, J.J. DPP4 as a Potential Candidate in Cardiovascular Disease. *J. Inflamm. Res.* **2022**, *15*, 5457–5469. [CrossRef] [PubMed]
24. Bostick, B.; Habibi, J.; Ma, L.; Aroor, A.; Rehmer, N.; Hayden, M.R.; Sowers, J.R. Dipeptidyl peptidase inhibition prevents diastolic dysfunction and reduces myocardial fibrosis in a mouse model of Western diet induced obesity. *Metabolism* **2014**, *63*, 1000–1011. [CrossRef] [PubMed]
25. Shah, Z.; Kampfrath, T.; Deiuliis, J.A.; Zhong, J.; Pineda, C.; Ying, Z.; Xu, X.; Lu, B.; Moffatt-Bruce, S.; Durairaj, R.; et al. Long-term dipeptidyl-peptidase 4 inhibition reduces atherosclerosis and inflammation via effects on monocyte recruitment and chemotaxis. *Circulation* **2011**, *124*, 2338–2349. [CrossRef] [PubMed]
26. Anderluh, M.; Kocic, G.; Tomovic, K.; Kocic, H.; Smelcerovic, A. DPP-4 inhibition: Capital A, Cyrillic novel therapeutic approach to the treatment of pulmonary hypertension? *Pharmacol. Ther.* **2019**, *201*, 1–7. [CrossRef] [PubMed]
27. Li, Y.; Yang, L.; Dong, L.; Yang, Z.W.; Zhang, J.; Zhang, S.L.; Niu, M.J.; Xia, J.W.; Gong, Y.; Zhu, N.; et al. Crosstalk between the Akt/mTORC1 and NF-kappaB signaling pathways promotes hypoxia-induced pulmonary hypertension by increasing DPP4 expression in PASMCs. *Acta Pharmacol. Sin.* **2019**, *40*, 1322–1333. [CrossRef] [PubMed]
28. Xu, J.; Wang, J.; He, M.; Han, H.; Xie, W.; Wang, H.; Kong, H. Dipeptidyl peptidase IV (DPP-4) inhibition alleviates pulmonary arterial remodeling in experimental pulmonary hypertension. *Lab. Invest.* **2018**, *98*, 1333–1346. [CrossRef]
29. Baggio, L.L.; Varin, E.M.; Koehler, J.A.; Cao, X.; Lokhnygina, Y.; Stevens, S.R.; Holman, R.R.; Drucker, D.J. Plasma levels of DPP4 activity and sDPP4 are dissociated from inflammation in mice and humans. *Nat. Commun.* **2020**, *11*, 3766. [CrossRef]
30. Koyanagi, Y.; Kawasaki, T.; Kasuya, Y.; Hatano, R.; Sato, S.; Takahashi, Y.; Ohnuma, K.; Morimoto, C.; Dudek, S.M.; Tatsumi, K.; et al. Functional roles of CD26/DPP4 in bleomycin-induced pulmonary fibrosis. *Physiol. Rep.* **2023**, *11*, e15645. [CrossRef]
31. Lindenschmidt, R.C.; Tryka, A.F.; Godfrey, G.A.; Frome, E.L.; Witschi, H. Intratracheal versus intravenous administration of bleomycin in mice: Acute effects. *Toxicol. Appl. Pharmacol.* **1986**, *85*, 69–77. [CrossRef] [PubMed]
32. Cutroneo, K.R.; White, S.L.; Phan, S.H.; Ehrlich, H.P. Therapies for bleomycin induced lung fibrosis through regulation of TGF-beta1 induced collagen gene expression. *J. Cell. Physiol.* **2007**, *211*, 585–589. [CrossRef] [PubMed]
33. Ohm, B.; Moneke, I.; Jungraithmayr, W. Targeting cluster of differentiation 26 / dipeptidyl peptidase 4 (CD26/DPP4) in organ fibrosis. *Br. J. Pharmacol.* **2023**, *180*, 2846–2861. [CrossRef] [PubMed]

34. Shi, S.; Srivastava, S.P.; Kanasaki, M.; He, J.; Kitada, M.; Nagai, T.; Nitta, K.; Takagi, S.; Kanasaki, K.; Koya, D. Interactions of DPP-4 and integrin beta1 influences endothelial-to-mesenchymal transition. *Kidney Int.* **2015**, *88*, 479–489. [CrossRef] [PubMed]
35. Soare, A.; Gyorfi, H.A.; Matei, A.E.; Dees, C.; Rauber, S.; Wohlfahrt, T.; Chen, C.W.; Ludolph, I.; Horch, R.E.; Bauerle, T.; et al. Dipeptidylpeptidase 4 as a Marker of Activated Fibroblasts and a Potential Target for the Treatment of Fibrosis in Systemic Sclerosis. *Arthritis Rheumatol.* **2020**, *72*, 137–149. [CrossRef] [PubMed]
36. Zakrzewicz, A.; Kouri, F.M.; Nejman, B.; Kwapiszewska, G.; Hecker, M.; Sandu, R.; Dony, E.; Seeger, W.; Schermuly, R.T.; Eickelberg, O.; et al. The transforming growth factor-beta/Smad2,3 signalling axis is impaired in experimental pulmonary hypertension. *Eur. Respir. J.* **2007**, *29*, 1094–1104. [CrossRef] [PubMed]
37. Wang, J.; Feng, W.; Li, F.; Shi, W.; Zhai, C.; Li, S.; Zhu, Y.; Yan, X.; Wang, Q.; Liu, L.; et al. SphK1/S1P mediates TGF-beta1-induced proliferation of pulmonary artery smooth muscle cells and its potential mechanisms. *Pulm. Circ.* **2019**, *9*, 1–8. [CrossRef]
38. Li, X.; Zhang, X.; Leathers, R.; Makino, A.; Huang, C.; Parsa, P.; Macias, J.; Yuan, J.X.; Jamieson, S.W.; Thistlethwaite, P.A. Notch3 signaling promotes the development of pulmonary arterial hypertension. *Nat. Med.* **2009**, *15*, 1289–1297. [CrossRef]
39. Tzavlaki, K.; Moustakas, A. TGF-beta Signaling. *Biomolecules* **2020**, *10*, 487. [CrossRef]
40. Yu, M.; Wu, X.; Wang, J.; He, M.; Han, H.; Hu, S.; Xu, J.; Yang, M.; Tan, Q.; Wang, Y.; et al. Paeoniflorin attenuates monocrotaline-induced pulmonary arterial hypertension in rats by suppressing TAK1-MAPK/NF-kappaB pathways. *Int. J. Med. Sci.* **2022**, *19*, 681–694. [CrossRef]
41. Karmouty-Quintana, H.; Zhong, H.; Acero, L.; Weng, T.; Melicoff, E.; West, J.D.; Hemnes, A.; Grenz, A.; Eltzschig, H.K.; Blackwell, T.S.; et al. The A2B adenosine receptor modulates pulmonary hypertension associated with interstitial lung disease. *FASEB J.* **2012**, *26*, 2546–2557. [CrossRef] [PubMed]
42. Hansen, T.S.; Bubb, K.J.; Schiattarella, G.G.; Ugander, M.; Tan, T.C.; Figtree, G.A. High-Resolution Transthoracic Echocardiography Accurately Detects Pulmonary Arterial Pressure and Decreased Right Ventricular Contractility in a Mouse Model of Pulmonary Fibrosis and Secondary Pulmonary Hypertension. *J. Am. Heart Assoc.* **2022**, *11*, e018353. [CrossRef] [PubMed]
43. Ashcroft, T.; Simpson, J.M.; Timbrell, V. Simple method of estimating severity of pulmonary fibrosis on a numerical scale. *J. Clin. Pathol.* **1988**, *41*, 467–470. [CrossRef] [PubMed]
44. Ciuclan, L.; Bonneau, O.; Hussey, M.; Duggan, N.; Holmes, A.M.; Good, R.; Stringer, R.; Jones, P.; Morrell, N.W.; Jarai, G.; et al. A novel murine model of severe pulmonary arterial hypertension. *Am. J. Respir. Crit. Care Med.* **2011**, *184*, 1171–1182. [CrossRef]
45. Li, L.; Zhang, X.; Li, X.; Lv, C.; Yu, H.; Xu, M.; Zhang, M.; Fu, Y.; Meng, H.; Zhou, J. TGF-beta1 inhibits the apoptosis of pulmonary arterial smooth muscle cells and contributes to pulmonary vascular medial thickening via the PI3K/Akt pathway. *Mol. Med. Rep.* **2016**, *13*, 2751–2756. [CrossRef]

CANCER RESEARCH COMMUNICATIONS

AACR American Association for Cancer Research

RESEARCH ARTICLE https://doi.org/10.1158/2767-9764.CRC-23-0215 OPEN ACCESS

HDAC Inhibition Induces CD26 Expression on Multiple Myeloma Cells via the c-Myc/Sp1-mediated Promoter Activation

Hiroko Nishida[1,2], Reiko Suzuki[3], Kiyora Nakajima[1], Mutsumi Hayashi[1], Chikao Morimoto[4], and Taketo Yamada[1,5]

ABSTRACT

CD26 is ubiquitously and intensely expressed in osteoclasts in patients with multiple myeloma, whereas its expression in plasma cells of patients with multiple myeloma is heterogeneous because of its cellular diversity, immune escape, and disease progression. Decreased expression levels of CD26 in myeloma cells constitute one of the mechanisms underlying resistance to humanized anti-CD26 mAb therapy in multiple myeloma. In the current study, we show that histone deacetylase inhibition (HDACi) with broad or class-specific inhibitors involves the induction of CD26 expression on CD26^{neg} myeloma cells both transcriptionally and translationally. Furthermore, dipeptidyl peptidase IV (DPPIV) enzymatic activity was concomitantly enhanced in myeloma cells. Combined treatment with HDACi plus CD26mAb synergistically facilitated lysis of CD26^{neg} myeloma cells not only by antibody-dependent cellular cytotoxicity but also by the direct effects of mAb. Of note, its combination readily augmented lysis of CD26^{neg} cell populations, refractory to CD26mAb or HDACi alone. Chromatin immunoprecipitation assay revealed that HDACi increased acetylation of histone 3 lysine 27 at the CD26 promoter of myeloma cells. Moreover, in the absence of HDACi, c-Myc was attached to the CD26 promoter via Sp1 on the proximal G-C box of myeloma cells, whereas, in the presence of HDACi, c-Myc was detached from Sp1 with increased acetylation of c-Myc on the promoter, leading to activation of the CD26 promoter and initiation of transcription in myeloma cells. Collectively, these results confirm that HDACi plays crucial roles not only through its anti-myeloma activity but by sensitizing CD26^{neg} myeloma cells to CD26mAb via c-Myc/Sp1-mediated CD26 induction, thereby augmenting its cytotoxicity.

Significance: There is a desire to induce and sustain CD26 expression on multiple myeloma cells to elicit superior anti-myeloma response by humanized anti-CD26 mAb therapy. HDACi upregulates the expression levels of CD26 on myeloma cells via the increased acetylation of c-MycK323 on the CD26 promoter, leading to initiation of CD26 transcription, thereby synergistically augments the efficacy of CD26mAb against CD26^{neg} myeloma cells.

Introduction

The therapeutic landscape for multiple myeloma has dramatically changed over the past decades and recent progress in the treatment options for multiple myeloma, in particular with the incorporation of anti-CD38 targeting mAbs into standard care regimens including proteasome inhibitors (PI) and immunomodulatory drugs (IMiD) has tremendously improved the prognosis of patients with multiple myeloma (1–3). However, the vast majority of patients still relapse and become refractory to existing treatments due to the heterogeneity of multiple myeloma, in which multiple clones have different clinical behaviors as well as acquired resistance (4). Notably, triple class–exposed patients with multiple myeloma typically have progressively shorter durations of responses (DOR) with subsequent lines of therapy and penta-class-refractory patients have extremely dismal outcomes with a median progression-free survival of 3 months and overall survival (OS) of less than 6 months (4). Therefore, the treatment of patients with relapsed or refractory multiple myeloma (RRMM) remains a major challenge and highlights the urgent need for the development of novel effective treatments to target alternative antigens or treatments with different mechanisms of action.

In recent years, in addition to naked mAbs, several novel targeted immunotherapies, including antibody–drug conjugates (ADC), bispecific antibodies (BsAb), and chimeric antigen receptor T-cells (CAR-T), have been developed to eliminate myeloma cells (5–7). B-cell maturation antigen, BCMA/TNFRSF17 is

[1]Department of Pathology, Keio University School of Medicine, Shinjuku-ku, Tokyo, Japan. [2]Division of Hematology, Department of Internal of Medicine, Keio University School of Medicine, Shinjuku-ku, Tokyo, Japan. [3]Department of Collaborative Research Resources, Keio University School of Medicine, Shinjuku-ku, Tokyo, Japan. [4]Department of Therapy Development and Innovation for Immune Disorders and Cancers, Juntendo University, Graduate School of Medicine, Bunkyo-ku, Tokyo, Japan. [5]Department of Pathology, Faculty of Medicine, Saitama Medical University, Saitama, Japan.

Corresponding Authors: Hiroko Nishida, Keio University, School of Medicine, 35 Shinanomachi, Shinjuku-ku, Tokyo, 160-8582, Japan. E-mail: hiroko@keio.jp; and Professor Taketo Yamada, Saitama Medical University, 38 Moroyama-machi, Iruma, Saitama, 350-0495, Japan. E-mail: taketo@saitama-med.ac.jp

doi: 10.1158/2767-9764.CRC-23-0215

highly expressed on most of malignant plasma cells and represents a promising novel target for multiple myeloma therapy (8). To date, three BCMA-directed therapies have been approved for patients with RRMM who have undergone at least four prior lines of therapy including PIs, IMiDs, and anti-CD38 mAbs (9–18). Belentamab mafodotin (belamaf), a first-in-class humanized, afucosylated IgG_1 BCMA-targeted ADC containing monomethyl auristatin F, eliminates myeloma cells by a multi-modal mechanism of action via direct myeloma cell killing and an anti-myeloma immune response (9). Belamaf has shown promising efficacy as a single agent, with an overall response rate of 32% and a DOR of 12.5 months in triple-refractory patients with RRMM (10–12). However, its clinical use is limited because of suboptimal disease control and the high incidence of off-target adverse events such as ocular toxicities and pancytopenia (5, 8–12).

Moreover, the substantial efficacy of cell-based immunotherapies that engage T cells to BCMA-expressing myeloma cells and redirect subsequent lysis of myeloma cells have recently been uncovered by the emergence of BCMA-directed CAR-T cell and BsAb constructs (8, 13, 14). Two BCMA-directed CAR-T cell therapies, idecabtagene vicleucel (ide-cel, abecma) and ciltacabtagene-autoleucel (cilta-cel) have shown remarkable efficacy with rapid, deep, and durable clinical responses. Similarly, a humanized BsAbs with dual binding sites targeting both CD3 expressed on T cells and BCMA on myeloma cells, Teclistamab (cqyv, JNJ64007957) has proven highly active as a single agent with a deep and durable response. All of these immunotherapies result in a substantial improvement of outcomes in triple class–exposed patients with RRMM (14–18).

CD26, a 110-kDa transmembrane glycoprotein with dipeptidyl peptidase IV (DPPIV) activity (19–22), is expressed on several tumor cells, including malignant lymphoma, and has been implicated in T-cell activation and tumorigenesis (23, 24). In first-in human phase I study, recombinant humanized anti-CD26mAb was generally well tolerated and revealed antitumor effects without significant side effects in 33 patients with advanced CD26-expressing tumors, including renal cell carcinoma ($n = 9$), malignant pleural mesothelioma (MPM, $n = 23$), and urothelial carcinoma ($n = 1$; ref. 25). Furthermore, CD26mAb also revealed modest antitumor efficacy, with partial remission in 1 patient and stable disease (SD) in 14 patients, leading to a median OS of 9.7 months in 31 Japanese patients with advanced MPM (26, 27). On the other hand, the roles of CD26 in plasma cell malignancies remain elusive. Recently, we identified that CD26 is uniformly and intensely expressed in osteoclasts, whereas its expression in the plasma cells of patients with multiple myeloma was heterogeneous, leading to marked differences of response to CD26mAb therapy in multiple myeloma (28, 29). Decreased expression levels of CD26 in myeloma cells is one of the mechanisms underlying innate or acquired resistance to CD26mAb therapy in multiple myeloma. Therefore, more detailed understanding of both host- and tumor-related factors that predict the response to this mAb may result in the novel design of CD26-based immunotherapeutic approach for boosting cytotoxic efficacy in RRMM.

Histone deacetylases (HDAC) are highly expressed in various cancer cells and regulate aberrant gene transcription, which contributes to tumorigenesis. Therefore, HDAC inhibition (HDACi) can restore the gene transcription, that is aberrantly expressed in cancer cells, leading to cell cycle arrest, cell differentiation, and apoptosis (30, 31). Moreover, HDACi also epigenetically modifies the expression of cell surface or immunomodulatory molecules in various cancer cells and immune effector cells (30–35).

In the current study, we elucidated for the first time the potential impacts and mechanisms of HDACi by isoform-selective as well as broad inhibitors on the regulation of CD26 expression in myeloma cells, thereby eliciting superior anti-myeloma efficacy by CD26mAb. We demonstrated that HDACi mediates c-Myc acetylation on the CD26 promoter of myeloma cells, which leads to activation of the promoter and initiation of CD26 transcription in myeloma cells as one of mechanisms for the induction of CD26 in myeloma cells. Our results point to a novel observation on the role of HDACi and highlight that the combination of an isoform-selective HDACi plus CD26mAb confers attractive therapeutic strategies by resensitizing $CD26^{neg}$ myeloma cells to CD26mAb and augmenting its cytotoxic efficacy, thereby overcoming therapeutic resistance to mAb in RRMM.

Materials and Methods

Cell Lines

Five multiple myeloma cell lines: KMS26, 27, 28, and RPMI8226 were obtained from the National Institute of Biomedical Innovation, Health and Nutrition (NIBIOHN, Osaka, Japan). KMS11 was obtained from ATCC. All cell lines were maintained in RPMI1640 (Invitrogen), containing 10% FBS (Life Technologies), 100 μg/mL penicillin, and 100 μg/mL streptomycin (Life Technologies) at 37°C in a humidified atmosphere of 5% CO_2.Contamination of *Mycoplasma* was regularly examined by PCR, and no contamination was detected during experiments concerning this work.

Reagents and Cells

Human bone marrow (BM) mononuclear cells (MNC) and peripheral blood mononuclear cells were purchased from Lonza and human natural killer (NK) cells were obtained from Biotherapy Institute of Japan (Tokyo, Japan). HDAC inhibitors; pan HDACi: panobinostat_50 μmol/L, vorinostat_1.0 μmol/L, isoform-selective HDACi: romidepsin (HDAC1i)_0.125 μmol/L, BG45 (HDAC1, 3i) 1.0 μmol/L, entinostat (HDAC1, 3i)_50 μmol/L, RG2833 (HDAC1, 3i)_0.5 μmol/L, nexturastat A (HDAC6i)_0.125 μmol/L, tubastatin A (HDAC6i)_25 μmol/L, ricolinostat (HDAC1, 3, 6i)_0.5 μmol/L were purchased from Selleck Chemical Co. LTD. for use as therapeutic agents. These compounds, reconstituted in DMSO were added to the medium in which myeloma cell lines were cultured at the indicated concentrations for indicated times from 24 to 72 hours. The CD26mAb, humanized IgG_1, employed in the current study was generously provided by Y's AC. The CD26mAb was generated by utilizing the complementarity-determining regions of the murine anti-human CD26mAb, 14D10 with no cross-reactivity to murine CD26. Isotype IgG_1 (Sigma-Aldrich) was used as a control. In the experiments, after the incubation with the treatment of each HDACi for 48 hours, CD26mAb was subsequently added to the medium in which myeloma cell lines were cultured at 10 μg/mL for 24 hours.

Cell Viability Assay

Myeloma cell lines were treated with one of nine HDACi or isotype (iso) control IgG_1 (BioLegend) and incubated for 48 hours, followed by the additional incubation with the treatment by isotype (iso) control IgG_1 or CD26mAb at 10 μg/mL for 24 hours at 37°C in a humidified atmosphere of 5% CO_2. At the end of each timepoints, myeloma cells were collected and cell viability was determined via the conversion of a soluble MTT [3-(4,5-dimethtlthiazol-2-yl)-2,5-diphenyltetrazolium bromide] to insoluble formazan using CellQuanti-MTT cell viability assay kit (BioAsssay Systems), according

to the manufacturer's instructions. The absorbance of each well was measured at 560 nm with GloMax-Muluti Detection System (Promega).

Apoptosis Assay

Apoptosis of myeloma cells was determined by staining cells with annexin and propidium iodide using Annexin V-FITC apoptosis detection kit (BioVision), according to the manufacturer's instructions. The intensity of each cell was analyzed by flow cytometry; CytoFLEX (Beckman Coulter).

Antibody-dependent Cellular Cytotoxicity Assay

Five myeloma cell lines: KMS11, 26, 27, 28, and RPMI8226 (1×10^6/mL), transduced with luciferase (Promega) were treated with one of nine HDACi at the indicated concentration iso control $IgG_1$and incubated at 37°C for 48 hours. Subsequently, these cells were additionally incubated with iso control IgG_1or CD26mAb (10 μg/mL) in the presence or absence of human NK effector cell at an effector to target (E/T) ratio of 20, at 37°C for 24 hours. Thereafter, D-luciferin substrate was added at 150 μg/mL and the bioluminescence (luciferase$^+$ cells) was measured using GloMax-Muluti Detection System (Promega). The cell viability (%) was calculated as mean signal in the presence of CD26mAb plus effector NK cells with or without the treatment of each HDACi × 100/optical density (OD) signal in the control IgG_1 and effector NK cells.

Complement-dependent Cellular Assay

Myeloma cell lines were incubated with the treatment by each HDACi at the indicated concentration or iso control IgG_1 for 48 hours, followed by the additional incubation with the treatment by either CD26mAb (10 μg/mL) or iso control IgG_1 in the presence or absence of 50% fresh human serum as a source of complement at 37°C for 1 hour. Cell viability was measured by MTT assay using CellQuanti-MTT cell viability assay kit (BioAsssay systems), according to the manufacturer's instructions. The absorbance of each well was measured at 560 nm with GloMax-Muluti Detection System (Promega).

Whole Transcriptome Profiling

The GeneChip Whole Transcript (WT) Pico Reagent Kit (Thermo Fisher Scientific) was used to prepare hybridization-ready targets of total RNA samples with GeneChip WT Expression Arrays (Thermo Fisher Scientific) according the user guide. Briefly, the assay workflow consists of three steps. First, after first-strand cDNA sysnthesis, 3′ adaptor cDNA synthesis, double-stranded (ds) cDNA sysnthesis and cRNA amplification by *in vitro* transcription of ds cDNA using T7 RNA polymerase, cRNA purification and quantification was performed. Subsequently, second cycle single-strand (ss-cDNA) synthesis and cRNA hydrolyzation by RNaseH were conducted followed by ss-cDNA purification and quantification, fragmentation and terminal labeling of ss-cDNA. Finally, hybridization to WT array was performed using GeneChip cartridge array according the user guide. Microarray signals were processed using a standard robust multi-array averaging algorithm. Observed signals were normalized using quantile normalization methods and genes that had no significant signals were ignored to reduce the signals.

Chromatin Immunoprecipitation (ChIP)-qPCR

For chromatin immunoprecipitation (ChIP) assays, anti-histone H3, GTX122148 (GENETEX), anti-acetyl histone H3 (H3K27ac), #39134, 39336 (Active Motief), anti-Sp1, GTX110593 (GENETEX), A19649 (ABclonal), anti-c-Myc, A19032 (ABclonal), C15410174 (Diagenode), anti-c-MycK323ac, C15410346 (Diagenode) were used. The detailed procedures were provided in Supplementary Data S1 and Supplementary Table S1. qPCR analysis was performed using the Thermal Cycle Dice (Takara Bio). Several amplifications were performed by classic PCR and products were run on 1.5% agarose gels and was visualized on iBrightFL1000 (Thermo Fisher Scientific). Primer sequences were available in Supplementary Table S1.

Statistical Analysis

All statistical analyses were performed using Student *t* test for two group comparisons and *P* values less than 0.05 were considered statistically significant. The data are presented as the mean values with 95% confidence intervals, and the results are representative of three independent experiments.

Supplementary Data S1 include details of protocols for immunophenotyping (Supplementary Table S2), quantitation and qualification of mRNA levels, IHC, immunoblotting, ELISA, and ChIP-qPCR.

Data Availability

All data are available in the main text or Supplementary Data. Further information in this article is available from the corresponding authors on request.

Results

HDACi Increases the Expression of CD26 on Myeloma Cell Lines

We have already shown that the BM tissues of patients with multiple myeloma contained intensely CD26-stained osteoclasts, whereas CD26 expression on plasma cells was heterogeneously distributed (28, 29). Indeed, analysis of primary BM tissues from multiple myeloma patient revealed that several CD138^{pos} plasma cells were stained with CD26, whereas other plasma cells were not (29). Moreover, those from several patients with multiple myeloma showed that CD138^{pos} plasma cells were rarely stained with CD26 (Fig. 1A). Therefore, it is not necessarily reasonable to target CD26 on myeloma cells by CD26-targeted immunotherapy to elicit extensive cytotoxicity against multiple myeloma. HDACi has the ability to modulate the expression of cell surface molecules such as tumor antigens or immunomodulatory molecules in tumor cells or immune effector cells (30–35). Consequently, we evaluated the effects of HDACi by broad or isoform-selective inhibitors on cell surface CD26 expression levels on myeloma cells. First, five myeloma cell lines KMS11, 26, 27, 28, and RPMI8226, were cultured in the presence or absence of HDACi; the broad inhibitors, panobinostat and vorinostat or the isoform-specific inhibitors, romidepsin (HDAC1i); BG45, entinostat and RG2833 (HDAC3i); and nexturastatA, ricolinostat, and tubastatinA (HDAC6i) for the indicated times (24, 48, 72 hours) and then, the expression levels of CD26 on myeloma cells were analyzed at each timepoints by flow cytometry. Although, cell surface CD26 expression levels on myeloma cell lines were relatively low or absent before treatment with each HDACi, an increase in CD26 expression levels was observed within 24 hours of the initiation of treatment. Moreover, CD26 levels increased further while exposure to each HDACi continued, and the maximum increase in CD26 expression was observed at 48 to 72 hours (Fig. 1B). Intriguingly, subsequent removal of the HDACi for 48 hours resulted in a decline of CD26 expression levels on myeloma cells to levels slightly positive or similar to pretreatment levels (Fig. 1B).

We also treated KMS27 and KMS28 with titrated concentrations of with panobinostat (0.5, 5.0, 50, 500 nmol/L), RG2833 (5.0, 50 nmol/L, 0.5, 1.0 μmol/L), and

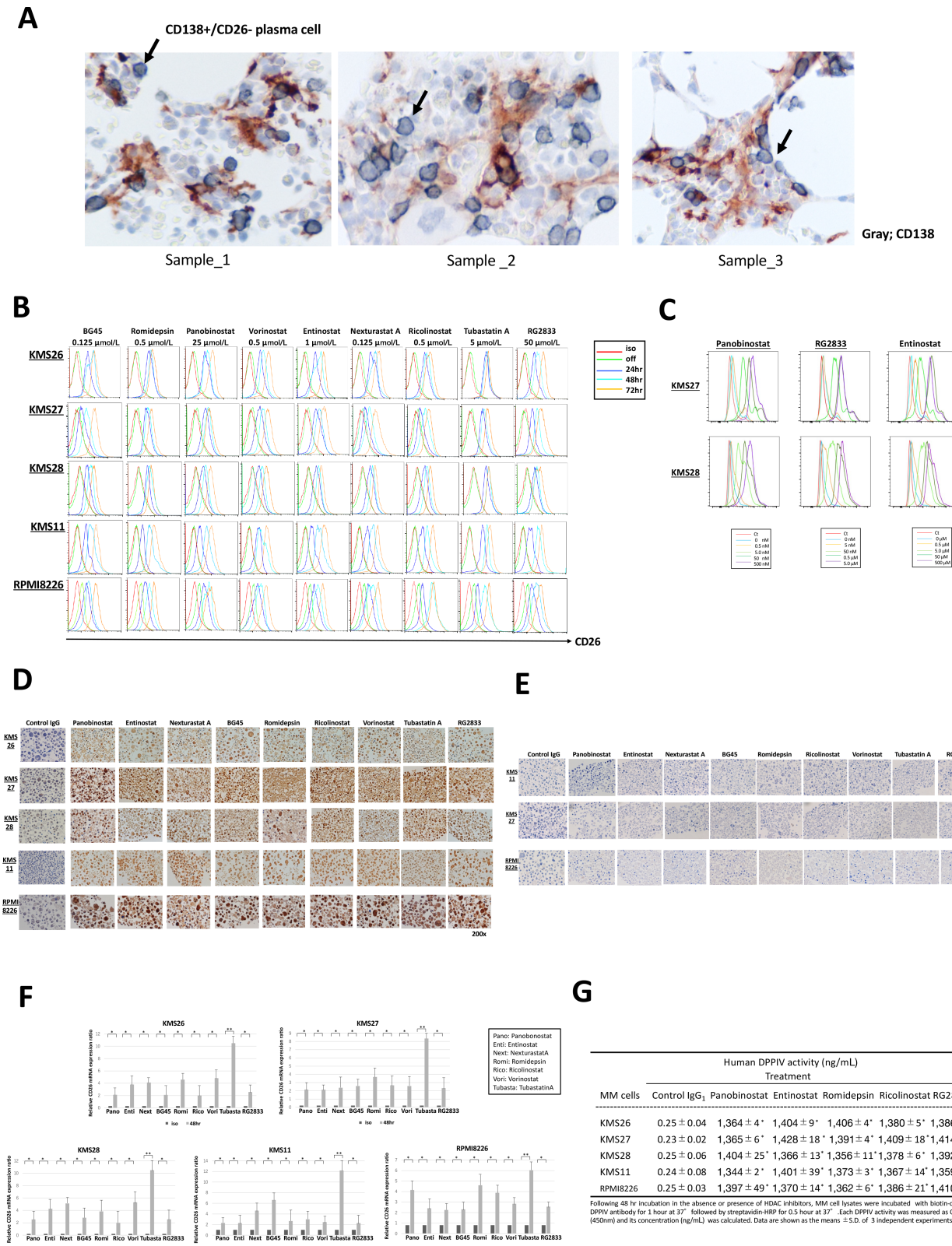

	Human DPPIV activity (ng/mL)				
	Treatment				
MM cells	Control IgG_1	Panobinostat	Entinostat	Romidepsin	Ricolinostat	RG2833
KMS26	0.25 ± 0.04	1,364 ± 4*	1,404 ± 9*	1,406 ± 4*	1,380 ± 5*	1,386 ± 7*
KMS27	0.23 ± 0.02	1,365 ± 6*	1,428 ± 18*	1,391 ± 4*	1,409 ± 18*	1,414 ± 9*
KMS28	0.25 ± 0.06	1,404 ± 25*	1,366 ± 13*	1,356 ± 11*	1,378 ± 6*	1,392 ± 10*
KMS11	0.24 ± 0.08	1,344 ± 2*	1,401 ± 39*	1,373 ± 3*	1,367 ± 14*	1,359 ± 12*
RPMI8226	0.25 ± 0.03	1,397 ± 49*	1,370 ± 14*	1,362 ± 6*	1,386 ± 21*	1,410 ± 23*

Following 48 hr incubation in the absence or presence of HDAC inhibitors, MM cell lysates were incubated with biotin-conjugate DPPIV antibody for 1 hour at 37° followed by streptavidin-HRP for 0.5 hour at 37° .Each DPPIV activity was measured as OD value (450nm) and its concentration (ng/mL) was calculated. Data are shown as the means ±S.D. of 3 independent experiments. *P<0.05.

FIGURE 1 Induction of CD26 expression on myeloma cell lines by HDACi. **A,** CD26 expression in plasma cells of bone marrow tissues of patients with multiple myeloma. Analysis of primary BM samples from several patients with multiple myeloma revealed that $CD138^{pos}$ plasma cells were rarely stained with CD26 (gray, CD138; red, CD26; original magnification, × 200). **B,** Flow cytometry with anti-CD26 (rat clone)-fluorescein (FITC) or isotype control IgG_1 was performed in five myeloma cell lines KMS11, 26, 27, 28, and RPMI8226. Overlay histograms show CD26 expression on myeloma cell lines before and after treatment with one of nine HDACi for the indicated times (24, 48, 72, and 48 hours after (*Continued on the following page.*)

(*Continued*) subsequent removal of each HDACi) at the indicated doses. HDACi elicited exposure time-dependent upregulation of CD26 expression on myeloma cells, whereas subsequent removal of HDACi resulted in a decline of CD26 expression to the decreased or near-pretreatment levels. **C,** KMS27 and KMS28 was incubated with titrated concentrations of panobinostat (0.5, 5.0, 50, and 100 nmol/L), RG2833 (5, 50 nmol/L, 0.5, and 5.0 μmol/L) and entinostat (0.5, 5.0, 50, and 500 μmol/L) for 48 hours, after which cells were harvested to analyze the levels of surface CD26 expression in myeloma cells by flow cytometry. Overlay histogram shows CD26 expression on each myeloma cell before and after 48 hours of treatment with each HDACi at the indicated doses. HDACi elicited a dose-dependent upregulation of CD26 expression on myeloma cells, whereas 5.0 μmol/L of RG2833 and 500 μmol/L of entinostat did not further/significantly enhance CD26 expression on myeloma cells, compared with 0.5 μmol/L of RG2833 and 50 μmol/L of entinostat. **D,** Myeloma cell lines KMS11, 26, 27, 28, and RPMI8226 were immunohistochemically stained for CD26 before and after treatment with one of nine HDACi. All tested myeloma cell lines cultured alone without each HDACi were either slightly stained for CD26 or completely lacked CD26 expression. In contrast, cell lines treated with each HDACi for 48 hours revealed moderate to intense CD26 expression (CD26, brown stain; original magnification, × 200). **E,** Thereafter, removal of the HDACi for 48 hours resulted in CD26 expression to the decreased or near-pretreatment levels again (CD26; brown-stained; original magnification, × 200). **F,** Expression levels of CD26 mRNA in myeloma cell lines KMS11, 26, 27, 28, and RPMI8226 before and after the treatment of one of nine HDACi for 48 hours were analyzed using real-time quantitative RT-PCR assay with specific primers for CD26 (Supplementary Table S1). The CD26 mRNA transcription levels in myeloma cell lines treated with each HDACi revealed a significant increase, compared with those of untreated myeloma cells. Results are shown as ratio of CD26mRNA/GAPDH mRNA. Bar diagrams represent the mean values ± SE. $n = 3$; *, $P < 0.05$; **, $P < 0.01$. **G,** The levels of DPPIV activity in supernatants derived from myeloma cell lines KMS11, 27, 28, and RPMI8226, cultured in the presence or absence of one of nine HDACi for 48 hours were determined by ELISA. The DPPIV levels in supernatants of myeloma cells, which were incubated in the presence of each HDACi were significantly elevated, compared with those of control IgG_1. The data represent the mean ± SE of triplicate wells from the representative of three independent experiments. The error bars represent the range, *, $P < 0.05$.

entinostat (0.5, 5, 50, 100 μmol/L) for 48 hours and observed a dose-dependent increase in CD26 expression on each myeloma cell by flow cytometry (Fig. 1C). Panobinostat-mediated increase in CD26 expression has been occurred at 0.5 nmol/L, whereas cytotoxicity against myeloma cells was not sufficient at this concentration. We observed a further increase in CD26 expression on myeloma cells following treatment with panobinostat at 5.0 to 50 nmol/L dose, correlated with dose-dependent enhanced anti-myeloma cytotoxic effect (Fig. 1C; Supplementary Fig. S1). Similarly, increasing concentrations of RG2833 or entinostat contributed to the enhanced expression levels of CD26 on myeloma cells at 5 nmol/L to 0.5 μmol/L dose of RG2833 as well as 0.5 to 50 μmol/L dose of entinostat. In parallel, more significant myeloma cell death was induced at 0.5 μmol/L dose of RG2833 and 50 μmol/L dose of entinostat. Although, higher doses of RG2833 at 5.0 μmol/L or entinostat at 500 μmol/L further reduced the viability of myeloma cells, these doses did not induce greater CD26 expression in myeloma cells anymore (Fig. 1C; Supplementary Fig. S1) Collectively, HDACi by both broad and isoform-selective inhibitors exposure-time dependently as well as dose-dependently induced the upregulation of CD26 protein expression on myeloma cells.

To verify whether upregulation of CD26 in each myeloma cell was induced by nonspecific effects due to drug-induced cell stress, we additionally examined the impacts of bortezomib or melphalan on CD26 modulation in each myeloma cell by flow cytometry. Indeed, neither agents altered the expression levels of CD26 in KMS11, 26, 27, 28, and RPMI8226, regardless of the duration of their treatment (Supplementary Fig. S2).

IHC analysis also revealed that myeloma cells that remained untreated with HDACi expressed low or slightly detectable level of CD26, whereas myeloma cells treated with each HDACi for 48 hours showed moderately or intensely stained CD26 expression (Fig. 1D). Subsequently, removal of the HDACi for 48 hours resulted in the expression levels of CD26 on myeloma cells to the reduced or near-pretreatment levels again (Fig. 1E).

Next, to assess the impact of HDACi on CD26mRNA transcription in myeloma cells, we performed qRT-PCR analysis to measure the expression of CD26mRNA in myeloma cell lines. In the current study, the cDNA of myeloma cells, preincubated for 48 hours with or without each HDACi, was used for qPCR amplification of CD26 with specific primers (Supplementary Table S2). The CD26mRNA levels in each myeloma cell line were significantly increased on treatment with each HDACi (Fig. 1F). These data demonstrated that the induction of CD26 protein in myeloma cells is paralleled with an increase in CD26 mRNA transcription and therefore occurs at the level of CD26 gene transcription. Moreover, ELISA analysis showed that increased DPPIV enzymatic activity in myeloma cells treated with each HDACi for 48 hours was correlated with the induction of CD26 protein in myeloma cells (Fig. 1G).

In addition, we analyzed whether each HDACi modulates the expression of other cell surface molecules used as therapeutic targets of multiple myeloma. The expression levels of CD38 were time-dependently increased in KMS11 on treatment with each HDACi excluding entinostat, whereas levels of CD38 were upregulated in KMS27 and RPMI8226 only on treatment with tubastatinA (Supplementary Fig. S3–S5). Moreover, BCMA expression was significantly upregulated in KMS27 and RPMI8226 treated with tubastatinA. SLAMF7/CS1 expression was also markedly enhanced in KMS11 and RPMI8226, treated with tubastatinA (Supplementary Fig. S3–S5).

Synergistic Anti-myeloma Efficacy of HDACi plus Humanized Anti-CD26mAb Against $CD26^{neg}$ Myeloma Cells

We demonstrated that HDACi retains the ability to induce the increased expression levels of CD26 on $CD26^{neg}$ myeloma cells, both at the mRNA and protein levels. Furthermore, we investigated the impact of HDACi on the viability of $CD26^{neg}$ myeloma cells in the presence or absence of CD26mAb. We pretreated myeloma cell lines KMS11, 26, 27, 28, and RPMI8226 with one of nine HDACi for 48 hours. Thereafter, these cells were treated with CD26mAb at 10 μg/mL or isotype control IgG_1 and additionally incubated for 24 hours in the presence or absence of human NK effector cells at an E/T ratio of 20:1 and then, the viability of each myeloma cell line was analyzed by antibody-dependent cellular cytotoxicity (ADCC) assay. The results showed that the treatment with each HDACi as a single agent induced significant myeloma

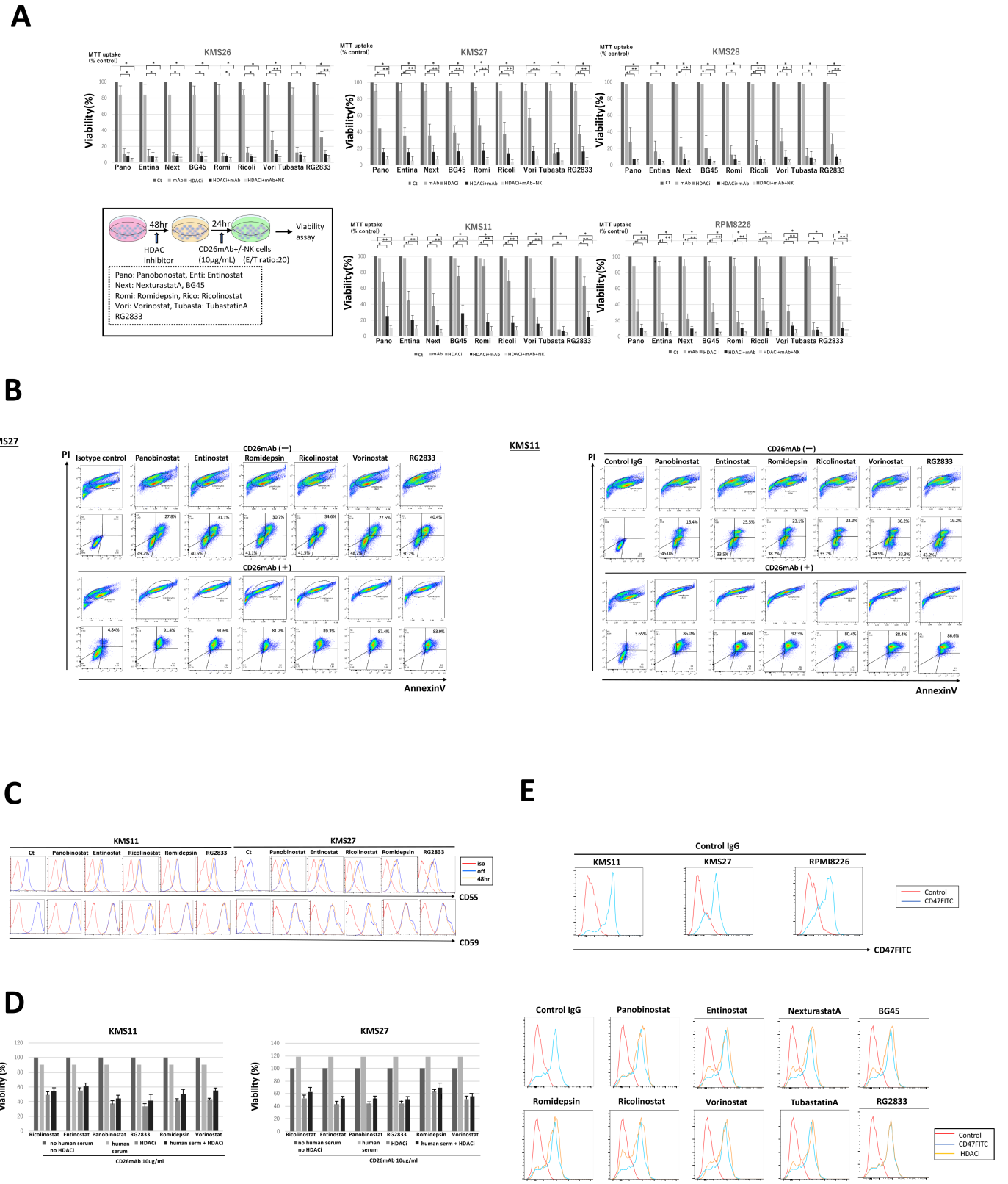

FIGURE 2 The effects of HDACi on the viability of CD26^{neg} myeloma cell lines treated with humanized anti-CD26 monoclonal antibody (CD26mAb). **A,** Cytotoxicity of CD26mAb against myeloma cell lines KMS11, 26, 27, 28, and RPMI8226 is shown with or without the treatment of HDACi. First, myeloma cells were pretreated with one of nine HDACi for 48 hours, followed by additional incubation with either CD26mAb at a concentration of 10 μg/mL or isotype control IgG$_1$ for 24 hours in the presence or absence of human NK effector cells at an E/T ratio of 20:1 and then, the viability of target myeloma cells was analyzed by the luciferase assay. Bar diagrams, indicating the percentage of viable (*Continued on the following page.*)

(*Continued*) myeloma cells show that CD26mAb alone did not induce significant lysis of $CD26^{neg}$ myeloma cells, whereas, the combination with HDACi plus CD26mAb synergistically facilitated lysis of $CD26^{neg}$ myeloma cells via direct effects as well as via NK effector cell-mediated ADCC by mAb. The data represent the mean ± SE of triplicate wells from the representative of three independent experiments. The error bars represent the range, *, $P < 0.05$; **, $P < 0.01$. **B,** KMS11 and KMS27 contained residual viable cell populations, which existed (Annexin/PI) after monotherapy with one of six HDACi for 48 hours. In contrast, combination with each HDACi plus CD26mAb overcame this refractoriness and synergistically augmented lysis of $CD26^{neg}$ cell populations in KMS11 and KMS27, which were refractory to HDACi or CD26mAb treatment as a single agent. **C,** Levels of CIPs (CD55, CD59) in myeloma cells in the presence or absence of one of five HDACi were examined using flow cytometry. Myeloma cells were positive for both CD55 and CD59 both before and after treatment with each HDACi. The expression levels of these proteins in myeloma cells underwent minor or no changes following treatment with each HDACi. **D,** The CDC lysis against $CD26^{neg}$ myeloma cells on treatment with CD26mAb was examined after the exposure to one of five HDACi for 48 hours. Incubation of target myeloma cells was performed for 1 hour in the presence of human serum plus CD26mAb at a concentration of 10 μg/mL or control IgG_1. No marked CDC lysis by CD26mAb was observed against myeloma cells, regardless of the pretreatment with each HDACi. **E,** The expression levels of CD47 in myeloma cell lines were examined by flow cytometry; KMS11, 27, and RPMI8226 were intensely stained with CD47. In addition, KMS11 was treated with each HDACi for 48 hours and the CD47 expression was also analyzed. Treatment with each HDACi resulted in no alterations in CD47 expression levels of KMS11.

cell death in KMS26 and KMS28, whereas KMS27 and KMS11 contained cell populations that were refractory to the treatment with each HDACi alone (Fig. 2A). Furthermore, although monotherapy with CD26mAb did not induce significant lysis of $CD26^{neg}$ myeloma cells in any of myeloma cell line, treatment with HDACi plus CD26mAb in combination synergistically facilitated lysis of $CD26^{neg}$ myeloma cells via direct effects as well as NK cell–mediated ADCC by CD26mAb and this combined treatment overcame the therapeutic refractoriness of $CD26^{neg}$ myeloma cells to CD26mAb (Fig. 2A). In particular, the combination with HDACi plus CD26mAb readily augmented the lysis of $CD26^{neg}$ cell populations in KMS27 or KMS11 that were refractory to treatment with HDACi or mAb alone (Fig. 2B).

To further explore the mechanisms that contribute to the refractoriness of myeloma cells toward CD26mAb therapy, we assessed the levels of complement inhibitory proteins (CIP) CD55 and CD59 in myeloma cells incubated with one of five HDACi for 48 hours. CIPs protect myeloma cells from a complement attack via complement-dependent cytotoxicity (CDC) by mAb (36); therefore, the elevated expression levels of CIPs observed in untreated myeloma cells indicate the inhibition of CDC by CD26mAb in myeloma cells. Moreover, the expression levels of these CIP proteins underwent only minor changes and were similar between HDACi-treated and nontreated cells (Fig. 2C). Consistent with our previous data (29), these results suggest that the induction of CD26 in myeloma cells by HDACi does not enhance CDC activity by CD26mAb against $CD26^{neg}$ myeloma cells (Fig. 2D).

CD47 expression in myeloma cells also leads to immune evasion through its interaction with signal regulatory proteins on dendritic cells or macrophages (37). Therefore, CD47 blockade may offer a therapeutic approach for preventing the immune escape of tumor cells. Indeed, the basal expression levels of CD47 were high in KMS11, KMS27, and RPMI8226. Furthermore, CD47 expression levels in KMS11 were shown to be sustained, but revealed no changes on treatment with each HDACi; this finding may be associated with therapeutic refractoriness (Fig. 2E).

Transcriptomic Alterations in Myeloma Cells, Treated with HDACi ± CD26mAb versus Untreated Cells

To gain the insight into the mechanisms by which HDACi modifies myeloma cell function, we analyzed the transcriptomic profiles of three myeloma cell lines in response to treatment with HDACi by either broad or isoform-specific inhibitor in the presence or absence of CD26mAb, compared with control IgG_1, further we identified the sets of genes with significantly altered expression levels. Briefly, KMS11, 27, and RPMI8226 were treated with panobinostat or RG2833 for 48 hours, followed by additional incubation with the CD26mAb for 24 hours and then, changes of mRNA expression levels in each myeloma cell line was explored at each timepoint (Fig. 3A). We showed that each myeloma cell line exhibited the majority of changes relative to control IgG_1 in the expression levels of mRNA transcripts following treatment with each HDACi, regardless of the presence or absence of CD26mAb (Fig. 3B). Transcriptomic profiles revealed that 27 and 26 genes, respectively were commonly upregulated in all three myeloma cell lines following treatment with panobinostat or RG2833. Of these genes, 16 genes were most significantly upregulated and shared by both HDACi (log_2 fold change > 20 to the control with $P < 0.05$; Fig. 3C). On the other hand, 229 and 46 genes, respectively were commonly downregulated in all three myeloma cell lines following treatment with panobinostat or RG2833. Of these genes, 36 genes were most significantly downregulated and sheared by both HDACi (log_2 fold change <−10) to the control with P value < 0.05; Fig. 3D). Moreover, of these overlapped 36 genes, 23 genes with consistently decreased expression levels were identified excluding 13 noncoding genes (log_2 fold change <−10) to the control with P value < 0.05; Fig. 3E; Supplementary Table S3). These results suggest that myeloma cells treated with HDACi alone as well as with HDACi plus CD26mAb in combination exhibited similar and distinct gene expression signatures, compared with those treated with control IgG_1. Furthermore, the downregulated genes shared among the three myeloma cell lines and treatment with both HDACi contained factors involved in cell cycle regulation, cell proliferation, cell differentiation, and apoptosis of cells such as Myc and Pim-2: the inhibition of which is associated with cell cycle arrest and apoptosis of myeloma cells (refs. 38–40; Fig. 3E and F). Notably, the majority of human cancers present with overexpression of Myc, which we also validated using qPCR analysis. Indeed, Myc expression affects gene instability and tumorigenesis via the activation or repression of a number of target genes as well as by the regulation of the gene promoter (38, 39). In addition, Myc expression is reportedly further upregulated during the course of disease progression in multiple myeloma (41). Therefore, next we sought to explore whether Myc regulation may contribute to the CD26 induction of in myeloma cells by HDACi.

The 5′-flanking Region of the Human CD26 Gene

The human CD26 gene, located on chromosome 2 (2q24.3): contains 300 bp of the 5′-flanking region (−359 to +1) which includes potential binding sites

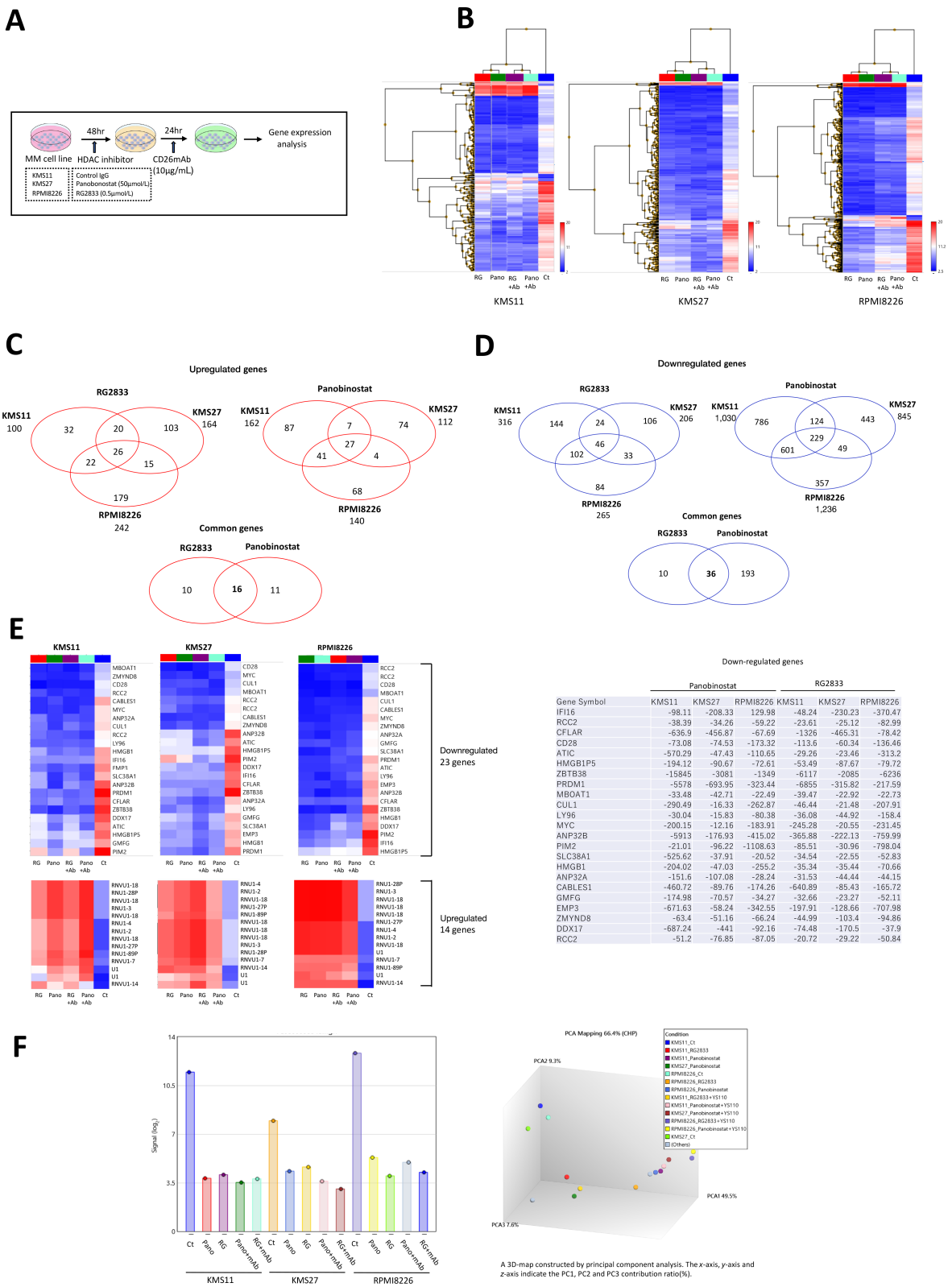

Down-regulated genes

	Panobinostat			RG2833		
Gene Symbol	KMS11	KMS27	RPMI8226	KMS11	KMS27	RPMI8226
IFI16	-98.11	-208.33	129.98	-48.24	-230.23	-370.47
RCC2	-38.39	-34.26	-59.22	-23.61	-25.12	-82.99
CFLAR	-636.9	-456.87	-67.69	-1326	-465.31	-78.42
CD28	-73.08	-74.53	-173.32	-113.6	-60.34	-136.46
ATIC	-570.29	-47.43	-110.65	-29.26	-23.46	-313.2
HMGB1P5	-194.12	-90.67	-72.61	-53.49	-87.67	-79.72
ZBTB38	-15845	-3081	-1349	-6117	-2085	-6236
PRDM1	-5578	-693.95	-323.44	-6855	-315.82	-217.59
MBOAT1	-33.48	-42.71	-22.49	-39.47	-22.92	-22.73
CUL1	-290.49	-16.33	-262.87	-46.44	-21.48	-207.91
LY96	-30.04	-15.83	-80.38	-36.08	-44.92	-158.4
MYC	-200.15	-12.16	-183.91	-245.28	-20.55	-231.45
ANP32B	-5913	-176.93	-415.02	-365.88	-222.13	-759.99
PIM2	-21.01	-96.22	-1108.63	-85.51	-30.96	-798.04
SLC38A1	-525.62	-37.91	-20.52	-34.54	-22.55	-52.83
HMGB1	-204.02	-47.03	-255.2	-35.34	-35.44	-70.66
ANP32A	-151.6	-107.08	-28.24	-31.53	-44.44	-44.15
CABLES1	-460.72	-89.76	-174.26	-640.89	-85.43	-165.72
GMFG	-174.98	-70.57	-34.27	-32.66	-23.27	-52.11
EMP3	-671.63	-58.24	-342.55	-197.91	-128.66	-707.98
ZMYND8	-63.4	-51.16	-66.24	-44.99	-103.4	-94.86
DDX17	-687.24	-441	-92.16	-74.48	-170.5	-37.9
RCC2	-51.2	-76.85	-87.05	-20.72	-29.22	-50.84

FIGURE 3 Transcriptomic profiles in three myeloma cell lines, either treated or untreated with HDACi or HDACi plus CD26mAb. **A,** Schema of transcriptomic analysis of three myeloma cell lines KMS11, 27, and RPMI8226, treated with one of two HDACi by panobinostat (50 μmol/L) or RG2833 (0.5 μmol/L) or HDACi plus CD26mAb in combination. **B,** Three myeloma cell lines were treated with panobinostat (50 μmol/L) or RG2833 (0.5 μmol/L) for 48 hours, followed by additional incubation with CD26mAb for 24 hours and transcriptomic profiles in each myeloma cell line were analyzed at each timepoints using microarray analysis. The heat maps show normalized relative mRNA expression differences, based on $\log_2$ fold change, with a cut-off *P* value <0.05. The color scale of the heat map from blue to red indicates low to (*Continued on the following page.*)

(*Continued*) high expression. **C,** Venn diagrams showing overlap in the most significantly upregulated genes (log_2 fold change >10, with a cut-off *P* value <0.05) among three myeloma cell lines treated with either panobinostat (50 μmol/L) or RG2833 (0.5 μmol/L) for 48 hours compared with the isotype control IgG_1. **D,** Venn diagrams showing overlap in the most significantly downregulated genes (log_2 fold change <−10, with a cut-off *P* value <0.05) among three myeloma cell lines treated with either panobinostat (50 μmol/L) or RG2833 (0.5 μmol/L) for 48 hours compared with the isotype control IgG_1. **E,** Among the 36 downregulated genes common to all three myeloma cell lines with the treatment of either panobinostat or RG2833, overlapped 23 genes excluding 13 noncoding genes were identified (log_2 fold change <−10, with a cut-off *P* value<0.05). The values show the fold changes of mRNA expression of transcripts in each myeloma cell line treated with each HDACi or either HDACi plus CD26mAb compared with control IgG_1. The color scale of the heat map from blue to red indicates low to high expression. Similarly, among the 16 genes, commonly upregulated in all three myeloma cell lines on treatment with each HDACi, overlapped 14 genes excluding noncoding genes were indicated. **F,** Left, c-Myc gene signal (log_2) in KMS11, KMS27, and RPMI8226, treated with isotype control IgG_1, HDACi; panobinostat or RG2833 and HDACi plus CD26mAb were shown. Myc is one of the genes, significantly downregulated in common, excluding noncoding genes in three myeloma cell lines following treatment with each HDACi or either HDACi plus CD26mAb. Right, A three-dimenisonal MAP was constructed by principal component analysis, indicating gene expression patterns based on transcriptome analysis.

for several transcriptional factors related to cell proliferation and differentiation such as Sp1 (specificity protein 1), Ap2, BRE (butyrate-responsive element), and HNF (hepatic nuclear factor 1; refs. 42, 43; Fig. 4). In particular, the 89 bp of G-C rich region (−91 to −3 relative to the translation initiation site), located at the proximal 5′-flanking region just upstream of the transcription initiation site, is essential for CD26 promoter activity (ref. 44; Fig. 4).

Sp1 is a transcription factor that is expressed in several solid tumor cells as well as in myeloma cells. Overexpression of Sp1 is involved in tumor progression or metastasis via regulation of the expression of Sp1-responsive genes related to cell growth, apoptosis, and angiogenesis (45, 46). These genes contain G-C rich regions, that is, G-C boxes on the promoter that interacts with Sp1 (47).

Indeed, the CD26 gene contains G-C boxes for Sp1 binding at both the proximal and distal regions within the promoter which regulate the expression of proto-oncogenes such as Myc, ras, and pim-1 (refs. 42, 43; Fig. 4). Furthermore, c-Myc not only affects proliferation, apoptosis, and metabolism in tumor cells via its modification but also forms complexes with Sp1 on several promoters and titrates the levels of Sp1, thereby affecting the promoter activity of several genes (47). Consequently, we postulated that modulation of c-Myc may play several roles in regulation of the CD26 promoter in myeloma cells. We therefore sought to elucidate the epigenetic impacts of histone as well as c-Myc as non-histone on the CD26 promoter of myeloma cells in the absence or presence of HDACi and determine whether it results in the induction of CD26 expression in myeloma cells.

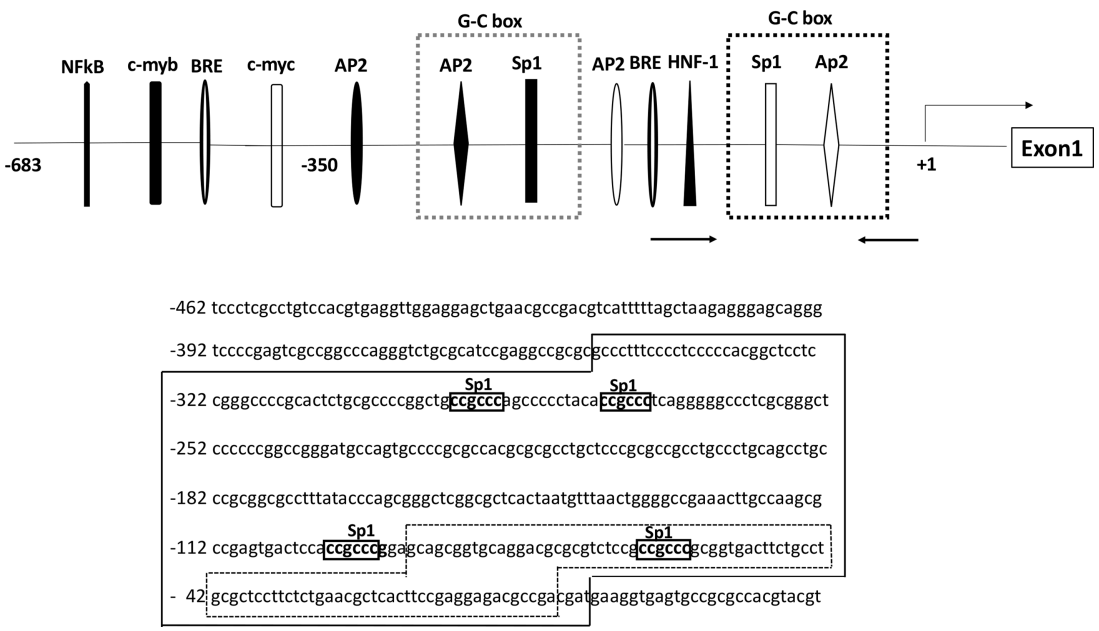

FIGURE 4 The 5′-flanking region of the human CD26 gene. The schematic representation of the 5′-flanking region of the human CD26 gene promoter constructs and the associated nucleotide sequences is shown. The 5′-flanking region of the CD26 gene contains 300 bp (−359 to +1) and incorporates potential binding sites for several transcriptional factors including G-C boxes for the binding of Sp1 and AP2, BRE, and HNF, the relative locations of which are indicated by the symbols in the figure. In particular, 89 bp of the G-C rich region (−91 to −3 relative to the translation initiation site) in the proximal 5′-flanking region is essential for CD26 promoter activity. The nucleotide sequences including the 5′-flanking region of the CD26 promoter are also shown. Position +1 indicates the initiation of the coding region in exon1. The nucleotide sequence has been shown in the GeneBank database with the accession number of AH005372.

HDACi Acetylates Histone 3 Protein on the CD26 Promotor Region of Myeloma Cells

First, we examined the epigenetic status in histone protein on the CD26 promoter region of myeloma cells after treatment with HDACi. ChIP assays were conducted on five myeloma cell lines, either treated or not treated with one of three HDACi, that is, panobinostat, RG2833 and tubasatinA, for 48 hours. The DNAs of immunoprecipitated chromatin of each myeloma cell line were analyzed using real-time qPCR with specific primers to amplify the CD26 promoter region (Supplementary Table S1). It was demonstrated that an increased levels of acetylation in histone 3 lysine 27 (H3K27) was detected on the CD26 promoter of each myeloma cell line after exposure to HDACi, suggesting its part of roles in the mechanisms involved in HDACi-dependent CD26 promoter activation in myeloma cells (Fig. 5A).

c-Myc Binds to the CD26 Promoter of Myeloma Cells Through Sp1 on the Proximal G-C Box

Next, we explored the epigenetic impacts of c-Myc on the CD26 promoter of myeloma cells and determined whether these contributed to the induction of CD26 expression in myeloma cells. We first examined the expression levels of c-Myc mRNA in five myeloma cell lines following the treatment with one of nine HDACi (Fig. 5B) and the significant reductions in mRNA expression levels of each myeloma cell were validated after 48 hours of exposure to each HDACi. Subsequently, the time course changes in c-Myc expression levels in KMS11, 27, and RPMI8226 with or without treatment by panobinostat or RG2833, were assessed in detail using real-time qPCR and immunoblotting (Fig. 5B and C). The expression levels of c-Myc were exposure time-dependently decreased both at mRNA and protein levels in myeloma cell lines on treatment with each HDACi (Fig 5B and C). Moreover, c-Myc was still significantly downregulated after 12 to 24 hours of exposure to each HDACi, which was fully consistent with the transcriptomic profiles of myeloma cell lines in the presence or absence of HDACi, as shown in Fig. 3E and F. Furthermore, the addition of cycloheximide did not restore HDACi-mediated c-Myc reduction in myeloma cells, implying that the c-Myc expression is regulated in myeloma cells not only transcriptionally and translationally but also posttranslationally (Supplementary Fig. S6). In addition, the acetylation status of c-Myc in each myeloma cell line was investigated in the presence or absence of each HDACi. The acetylation of c-Myc on lysine 323 (K323Ac) in each myeloma cell line was evident after 3 to 6 hours of exposure to panobinostat and was further increased after 12 to 24 hours of its exposure. It was also potentiated after 12 to 24 hours of the exposure to RG2833 (Fig. 5C). These results indicated that the expression levels of c-MycK323ac were time-dependently increased in myeloma cells after treatment with each HDACi and were inversely correlated with the time-dependent decrease in c-Myc expression (Fig. 5C). On the other hand, expression levels of both c-Myc and acetylated c-Myc were unaltered in normal human mononuclear cells on treatment with HDACi, implying that c-Myc regulation in myeloma cells is a tumor-specific process (Fig. 5C).

We further investigated the interaction between c-Myc and the CD26 promoter in myeloma cells with or without treatment by HDACi. ChIP analysis was conducted in KMS11, 27, and RPMI8226 in the presence or absence of panobinostat or RG2833 at the indicated times (3.0, 6.0, 12, 24 hours) using antibodies for c-Myc and c-MycK323ac. Thereafter, DNAs of immunoprecipitated chromatin in each myeloma cell line were subjected to qPCR to amplify the CD26 promoter region, including the proximal G-C box (Supplementary Table S1). It was revealed that the recovery percentages of IP/INPUT, indicating the binding of c-Myc to the CD26 promoter via the proximal G-C box was exposure time-dependently decreased on treatment with HDACi, whereas the binding of c-MycK323ac to the promoter showed a time-dependent increase in each myeloma cell line following treatment with HDACi. These findings suggest that the occupancy of c-Myc was replaced by that of c-MycK323ac on the CD26 promoter of myeloma cells on treatment with HDACi (Fig 5D).

Finally, on the basis of these observations, we further examined the interaction between c-Myc and Sp1 on the CD26 promoter of myeloma cells in the presence or absence or HDACi. DNAs of chromatin, immunoprecipitated by ChIP and re-ChIP assay using antibodies for Sp1 and c-Myc in each myeloma cell line, either treated or untreated with each HDACi for the indicated times (3.0, 6.0, 12, 24 hours), were subject to qPCR and amplified at the CD26 promoter, including the proximal G-C box (Supplementary Table S1). The recovery percentages of IP/INPUT, indicating the binding of c-Myc to the Sp1 was exposure time-dependently reduced on the CD26 promoter of myeloma cells on treatment with each HDACi (Fig. 5E).

These results suggest that in the absence of HDACi, c-Myc is attached to the CD26 promoter via binding to Sp1 and thereby represses the promoter, leading to interruption of CD26 transcription in myeloma cells. In contrast, in the presence of HDACi, c-Myc is detached from the CD26 promoter via Sp1 with the increased acetylation of c-MycK323 and the promoter is thereby activated, leading to initiation of CD26 transcription as well as activation of cytotoxicity in several myeloma cells (Fig 5F).

The Effect of HDACi and CD26mAb on the Activity of Human NK Cells in Multiple Myeloma

NK cells are crucial mediators of ADCC against myeloma cells by mAb therapy targeting CD38, CS1, and BCMA in multiple myeloma. Moreover, our previous study revealed that IMiDs potentiated human NK cell activity, leading to enhanced ADCC by CD26mAb against $CD26^{pos}$ myeloma cells (29).

To clarify the effect of HDACi or CD26mAb on NK cell activity in multiple myeloma, the expression levels of CD26 in NK cells in the presence or absence of one of nine HDACi was explored. Flow cytometry analysis showed that human NK cells exhibited high expression levels of CD26: these expression levels were not significantly affected by exposure to either HDACi or CD26mAb for the indicated times (24, 48, 72 hours; Fig. 6A and B). Furthermore, the effects of HDACi or CD26mAb on the viability of NK cells were assessed using MTT assay. Our findings demonstrated that although both HDACi and CD26mAb moderately affected the viability of NK cells, its viability did not show significant change, implying that ADCC activity against myeloma cells is likely not severely disrupted by treatment with HDACi plus CD26mAb in combination.

Discussion

Recent development of novel antibody and cellular-based therapies, directly targeting antigens such as BCMA on myeloma cells has resulted in durable responses in patients with RRMM (8–18). Our previous studies demonstrated favorable preclinical results showing potent *in vitro* and *in vivo* cytotoxic efficacy of CD26mAb against both $CD26^{pos}$ myeloma cells and $CD26^{pos}$ osteoclasts in multiple myeloma (28, 29). However, BM tissues of patients with multiple myeloma revealed heterogeneous and sometimes decreased expression levels of CD26 in plasma cells in contrast to osteoclasts in which CD26 is uniformly and intensely expressed (refs. 28, 29; Fig. 1). These results might indicate barriers to elicit robust responses in multiple myeloma by CD26mAb.

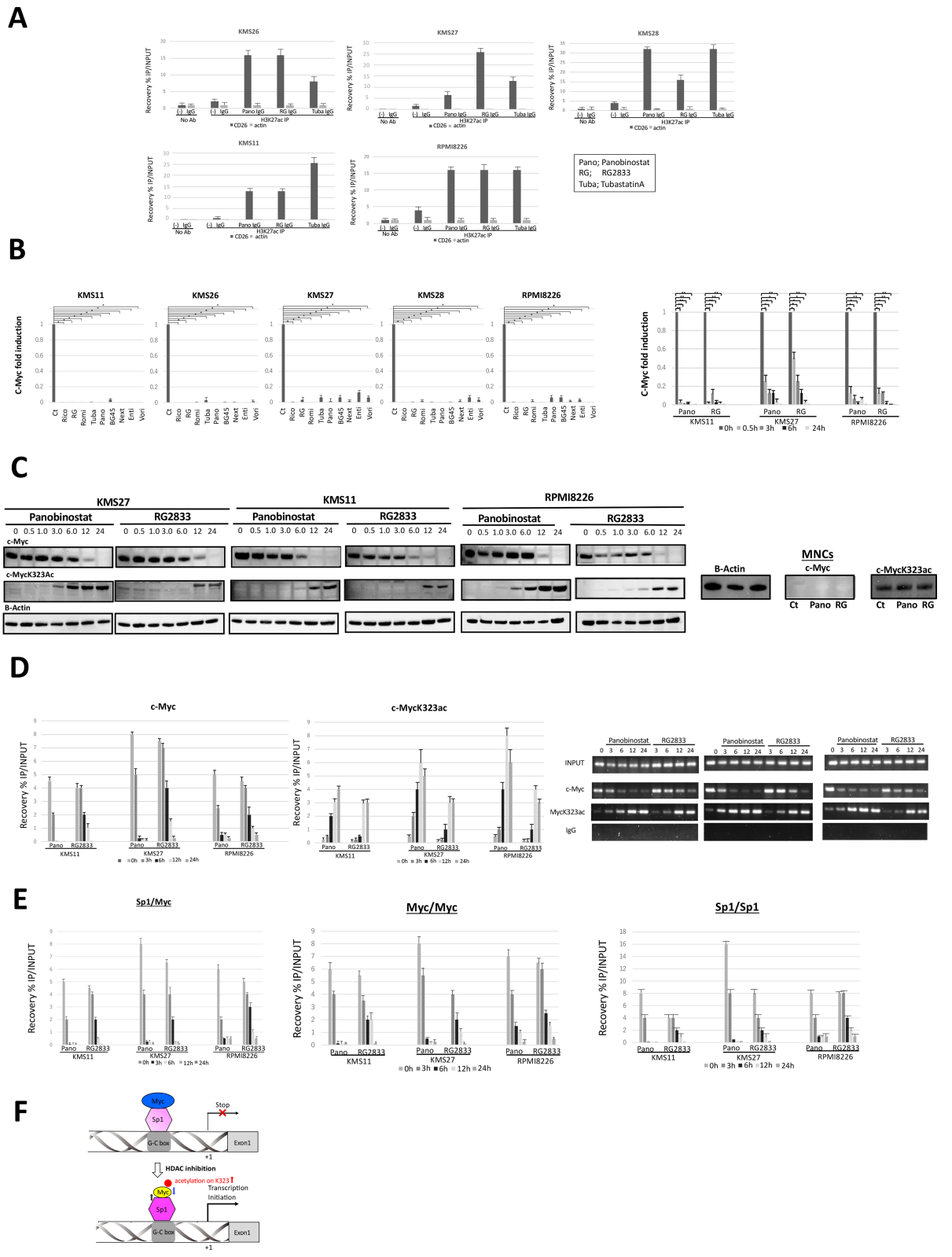

FIGURE 5 Epigenetic modification at the CD26 promoter of myeloma cells on treatment with HDACi. **A,** The effects of HDACi on histone H3 acetylation on the CD26 promoter of myeloma cells are shown. Myeloma cell lines KMS11, 26, 27, 28, and RPMI8226, treated with either panobinostat (50 μmol/L), RG2833 (0.5 μmol/L), or tubastatinA (2.5 μmol/L) or control IgG_1 for 48 hours were investigated by ChIP assay using anti-histone 3 on lysine 27 acetylated (H3K27Ac) antibody or rabbit IgG and then, the DNAs of immunoprecipitated chromatin were amplified and quantified by real-time qPCR with the primer pairs for the CD26 promoter shown in Supplementary Table S1. NoAb means (*Continued on the following page.*)

(*Continued*) samples prepared without antibodies as a control and INPUT indicates that PCR was performed with genomic DNA. Increased levels of acetylation at H3K27 was observed on the CD26 promoter of myeloma cells treated with each HDACi, compared with control IgG_1. Values represent percentage of IP/INPUT. Bars represent the mean ± S.D. of three independent experiments done in triplicate. **B,** qRT-PCR for c-Myc expression in myeloma cell lines KMS11, 26, 27, 28, and RPMI8226 treated with one of nine HDACi, namely, BG45 (1 μmol/L), romidepsin (0.125 μmol/L), ricolinostat (0.5 μmol/L), panobinobinostat (50 μmol/L), entinostat (50 μmol/L), nexturastatA (0.125 μmol/L), vorinostat (1 μmol/L), tubastatinA (25 μmol/L), RG2833 (0.5 μmol/L), or control IgG for 48 hours. The expression of c-Myc mRNA was significantly reduced in each myeloma cell line after exposure to each HDACi for 48 hours (*, $P < 0.01$). Furthermore, the expression levels of c-Myc mRNA in KMS11, 27, and RPMI8226 were examined at the indicated times (3.0, 6.0, 12, 24 hours) following treatment with panobinostat or RG2833 (*, $P < 0.05$; **, $P < 0.01$). The expression levels of c-Myc were normalized to that of GAPDH and quantified by the $2^{-\Delta\Delta Ct}$ method. Data are shown as the ratio of c-Myc mRNA/GAPDH mRNA and represent the means ± S.D. of three independent experiments. **C,** Expression levels of c-Myc and c-MycK323ac protein in KMS11, 27, and RPMI8226 were examined in the presence or absence of panobinostat (50 μmol/L) or RG2833 (0.5 μmol/L) at the indicated times (0.5, 1.0, 3.0, 6.0, 12, 24 hours) by immunoblotting. Levels of these proteins in normal MNCs, incubated with panobinostat, RG2833 or control IgG_1 for 24 hours were also analyzed. **D,** To investigate the binding of c-Myc and c-MycK323ac to the CD26 promoter of myeloma cells, KMS11, 27, and RPMI8226 were treated with panobinostat (50 μmol/L), RG2833 (0.5 μmol/L), or control IgG_1 for the indicated times (3.0, 6.0, 12, 24 hours) and then, ChIP assays were conducted in each myeloma cell using anti-c-Myc or c-MycK323ac antibody or rabbit IgG. Thereafter, the DNAs of each immunoprecipitated chromatin suspension were amplified and quantified by real-time qPCR with specific primers for the CD26 promoter via the proximal G-C box (Supplementary Table S1). The recovery of ChIP's DNAs was calculated as the percentages of IP/INPUT. The time-dependent decrease of the binding of c-Myc to the promoter, concomitant with a time-dependent increase in the binding of c-MycK323ac to the promoter, was observed in each myeloma cell line treated with each HDACi, compared with control IgG_1. Bars represent the mean ± S.D. of three independent experiments done. The amplified products were also visualized by MIDORI^{green} Direct staining following 1.5% agarose gel electrophoresis. Representative data of 40 cycles are shown. INPUTs show that PCR was conducted with genomic DNA. The actin signal shows equal loading as a control. **E,** The binding of c-Myc to the transcriptional factor, Sp1 in myeloma cell lines is shown after exposure to each HDACi. The binding of c-Myc to the Sp1 on the CD26 promoter via the proximal G-C box of KMS11, 27, and RPMI8226 after exposure to panobinostat (50 μmol/L) or RG2833 (0.5 μmol/L) was examined by ChIP and re-ChIP assay using antibodies for c-Myc and Sp1, followed by real-time qPCR using specific primers to amplify the CD26 promoter, including the proximal G-C box. The recovery of ChIP's DNAs was calculated as the percentages of IP/INPUT for each sample. In the absence of HDACi, c-Myc binds to the Sp1 on the proximal G-C box of the CD26 promoter in each myeloma cell line, whereas in the presence of HDACi, this binding was time-dependently detached. Bars represent the mean ± S.D. of three independent experiments. **F,** Schema of HDACi-regulated CD26 induction in myeloma cells.

In the current study, we demonstrated that epigenetic regulation by HDACi in myeloma cells, especially isoform-selective inhibition of HDAC1, 2, 3, and 6 as well as broad inhibition induces an increase in CD26 transcripts by RT-PCR and CD26 protein expression by flow cytometry and IHC. Therefore, concurrent use of HDACi conferred superior cytotoxic efficacy of CD26mAb against CD26^{neg} myeloma cells or those with CD26 antigen loss. Consequently, we further elucidated the precise mechanisms involved in the induction of CD26 expression in myeloma cells by HDACi.

Comparison of the transcriptomic profiles of three myeloma cell lines between those treated with HDACi by broad or isoform-selective inhibitor and those left untreated identified Myc as one of the aberrantly deregulated genes, which is known to be a hallmark in the majority of human cancers: it regulates cell proliferation, differentiation, and apoptosis via regulation of a number of target genes and is involved in tumorigenesis (38, 48, 49). HDACs are known to have majority of substrates including histone and non-histone proteins which are involved in biological processes such as cell proliferation, differentiation, apoptosis, and cell death. In particular, non-histone proteins regulate the activity of tumor suppressor genes and oncogenes which have crucial roles in tumorigenesis (30, 31). Therefore, HDACi induce different phenotypes in tumor cells and antitumor effects via cell cycle arrest, activation of apoptosis, mitotic cell death, autophagic cell death, and reactive oxygen species–induced cell death (30, 31). The c-Myc is one of the non-histone proteins as a substrate of HDACs, which is also subject to posttranslational modifications such as phosphorylation, acetylation, and ubiquitinylation (39). It plays crucial roles in the development of plasma cell malignancies during the progression from monoclonal gammopathy of unknown significance to smoldering multiple myeloma, symptomatic multiple myeloma, and plasma cell leukemia (41, 48, 49). Moreover, BM microenvironment upregulates c-Myc, thereby promoting myeloma cell growth. Therefore, Myc may become an attractive therapeutic target for the treatment of multiple myeloma (48, 49). The c-Myc is strongly modulated (i.e., downregulated or acetylated) by HDACi, which correlates with cell cycle arrest and apoptosis of cells via restoring the expression of genes aberrantly repressed in tumor cells, leading to tumor reduction (38, 48, 49). Indeed, in the current study, we validated the time-dependent reduction of c-Myc as well as an increase of c-MycK323ac in myeloma cell lines on treatment with class I/II and class I HDACi, compared with those treated with control IgG_1 at protein levels (Fig. 5C), but not in human normal MNCs, highlighting that c-Myc modification by HDACi is tumor-selective and may correlate with cytotoxic response in myeloma cells.

Our results demonstrated that the cell surface CD26 expression in KMS26, 27, 28 and RPMI8226 was upregulated in parallel to anti-myeloma cytotoxicity on treatment with HDACi. On the other hand, despite the upregulation of CD26 expression in KMS11, its cytotoxic effect was not sufficiently clear following treatment with several class Our results demonstrated that the cell surface CD26 expression in KMS26, 27, 28, and RPMI8226 was upregulated in parallel to anti-myeloma cytotoxicity on treatment with HDACi. On the other hand, despite the upregulation of CD26 expression in KMS11, its cytotoxic effect was not sufficiently observed following treatment with several class I/II or class I HDACi, suggesting that the upregulation of CD26 in myeloma cells was not necessarily correlated with anti-myeloma cytotoxicity by HDACi. Moreover, our findings have important clinical implications indicating that modest HDACi contributes to synergistic anti-myeloma cytotoxicity by CD26mAb. Namely, potent HDACi

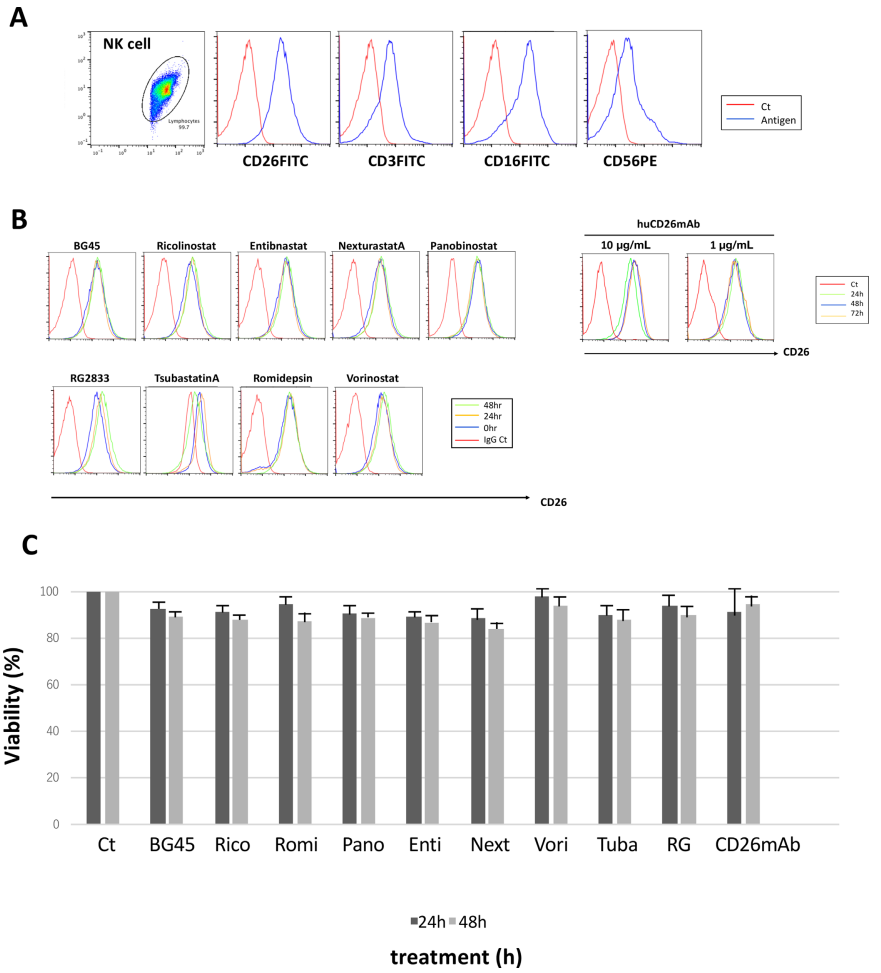

FIGURE 6 The effect of HDACi and CD26mAb on human NK cells in multiple myeloma. **A,** Expression of CD26, CD3, and CD56 on human NK cells was examined by flow cytometry. Representative overlay histograms show that human NK cells were positive for CD26. **B,** Expression levels of CD26 on human NK cells were investigated before and after exposure to one of nine HDACi or CD26mAb at 10 μg/mL for indicated times (24, 48, 72 hours). Representative overlay histograms show the expression levels of CD26 on NK cells: these levels were not altered following treatment with each HDACi. **C,** After NK cells were treated with one of nine HDACi or CD26mAb at 10 μg/mL for 24 and 48 hours, the viability of NK cell was examined by MTT assay. Bar diagrams show the percentage of viable cells. Data are presented as mean values ± S.D of three independent experiments.

may trigger adverse reactions, thereby compromising the combination with HDACi plus CD26mAb for the treatment of multiple myeloma.

The promoter region of the CD26 gene contains several potential transcription factor binding sites including Sp1 (Fig 4) and this site is shown to be a potent transcriptional activator for the transcription of several genes (42–46). The c-Myc reportedly binds to the DNA-binding domain of Sp1 on the promoter of several genes and titrates the levels of Sp1, thereby affecting promoter activity (47). Intriguingly, the c-Myc gene contains multiple Sp1-binding sites within its promoter, and represses its own transcription through the interaction between c-Myc and Sp1 at the promoter (47, 48, 50). Therefore, we postulated that the interaction between c-Myc and Sp1 on the CD26 promoter of myeloma cells may be one of mechanisms which regulate the activity of the CD26 promoter gene to induce CD26 expression in myeloma cells. ChIP-qPCR analysis confirmed that in the absence of HDACi, c-Myc is present on the CD26 promoter of myeloma cells via binding to Sp1 located on the proximal G-C box, thereby repressing the promoter and leading to reduced CD26 transcription in myeloma cells (Fig. 5D and E). In contrast, in the presence of HDACi, c-Myc was shown to be dissociated from Sp1 and its binding was replaced by acetylated c-Myc on K323 on the CD26 promoter of myeloma cells, leading to activation of the promoter and initiation of CD26 transcription (Fig. 5D and E).

The current study elucidated crucial roles of HDACi in the induction of CD26 expression in myeloma cells. First, class I or class II HDACi triggers modification of c-Myc in myeloma cells, associated with cytotoxicity in several myeloma cells. Second, HDACi plays the role of chemosensitizer via the induction of CD26 expression in myeloma cells with CD26 antigen loss. It results from increased acetylation of H3K27 as well as c-MycK323 on the CD26 promoter of myeloma cells and is inversely correlated with the decreased acetylation and expression of c-Myc. These changes lead to elicit superior cytotoxic efficacy of CD26mAb against $CD26^{neg}$ or $CD26^{dim}$ myeloma cells and restore refractoriness of myeloma cells to CD26mAb.

Currently, several HDAC inhibitors have received regulatory approval for solid tumors or hematologic malignancies including multiple myeloma (51).

In particular, panobinostat have emerged as the only HDACi approved for the treatment of multiple myeloma which nonselectively inhibits class I/II HDACs. HDACi has already shown synergistic antitumor effects with antitumor agents in combination. Indeed, the phase III PANORAMA1 trial demonstrated that 3-drug regimen containing panobinostat in combination with bortezomib plus dexamethasone led to a modest OS benefit, compared with 2-drug regimens containing bortezomib plus dexamethasone in patients with RRMM (52). Moreover, the combination of HDACi with immunotherapy has also been expected to reveal a dual efficacy as double epigenetic options. However, nonselective class I/II pan HDACi reveals profound anti-myeloma efficacy, whereas its clinical utility is limited because of unfavorable toxicities due to the inhibition of the broad range of HDAC isoforms (31, 51). Indeed, panobinostat causes severe toxic reactions such as BM suppression, severe diarrhea, bleeding tendency, liver or renal dysfunction, arrhythmia, and deep vein thrombosis, all of which were serious for elderly patients with multiple myeloma, resulting in the high rates of discontinuation in its treatment (31, 51). Therefore, alternatively, isoform-selective HDACi that exploits anti-myeloma cytotoxicity, while minimizing toxicities or combination regimens have recently been developed as a promising therapeutic option to improve the outcome of patients with multiple myeloma (53). Our findings also confirmed that isoform-selective (class I or class IIb) HDACi plus CD26mAb in combination may induce synergistic cytotoxicity against myeloma cells via the upregulation of CD26 on myeloma cells and enhanced ADCC activity by CD26mAb. In particular, HDAC3 has been reported to regulate c-Myc protein levels, thereby HDAC3 inhibition increased acetylation of c-Myc as well as DNMT1 in myeloma cells, leading to degradation of DNMT1 and inhibition of myeloma cell growth (54). Therefore, combination with HDAC3-selective inhibitor plus CD26mAb may be a promising therapeutic option to induce enhanced myeloma cell growth by CD26mAb.

To date, several studies have demonstrated that the efficacy of targeted immunotherapies in hematologic malignancies is partly dependent on the expression levels of the target antigen on the surface of tumor cells. Indeed, $CD20^{high}$ malignant lymphoma cells or chronic lymphocytic leukemia cells potentiate cytotoxic efficacy of rituximab via CDC and ADCC, whereas $CD20^{low}$ lymphoma or leukemia cells elicit a poor response to these mAbs (55, 56). Similarly, in multiple myeloma, the expression levels of CD38 in myeloma cells determine the efficacy of CD38 mAb-mediated cytotoxicity (34, 35). Specifically, $CD38^{high}$ myeloma cells were rapidly eliminated by daratumumab via immune selection, indicating that the remaining myeloma cells had lower CD38 expression levels. In addition, the trogocytic transfer of complexes consisting of CD38 and daratumumab from the myeloma cell surface to immune effector cells is an additional important mechanism for CD38 antigen loss on both myeloma cells and immune cells. These processes reduce the therapeutic efficacy of daratumumab-mediated ADCC and CDC in multiple myeloma (57). Moreover, although BCMA is expressed on most of malignant plasma cells and is recognized as a validated target in multiple myeloma therapy, its expression levels are heterogeneous, resulting in variable responses in patients with multiple myeloma (5, 58). To date, BCMA antigen loss in myeloma cells remains poorly understood. Indeed, BCMA loss in myeloma cells is not common on treatment with anti-BCMA immunotherapies because BCMA is essential for the survival of malignant plasma cells (59). Moreover, the majority of cases of BCMA loss occur by immune selection after anti-BCMA targeted immunotherapies, and the expression levels of BCMA in myeloma cells recover to the pretreatment levels at a later time. Consequently, sequential anti-BCMA retreatment with different BCMA-directed immunotherapies is considered to be feasible (60).

The relation between CD26 expression and the efficacy of CD26mAb against $CD26^{pos}$ malignancies has been controversial. Indeed, our previous studies demonstrated that CD26mAb revealed significant ADCC against $CD26^{pos}$ myeloma cells but not against $CD26^{neg}$ myeloma cells *in vitro* and *in vivo* (29). Likewise, in the treatment of solid tumors, Inamoto and colleagues showed that CD26mAb had inhibitory effects against $CD26^{pos}$ MPM cells *in vitro* and exhibited antitumor effects in a $CD26^{pos}$ MPM-bearing mouse model (61, 62). Consistent with preclinical results, CD26mAb has already been indicated as a promising therapy with well-tolerated toxicity profiles and modest efficacy as a single agent among patients with advanced MPM (26, 27); however, substantial differences in treatment response were also indicated against MPM. Indeed, a phase II study of CD26mAb in relapsed or refractory Japanese patients with MPM demonstrated that several cases with low CD26 expression in MPM cells could attain SD after treatment with CD26mAb (27). This finding implies that anti-MPM cytotoxicity may also be associated with mechanisms of action other than ADCC activity. In other words, refractoriness to targeted immunotherapies is not solely explained by antigen loss, but additional tumor- or host-related mechanisms underlying acquired resistance are also involved. First, an increase in the expression of CIPs, including CD55 and CD59, protects myeloma cells from complement attack via CDC, leading to refractoriness to mAb (36). Indeed, expression levels of CIPs on myeloma cell lines, cultured alone were increased but were not altered by HDACi, which may contribute to the inhibition of CDC lysis by CD26mAb in multiple myeloma, regardless of the presence or absence of HDACi (Fig. 2C and D). Second, myeloma cells reside in the BM microenvironment by binding to various stromal cells (BMSCs) through the upregulation of antiapoptotic proteins, which may also contribute to the development of resistance via the evasion of mAb or cytotoxic T cell–mediated killing of myeloma cells (63). We previously demonstrated that CD26mAb impaired the adhesion of $CD26^{pos}$ myeloma cell to BMSCs which inhibits myeloma cell growth (29). Third, mAbs are not necessarily capable of eliminating clones in myeloma cells with high-risk chromatin alteration such as t(4;14)(p16.3;q32.3), gain 1q21 or del(17p) or drug-efflux pump such as side population (SP) cells, both of which indicate refractoriness to anticancer agents and result in inferior impacts on survival of patients with myeloma. Specifically, KMS11 cells contain both t(4;14) alteration and SP cells, parts of which revealed resistance to HDACi monotherapy; however, it was restored by treatment with HDACi plus CD26mAb in combination (Fig. 2A). Moreover, the activity of immune effector cells is also associated with refractoriness to targeted immunotherapy. CD38 is expressed not only on myeloma cells but also on NK cells. Therefore, rapid depletion of $CD38^{pos}$NK cells was observed after treatment with daratumumab, which may lead to a decrease in the ADCC activity of daratumumab against myeloma cells (64, 65). In the current study, although CD26 was also highly expressed in NK cells, neither HDACi nor CD26mAb altered the expression levels of CD26 on NK cells (Fig. 6B). Moreover, the viability of NK cells was not affected by either treatment. This finding implies that NK cell–mediated ADCC against myeloma cells by CD26mAb is not impeded by the diminished frequency or activity of NK cells, unlike CD38mAb treatment, which may indicate a clinical benefit for the treatment of multiple myeloma by CD26mAb (Fig. 6C).

In summary, to overcome both innate and acquired refractoriness of myeloma cells with CD26 antigen loss to CD26mAb, the concurrent use of HDACi confers therapeutic benefit by the induction of CD26 expression in myeloma

cells. Importantly, our findings point to a novel observation on the role of HDACi. Namely, epigenetic modification with isoform-selective (class I or class IIb) HDACi not only shows anti-myeloma activity in itself but also acts as a chemosensitizer by resensitizing $CD26^{neg}$ myeloma cells or those with CD26 antigen loss to CD26mAb, thereby eliciting superior anti-myeloma cytotoxicity that may lead to restore the refractoriness to mAb in RRMM.

Authors' Disclosures

No disclosures were reported.

Authors' Contributions

H. Nishida: Conceptualization, resources, data curation, software, formal analysis, funding acquisition, validation, investigation, visualization, methodology, writing-original draft, writing-review and editing, designed and performed the experiments analyzed data and wrote original draft manuscript. **R. Suzuki:** Formal analysis, investigation, methodology, designed and performed the experiments in transcriptome profiling. **K. Nakajima:** Formal analysis, investigation, methodology, performed the experiments in IHC. **M. Hayashi:** Investigation, conceptualized and curated the data. **C. Morimoto:** Investigation, conceptualized and curated the data. **T. Yamada:** Resources, supervision, funding acquisition, investigation, project administration, provided samples, performed the experiments, analyzed pathological results, conceptualized and curated the data and wrote review.

Acknowledgments

We thank Mari Fujiwara, Akira Sonoda at Core Instrumentation Facility, Keio University, School of Medicine for their technical assistance in executing experiments of flow cytometry and cell sorting, Maiko Matsushita, division of clinical physiology and therapeutics, at Keio University, Faculty of Pharmacy for helpful advice of drug use, Satoru Kobayashi and Hisahito Yamazaki at Thermo Fisher Scientific Co. Ltd. for the technical support. This work was supported in by Grant-in-Aid for Scientific Research from the Ministry of Education, Culture, Sports, Science and Technology of Japan (C; 20K07682, 16K07180) to H. Nishida., (B; 19H03519) and Grant-in-Aid for Exploratory Research (19K22542) to H. Nishida. and T. Yamada.

Note

Supplementary data for this article are available at Cancer Research Communications Online (https://aacrjournals.org/cancerrescommun/).

Received May 15, 2023; revised November 13, 2023; accepted January 24, 2024; published first February 09, 2024.

References

1. van de Donk N, Pawlyn C, Yong KL. Multiple myeloma. Lancet 2021;397: 410-27.
2. Dimopoulos MA, Oriol A, Nahi H, San-Miguel J, Bahlis NJ, Usmani SZ, et al. Daratumumab, lenalidomide, and dexamethasone for multiple myeloma. N Engl J Med 2016;375: 1319-31.
3. Landgren O, Hultcrantz M, Diamond B, Lesokhin AM, Mailankody S, Hassoun H, et al. Safety and effectiveness of weekly carfilzomib, lenalidomide, dexamethasone and daratumumab combination therapy for patients with newly diagnosed multiple myeloma. JAMA Oncol 2021;7: 862-8.
4. Gandhi UH, Cornell RF, Lakshman A, Gahvari ZJ, McGehee E, Jagosky MH, et al. Outcomes of patients with multiple myeloma. Leukemia 2019;33: 2266-75.
5. Lakshman A, Kumar SK. Chimeric antigen receptor T-cells, bispecific antibodies, and antibody-drug conjugates for multiple myeloma: an update. Am J Hematol 2022;97: 99-118.
6. Velasquez MP, Bonifant CL, Gottschalk S. Redirecting T cells to hematological malignancies with bispecific antibodies. Blood 2018;131: 30-8.
7. Mikkilineni L, Kochenderfer JN. Chimeric antigen receptor T-cell therapies for multiple myeloma. Blood 2017;130: 2594-602.
8. Tan CR, Shah UA. Targeting BCMA in multiple myeloma. Curr Hematol Malig Rep 2021;16: 367-83.
9. Tai YT, Mayes PA, Acharya C, Zhong M, Cea M, Cagnetta A, et al. Novel anti-B-cell maturation antigen antibody-drug conjugate (GSK2857916) selectively induces killing of multiple myeloma. Blood 2014;123: 3128-38.
10. Trudel S, Lendvai N, Popast R, Voorhees PM, Reeves B, Libby EN, et al. Targeting B-cell maturation antigen with GSK2857916 antibody drug conjugate in relapsed or refractory multiple myeloma (BMA117159): a dose escalation and expansion phase 1 trial. Lancet Oncol 2018;19: 1641-53.
11. Lonial S, Lee HC, Badros A, Trudel S, Nooka AK, Chari A, et al. Blentamab mafodotin for relapsed or refractory multiple myeloma (DREAMM-2): a two-arm randomized, open-label, phase 2 study. Lancet Oncol 2020;21: 207-21.
12. Nooka AK, Cohen A, Lee HC, Badros A, Suvannasankha A, Callander N, et al. Single-agent blentamab mafodotin in patients with relapsed or refractory multiple myeloma: final analysis of the DREAMM-2 trial. Cancers 2023;129: 3746-60.
13. Carpenter RO, Evbuomwan MO, Pittaluga S, Pittaluga S, Rose JJ, Raffeld M, et al. B-cell maturation antigen is promising target for adoptive T-cell therapy of multiple myeloma. Clin Cancer Res 2013;19: 2048-60.
14. Hipp S, Tai Y, Blanset D, Deegen P, Wahl J, Thomas O, et al. A novel BCMA/CD3 bispecific T-cell engager for the treatment of multiple myeloma induces selective lysis *in vitro* and *in vivo*. Leukemia 2017;31: 1743-51.
15. Munshi NC, Anderson LD Jr, Shah N, Madduri D, Berdeja J, Lonial S, et al. Idecabtagene Vicleucel in relapsed and refractory multiple myeloma. N Engl J Med 2021;384: 705-16.
16. Berdeja JG, Madduri D, Usmani SZ, Jakubowiak A, Agha M, Cohen AD, et al. Ciltacabtagebe autoleucel, a B-cell maturation antigen-targeted chimeric antigen receptor T-cell therapy in patients with relapsed or refractory multiple myeloma (CARTITUDE-1): a phase 1b/2 open label study. Lancet 2021;298: 314-24.
17. Martin T, Usmani SZ, Berdeja JG, Agha M, Cohen AD, Hari P, et al. Ciltacabtagene autoleucel, anti-B-cell maturation chimeric antigen receptor T-cell therapy, for relapsed/refractory multiple myeloma: CARTITUDE-12-year follow-up. J Clin Oncol 2022;41: 1265-74.
18. Usmani SZ, Garfall AL, van de Donk NWCJ, Nahi H, San-Miguel JF, Oriol A, et al. Teclistamab, a B-cell maturation antigen xCD3 bispecific antibody, in patients with relapsed or refractory multiple myeloma (MajesTEC-1): a multicentre, open-label, single-arm, phase 1 study. Lancet 2021;398: 665-74.
19. Fleischer B. CD26: a surface protease involved in T-cell activation. Immunol Today 1994;15: 180-4.
20. Tanaka T, Camerini D, Seed B, Torimoto Y, Dang NH, Kameoka J, et al. Cloning and functional expression of the T cell activation antigen CD26. J Immunol 1992;149: 881-6.
21. Dang RP, Tachibana K, Hegen M, Scharpe S, Schlossma SF, Morimoto C. Correlation of the epitope defined anti-CD26mAbs and CD26 function. Mol Immnol 1998;35: 13-21.
22. Torimoto Y, Dang NH, Tanaka T, Prado C, Schlossman SF, Morimoto C. Biochemical characterization of CD26 (dipeptidyl peptidase IV): functional comparison of distinct epitopes recognized by various anti-CD26 monoclonal antibodies. Mol Immunol 1992;29: 183-92.

23. Ohnuma K, Takahashi N, Tamochi T, Hosono O, Dang NH, Morimoto C. Role of CD26/dipeptidyl peptidase IV in human T cell activation and function. Front Biosci 2008;13: 2299-310.
24. Havre PA, Abe M, Urasaki Y, Ohnuma K, Morimoto C, Dang NH. The role of CD26/dipeptidyl peptidase IV in cancer. Front Biosci 2008;13: 1634-45.
25. Angevin E, Isambert N, Trillet-Lenoir V, You B, Alexandre J, Zalcman G, et al. First-in-human phase 1 of YS110, a monoclonal antibody directed against CD26 in advanced CD26-expressing cancers. Br J Cancer 2017;116: 1126-34.
26. Takeda M, Ohe Y, Horinouchi H, Hida T, Sjimizu J, Seto T, et al. Phase I study of YS110, a recombinant humanized monoclonal antibody to CD26, in Japanese patients with advanced malignant pleural mesothelioma. Lung Cancer 2019;137: 64-70.
27. Nakagawa K, Kijima T, Okada M, Morise M, kato M, Hirano K, et al. Phase 2 study of YS110, a recombinant humanized anti-CD26 monoclonal antibody, in Japanese patients with advanced malignant pleural mesothelioma. JTO Clin Res Rep 2021;2: 100178.
28. Nishida H, Suzuki H, Madokoro H, Hayashi M, Morimoto C, Sakamoto M, et al. Blockade of CD26 signaling inhibits osteoclast differentiation. J Bone Miner Res 2014;29: 2439-55.
29. Nishida H, Hayashi M, Morimoto M, Sakamoto M, Yamada T. CD26 is a potential therapeutic target by humanized monoclonal antibody for the treatment of multiple myeloma. Blood Cancer J 2018;8: 99.
30. Ropero S, Esteller M. The role of histone deacetylases (HDACs) in human cancer. Mol Oncol 2007;1: 19-25.
31. Xu WS, Parmigiani MPA. Histone deacetylase inhibitors: molecular mechanisms of action. Oncogene 2007;26: 5541-52.
32. Bobrowicz M, Dwojak D, Pyrzynska B, Stachura J, Muchowicz A, Berthel E, et al. HDAC6 inhibition upregulates CD20 levels and increases the efficacy of anti-CD20 monoclonal antibodies. Blood 2017;130: 1628-38.
33. Shimizu R, Kikuchi J, Wada T, Ozawa K, Kano Y, Furukawa Y. HDAC inhibitors augment cytotoxic activity of rituximab by upregulating CD20 expression on myeloma cells. Leukemia 2010;24: 1760-8.
34. Garicia-Guerreri E, Gotz R, Doose S, Sauer M, Rodriguez-Gil A, Nerreter T, et al. Upregulation of CD38 expression on multiple myeloma cells by novel HDAC6 inhibitor is a class effect and augments the efficacy of daratumumab. Leukemia 2021;35: 201-14.
35. Nijhof IS, Grosen RWJ, Lokhorst HM, Van Kessel B, Bloem AC, Van Velzen J, et al. Upregulation of CD38 expression on multiple myeloma cells by all-trans retinoic acid improves the efficacy of daratumumab. Leukemia 2015;29: 2039-49.
36. Nihof IS, Casneuf T, Van Kessel B, Axel AE, Syed K, Groen RWJ, et al. CD38 expression and complement inhibitors affect response and resistance to daratumumab therapy in myeloma. Blood 2016;128: 959-70.
37. Barclay AN, van den Berg TK. The interaction between signal regulatory protein alpha (SIRPα): structure, function and therapeutic target. Ann Rev Immunol 2014;32: 25-50.
38. Gartel AL, Goufman XYE, Shianov P, Hay N, Najmabadi F, Tyner AL. Myc represses the p21WAF1/CIP1 promoter and interacts with Sp1/Sp3. Proc Natl Acad Sci U S A 2001;98: 4510-5.
39. Vervoorts J, Luscher-Firzlaff J, Luscher B. The ins and outs of MYC regulation by posttranslational mechanisms. J Biol Chem 2006;281: 34725-9.
40. Nair JR, Caserta J, Belko K, Howell T, Fetterly G, Baldino C, et al. Novel inhibition of PIM2 kinase has significant anti-tumor efficacy in multiple myeloma. Leukemia 2017;31: 1715-26.
41. Jang JS, Li Y, Mitra AK, Bi L, Abyzov A, van Wijnen AJ, et al. Molecular signatures of multiple myeloma progression through single cell RNA-Seq. Blood Cancer J 2019;9: 2.
42. Bohm SK, Gum JR Jr, Erickson RH, Hicks JW, Kim YS. Human dipeptidyl peptidase IV gene promoter: tissue-specific regulation from TATA-less GC-rich sequence characteristic of a housekeeping gene promoter. Biochem J 1995;311: 835-43.
43. Abbott CA, Baker E, Sutherland GR, McCaughan GW. Genomic organization, exact localization, and tissue expression of the human CD26 (dipeptidyl peptidase IV) gene. Immunogenetics 1994;40: 331-8.
44. Qvist H, Sjostrom H, Noren O. The TATA-less, GC-rich proline dipeptidylpeptidase IV (DPPIV) promoter shows bidirectional activity. Bio Chem 1998;379: 75-81.
45. Suske G. The SP1-family of transcription factors. Gene 1999;238: 291-300.
46. Lania L, Majello B, De Luca P. Transcriptional regulation by the Sp family proteins. Int J Biochem Cell Biol 1997;29: 1313-23.
47. DesJardins E, Hay N. Repeated CT elements bound by zinc finger proteins control the absolute and relative activities of the two principal human c-myc promoters. Mol Cell Biol 1993;13: 5710-24.
48. Thompson EB. The many roles of c-Myc in apoptosis. Annual Rev Physiol 1998;60: 575-600.
49. Dang CV. c-Myc target genes involved in cell growth, apoptosis and metabolism. Mol Cell Biol 1999;19: 1-11.
50. Penn LJ, Brooks MW, Laufer EM, Land H. Negative autoregulation of c-myc transcription. EMBO J 1990;9: 1113-21.
51. Ho TCS, Chan AHY, Ganesan A. Thirty years of HDAC inhibitors: 2020 Insight and hindsight. J Med Chem 2020;63: 12460-84.
52. San-Miguel JF, Hungria VTM, Yoon SS, Beksac M, Dimopoulos MA, Elghandour A, et al. Overall survival of patients with relapsed multiple myeloma treated with panobinostat or placebo plus bortezomib and dexamethasone (the PANORAMA 1 trial). A randomized placebo-controlled, phase 3 trial. Lancet Haematol 2016;3: e506-15.
53. Banik D, Moufarrij S, Villagra A. Immunogenetics combination therapies: an overview of the role of HDACs in cancer immunotherapy. Int J Mol Sci 2019;20: 2241.
54. Harada T, Ohguchi H, Grondin Y, Kikuchi S, Sagawa M, Tai YT, et al. HDAC3 regulates DNMT1 expression in multiple myeloma: therapeutic implications. Leukemia 2017;31: 2670-7.
55. Jilani I, O'Brien S, Manshuri T, Thomas DA, Thomazy VA, Imam M, et al. Transient down-modulation of CD20 by rituximab in patients with chronic lymphocytic leukemia. Blood 2003;102: 3514-20.
56. Davis TA, Czerwinski DK, Levy R. Therapy B-cell lymphoma with anti-CD20 antibodies can result in the loss of CD20 antigen expression. Clin Cancer Res 1999;5: 611-5.
57. Krejcik J, Frerichs KA, Nihof IS, van Kessel B, van Velzen JF, Bloem AC, et al. Monoctytes and glanulocytes reduce CD38 expression levels on myeloma cells on patients treated with daratumumab. Clin Cancer Res 2017;23: 7498-511.
58. Zhou X, Rasche L, Kortum KM, Mersi J, Einsele H. BCMA loss in the epoch of novel immunotherapy for multiple myeloma. Haematologica 2022;108: 958-68.
59. O'Connor BP, Raman VS, Erickson LD, Cook WJ, Weaver LK, Ahonen C, et al. BCMA is essential for the survival of long-lived bone marrow plasma cells. J Exp Med 2004;199: 91-8.
60. Gazeau N, Beauvais D, Yakoub-Agha I, Mitra S, Campbell TN, Facon T, et al. Effective anti-BCMA retreatment in multiple myeloma. Blood Adv 2021;5: 3016-20.
61. Inamoto T, Yamada T, Ohnuma K, Kina S, Takahashi N, Yamochi T, et al. Humanized anti-CD26 monoclonal antibody as a treatment for malignant mesothelioma tumors. Clin Cancer Res 2007;13: 4191-200.
62. Inamoto T, Yamochi T, Ohnuma K, Iwata S, Kina S, Inamoto S, et al. Anti-CD26 monoclonal antibody-mediated G1-S arrest of human renal clear cell carcinoma Caki-2 is associated with retinoblastoma substrate dephosphorylation, cyclin dependent kinase 2 reduction p27(kip1) enhancement, and disruption of binding to the extracellular matrix. Clin Cancer Res 2006;12: 3470-7.
63. de Haart SJ, van de Donk NWCJ, Minnema MC, Huang JH, Aarts-Riemens T, Bovenschen N, et al. Accessory cell of the microenvironment protect multiple myeloma from T-cell cytotoxicity through cell adhesion-mediated immune resistance. Clin Cancer Res 2013;19: 5591-601.
64. Wang Y, Zhang Y, Hughes T, Zhang J, Caligiuri MA, Benson DM, et al. Fratricide of NK cells in daratumumab therapy for multiple myeloma overcome by *ex vivo*-expanded autologous NK cells. Clin Cancer Res 2018;24: 4006-617.
65. Casneuf T, Xu XS, Adams HC III, Axel AE, Chiu C, Khan I, et al. Effects of daratumumab on natural killer cells and impact on clinical outcomes in relapsed or refractory multiple myeloma. Blood Adv 2017;1: 2105-14.